



## **AFFIDAVIT**

I declare that I have authored this thesis independently, that I have not used other than the declared sources/resources, and that I have explicitly indicated all material which has been quoted either literally or by content from the sources used. The text document uploaded to TUGRAZonline is identical to the present doctoral thesis.

---

Date

---

Signature

## **Acknowledgment**

Firstly, I would like to express my gratitude to my supervisor Prof. Bernd Nidetzky who provided me an opportunity to join his research group and for the continuous support of my PhD study and related research. Besides my advisor, my sincere thanks also go to my co-supervisor, Dr. Juan Manuel Bolivar who helped me to fulfill my research within the whole years of my Ph.D. I am also deeply thankful to Martin Pfeiffer, Dr. Alexander Dennig and Dr. Zdenek Petrsek for their help in some parts of my PhD research. Furthermore, I am extending my heartfelt thanks to Sabine Schelch, Marco A. Tribulato and Dr. Martina Viefhues for their support during my PhD period. Also, I express my thanks to all members of the Institute of Biotechnology and Biochemical Engineering of TU Graz for assistance wherever it was needed.

Last but not the least; I would like to thank my family: my parents and friends for supporting me spiritually throughout my PhD study but also my life in general.

## Abstract

Microstructured reactors are promising engineering tools to develop emerging flow-chemistry applications. Apart from their purely chemical applications, microreactors have also drawn significant attention for use in biocatalysis. A promising layout involves flow microchannels that are wall-coated with enzyme. In this study, an immobilization procedure was developed that involves fusion of the target enzyme to the cationic binding module  $Z_{\text{basic2}}$  (58 amino acids; 7 kDa mass) to enable oriented immobilization on negatively charged surfaces based on convenient charge complementarity. The effects of multiple  $Z_{\text{basic2}}$  modules in a single enzyme molecule on immobilized performance in a glass microreactor were studied for sucrose phosphorylase (SPase). Results showed that multivalent constructs reached a higher value of space-time yield and operational stability as compared to monovalent construct contains one  $Z_{\text{basic2}}$ .

A fundamental problem of enzyme microreactor design is that plain microchannels without extensive static internals, or packings, offer limited exposed surface area for immobilizing the enzyme. To boost the immobilization in a manner broadly applicable to enzymes, we coated borosilicate microchannels with silica nanosprings. Using a multivalent  $Z_{\text{basic2}}$  construct of SPase, it was shown that the nanosprings-coated microchannel boosted the conversion rate, but also the operational stability, as compared to the plain microchannel.

To explore the application of immobilized enzyme microreactors in another aspect, we also studied the easy integration of  $O_2$  sensor systems into microreactors to study the performance of an  $O_2$ -dependent enzyme, namely glucose oxidase.

Considering the high efficiency of the  $Z_{\text{basic2}}$  immobilization method demonstrated in proof of principle studies, we expanded the research to the development of a self-sufficient monooxygenase biocatalyst. Cytochrome P450 monooxygenases (P450s) promote hydroxylations, via oxygen insertion from  $O_2$ , in a broad variety of substrates. However, operating P450 reactions involves complex management of the main substrate,  $O_2$  and NADPH reducing equivalents against an overall background of low enzyme operational stability. Using enzymes as fusion proteins with  $Z_{\text{basic2}}$ , the canonical P450 monooxygenase (P450 BM3) was co-immobilized with glucose dehydrogenase (as a cofactor regeneration enzyme) on anionic sulfopropyl-activated carrier (ReliSorb SP). The immobilized P450 BM3 showed a high total turnover number and remarkable number of reusability. This study therefore supports the idea of practical heterogeneous catalysis by P450 monooxygenase systems immobilized on solid support. The results provide an important step towards the application of complex biocatalysts in continuous microreactors.

## Zusammenfassung

Mikrostrukturierte Reaktoren sind vielversprechende technische Werkzeuge für die Entwicklung von Anwendungen der Flow Chemistry. Abgesehen von ihrer reinen chemischen Anwendung, haben Mikroreaktoren auch durch ihre Anwendung in der Biokatalyse Aufmerksamkeit auf sich gezogen. Eine vielversprechende Ausführung beinhaltet Durchfluss-Mikrokanäle, deren Wände mit Enzym gesättigt sind. In dieser Arbeit wurde eine Immobilisierungsmethode entwickelt, welche auch die Fusion des gewünschten Enzyms an ein kationisches Bindungsmodul  $Z_{\text{basic2}}$  (58 Aminosäuren; 7 kDa Masse) miteinschließt, um eine geordnete Immobilisierung an negativ geladene Oberflächen basierend auf nützlicher Ladungskomplementarität zu ermöglichen. Untersucht wurden die Effekte auf die Immobilisierungseffizienz von mehreren  $Z_{\text{basic2}}$  Modulen an einem einzigen Enzym Molekül für Sucrose Phosphorylase (SPase). Die Resultate zeigten, dass Konstrukte mit mehreren Modulen  $Z_{\text{basic2}}$ , im Vergleich zu Konstrukten mit einem Modul, einen höheren Wert bei der Space-Time-Yield und der operative Stabilität erreichten.

Ein elementares Problem des Enzym-Mikroreaktor-Designs ist das einfache Mikrokanäle ohne umfangreiche statische Einbauten oder Füllkörper nur wenig freiliegende Oberfläche für die Immobilisierung der Enzyme anbieten. Um die Immobilisierung für eine erweiterte Anwendbarkeit für Enzyme zu steigern, haben wir die Oberfläche der Borosilikat-Mikrokanäle mit Silica-Nanosprings beschichtet. Durch Verwendung von einem Konstrukt mit mehreren Modulen  $Z_{\text{basic2}}$ , konnte gezeigt werden, dass mit Nanosprings-beschichteten Mikrokanälen im Vergleich zu unbeschichteten Mikrokanälen sowohl die Konversionsrate als auch die operative Stabilität gesteigert werden konnte. Um einen anderen Aspekt der Anwendung von immobilisierten Enzym-Mikroreaktoren zu erforschen, haben wir die einfache Integration von  $O_2$  Sensorsystemen untersucht, um die Effizienz des  $O_2$  abhängigen Enzyms Glucose Oxidase zu erforschen. Unter Berücksichtigung der hohen Effizienz der Immobilisierungsmethode mit  $Z_{\text{basic2}}$  in „Beweis des Prinzips“-Studien, haben wir unsere Erforschung auf die Entwicklung eines autarken Monooxygenase Biokatalysators erweitert. Cytochrome P450 Monooxygenasen (P450s) begünstigen Hydroxylierungen durch die Einbringung von Sauerstoff in eine breitgefächerte Menge an Substraten. Allerdings ist für die Anwendung von P450 Reaktionen ein komplexes Management des Hauptsubstrats,  $O_2$  und NADPH reduzierende Äquivalente notwendig im Gegenzug zur niedrigen operativen Enzymstabilität. Durch Verwendung von Enzymen als Fusionsproteine mit  $Z_{\text{basic2}}$ , wurde die kanonische P450 Monooxygenase (P450 BM3) mit Glucose Dehydrogenase (als Cofaktor regenerierendes Enzym) auf anionischem Sulfopropyl-aktiviertem Trägermaterial (ReliSorb SP) coimmobilisiert. Das immobilisierte P450 BM3 zeigte eine hohe total turn over number und eine bemerkenswerte Wiederverwendbarkeit. Diese Arbeit unterstützt aufgrund dessen die Idee der praktischen heterogenen Katalyse von P450 Monooxygenase Systemen immobilisiert auf festen Trägermaterialien. Die Resultate liefern einen wichtigen Beitrag für die Anwendung von komplexen Biokatalysatoren in kontinuierlichen Mikroreaktoren.

## Table of Contents

<b>Multivalency Effects on the Immobilization of Sucrose Phosphorylase in Flow Microchannels and Their Use in the Development of a High-Performance Biocatalytic Microreactor</b>	
Donya Valikhani, Juan M. Bolivar, Martin Pfeiffer, Bernd Nidetzky	
<i>ChemCatChem</i> , 2017, 9, 161 – 166	5
Supporting Information	11
<b>A Spring in Performance: Silica Nanosprings Boost Enzyme Immobilization in Microfluidic Channels</b>	
Donya Valikhani, Juan M. Bolivar, Martina Viefhues, David N. McIlroy, Elwin X. Vrouwe, Bernd Nidetzky	
<i>ACS Appl. Mater. Interfaces</i> , 2017, 9, 34641–34649	26
Supporting Information	35
<b>Tailor-made resealable micro(bio)reactors providing easy integration of <i>in situ</i> sensors</b>	
Martina Viefhues, Shiwen Sun, Donya Valikhani, Bernd Nidetzky, Elwin X Vrouwe, Torsten Mayr, Juan M. Bolivar	
<i>J. Micromech. Microeng.</i> , 2017, 27, 065012	41
Supporting Information	52
<b>Tailor-made, Self-sufficient and Recyclable Monooxygenase Catalyst Based on Co-immobilized Cytochrome P450 BM3 and Glucose Dehydrogenase</b>	
Donya Valikhani, Juan M. Bolivar, Alexander Dennig, Bernd Nidetzky	
Manuscript in preparation	60
Supporting Information	89
<b>Scientific record</b>	94

**Multivalency Effects on the Immobilization of Sucrose Phosphorylase in Flow Microchannels and Their Use in the Development of a High-Performance Biocatalytic Microreactor**

# Multivalency Effects on the Immobilization of Sucrose Phosphorylase in Flow Microchannels and Their Use in the Development of a High-Performance Biocatalytic Microreactor

Donya Valikhani,<sup>[a]</sup> Juan M. Bolivar,<sup>[a]</sup> Martin Pfeiffer,<sup>[a]</sup> and Bernd Nidetzky<sup>\*[a, b]</sup>

Microstructured reactors are emerging engineering tools for the development of biocatalytic conversions in continuous flow. A promising layout involves flow microchannels that are wall-coated with enzyme. As protein immobilization within closed microstructures is challenging, we suggested a confluent design of enzyme and microreactor: fusion to the silica-binding module  $Z_{\text{basic}2}$  is used to engineer enzymes for high-affinity oriented attachment to the plain wall surface of glass microchannels. In this study of sucrose phosphorylase, we examined the effects of multiple  $Z_{\text{basic}2}$  modules in a single enzyme molecule on the activity and adsorption stability of the phosphorylase immobilized in a glass microchannel reactor. Compared to the "monovalent" enzyme, two  $Z_{\text{basic}2}$  modules, present in tandem repeat at the N-terminus, separated at the N- and C-

terminus of an enzyme monomer, or arranged N-terminally in a protein homodimer, boosted the effectiveness of the immobilized phosphorylase by up to twofold. They attenuated (up to 12-fold) the elution of the wall-coated enzyme during continuous reactor operation. The divalent phosphorylase was distributed uniformly on the microchannel surface and approximately 70% activity could still be retained after 690 reactor cycles. Reaction-diffusion regime analysis in terms of the second Damköhler number ( $Da_{II} \leq 0.02$ ) revealed the absence of mass transport limitations on the conversion rate. The synthesis of  $\alpha$ -D-glucose 1-phosphate occurred with a productivity of  $\sim 14 \text{ mm min}^{-1}$  at 50% substrate conversion (50 mM). The use of wall-coated enzyme microreactors in high-performance biocatalytic reaction engineering is supported strongly.

## Introduction

Flow chemistry has aroused a great deal of interest in various fields.<sup>[1–5]</sup> Microstructured reactors are promising engineering tools to develop emerging flow-chemistry applications. Their design usually involves a functional network of narrow microchannels, each 10–100  $\mu\text{m}$  wide, into which the fluid flow is directed. In addition to offering a general "flow format" for chemical conversions, microstructured reactors support highly efficient mass and heat transport because of the large specific surface area and short diffusion distances in the microchannels.<sup>[6,7]</sup> Apart from their purely chemical applications, microreactors have also drawn significant attention for use in biocatalysis.<sup>[8–12]</sup> However, whenever enzymes are applied to continuous conversions, the question about their recycling arises, enzyme reuse is then a practical necessity.<sup>[13–15]</sup> As in macro-scale reactors, the use of solid-supported immobilized enzymes

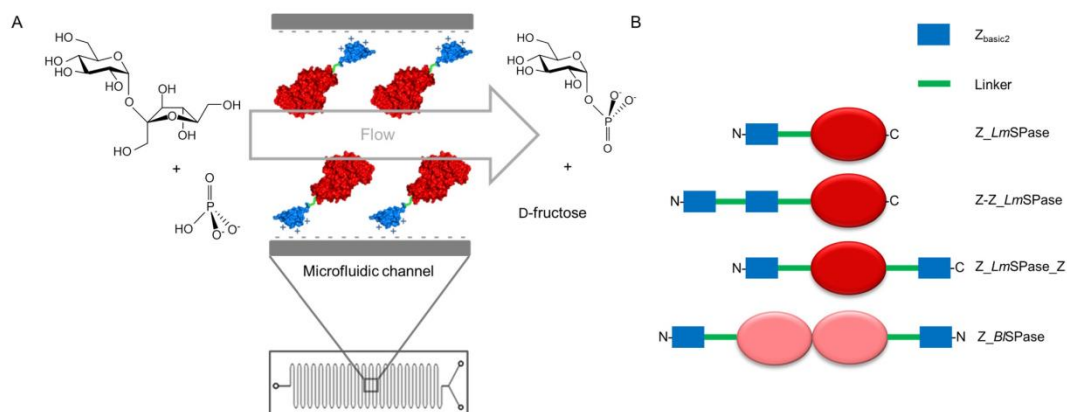
is appropriate,<sup>[16–24]</sup> but in closed microstructures enzyme immobilization is a difficult problem.<sup>[9,11,25]</sup> A promising microreactor design that integrates the immobilization is one in which the flow microchannels are wall-coated with the enzyme used.<sup>[9,11,25]</sup> However, to create a wall surface that offers the enzyme activity in the required amount presents a fundamental challenge in biocatalytic microreactor development.

To overcome these limitations, we suggested fusion to the strongly positively charged silica-binding module  $Z_{\text{basic}2}$  (58 amino acids; 7 kDa mass) to engineer enzymes for immobilization on the wall surface of silica microchannels based on convenient charge complementarity.<sup>[26,27]</sup> Silica was considered for its widespread use in microstructure fabrication. Fixation through  $Z_{\text{basic}2}$  offers decisive advantages for enzyme immobilization on silica materials. By decoupling the function of surface adsorption from the enzymatic function in the protein structure, the immobilization is generally applicable to enzymes. It is highly selective for enzymes that contain  $Z_{\text{basic}2}$  so a one-step purification and immobilization from crude protein mixtures is usually possible.<sup>[27–30]</sup> It does not require the derivatization of the silica surface. As a result of the defined molecular orientation of the adsorption, the immobilized enzyme usually retains its intrinsic activity. The immobilization is readily reversible. By simply washing the enzyme off, the recycling of the microstructured element is achieved conveniently.

[a] D. Valikhani, Dr. J. M. Bolivar, M. Pfeiffer, Prof. Dr. B. Nidetzky  
Institute of Biotechnology and Biochemical Engineering  
Graz University of Technology, NAWI Graz  
Petersgasse 12  
A-8010 Graz (Austria)  
E-mail: bernd.nidetzky@tugraz.at

[b] Prof. Dr. B. Nidetzky  
Austrian Centre of Industrial Biotechnology  
Petersgasse 14  
A-8010 Graz (Austria)

 Supporting information for this article can be found under:  
<http://dx.doi.org/10.1002/cctc.201601019>.



**Scheme 1.** Development and operation of a biocatalytic microreactor fabricated from glass that features sucrose phosphorylase immobilized on the walls of the meandering flow microchannel. A) The enzyme is attached to microchannel walls through its  $Z_{\text{basic}2}$  binding module, which is highly positively charged and, therefore, binds to negatively charged silica surfaces with high affinity. The enzymatic reaction that gives  $\alpha\text{Glc 1-P}$  as the product is shown. B) Different chimeric forms of sucrose phosphorylase are used to explore multivalency effects from two  $Z_{\text{basic}2}$  modules on activity and stability of the immobilized enzyme. The locations of the N- and C-termini of the enzyme constructs used are indicated. The enzyme from *Leuconostoc mesenteroides* (*LmSPase*) is a - functional monomer, whereas the enzyme from *Bifidobacterium longum* (*BISPase*) is a homodimer.

Surface attachment through  $Z_{\text{basic}2}$  involves only noncovalent bonds, which gives rise to the caveat that the immobilized enzyme might be washed off quickly on application of the fluid flow. Therefore, this study was performed to analyze multivalency effects from two  $Z_{\text{basic}2}$  modules in the functional enzyme, instead of just one, on the activity and adsorption stability of enzyme immobilized in a glass microchannel reactor. A comparison between the “divalent” and “monovalent” enzyme was done using sucrose phosphorylase (EC 2.4.1.7), a well-known transglucosidase that has important applications in glycoside and sugar phosphate synthesis.<sup>[31]</sup> Irrespective of the spatial arrangement in the phosphorylase structure (Scheme 1), the presence of two  $Z_{\text{basic}2}$  modules compared to only one was correlated with a strong boost in enzyme reactor stability during continuous operation. It is also shown that the wall-coated enzyme was distributed homogeneously on the microchannel surface; and that, contrary to monovalent binding, which gave relatively fast “bleeding” of the immobilized phosphorylase, divalent binding attenuated the enzyme elution strongly under continuous-flow conditions. We analyzed the synthesis of  $\alpha\text{-D-glucose 1-phosphate}$  ( $\alpha\text{Glc 1-P}$ ) from sucrose and phosphate (Scheme 1), and the immobilized enzyme microreactor gave an outstanding performance regarding conversion rate and space-time yield in the absence of diffusional limitations.

## Results and Discussion

### Creating multivalency from two $Z_{\text{basic}2}$ modules within a single enzyme molecule

We used the monomeric sucrose phosphorylase from *Leuconostoc mesenteroides* (*LmSPase*) as the “monovalent reference”, and two approaches to induce  $Z_{\text{basic}2}$  multivalency were pur-

sued (Scheme 1; Figure S1). One was to append  $Z_{\text{basic}2}$  to the N-terminus of the homodimeric sucrose phosphorylase from *Bifidobacterium longum* (*BISPase*), and the other was to incorporate two  $Z_{\text{basic}2}$  modules in tandem repeat at the N-terminus of the *LmSPase*. The effect of the presence of two  $Z_{\text{basic}2}$  modules separated from each other in the *LmSPase* structure was examined with a fusion protein that contained  $Z_{\text{basic}2}$  both at the N- and the C-termini. All constructs were expressed in *E. coli* to a level of 10% of total intracellular protein or greater. Purified proteins (Figure S2) showed specific phosphorylase activities ( $69\text{--}90\text{ U mg}^{-1}$ ) comparable to that of the *LmSPase* reference. Some basic properties of the enzymes used are reported in Table S1.

### Immobilization in the glass microchannel reactor

A microfluidic chip fabricated from borosilicate glass was used. It contained a single meandering flow channel (width:  $150\text{ }\mu\text{m}$ ; depth:  $150\text{ }\mu\text{m}$ ; length:  $771\text{ mm}$ ) with an approximately triangular cross-section (Scheme 1; Figure S3). The hydraulic diameter was calculated to be  $92\text{ }\mu\text{m}$ .<sup>[27]</sup> The internal surface area was calculated as  $374\text{ mm}^2$  by assuming a flat wall surface, which is explained in the Supporting Information (subsection S2.1). The calculated volume of the microreactor was  $8.67\text{ }\mu\text{L}$ . The atomic resolution structure of the dimeric sucrose phosphorylase from *Bifidobacterium adolescentis* was used to assess the footprint area of the adsorbed enzymes (Supporting Information, subsection S2.1). We estimated that approximately  $1.0\text{--}1.3\text{ }\mu\text{g}$  of protein could be bound maximally to the microchannel wall surface by monolayer adsorption (Table S1). With the known specific enzyme activity, a maximum volumetric rate in the range  $8\text{--}12\text{ mm min}^{-1}$  was calculated (Table S1). In the immobilization experiments described below, the amount of enzyme was offered in suitable excess ( $\sim 40\%$ ) over the esti-

mated monolayer adsorption in the case that all of the soluble target protein had been immobilized.

The parameters varied in the immobilization were flow conditions and time, and representative results are shown in Figure S4. The immobilization was evaluated based on the apparent enzyme activity bound to the plate ( $E_{app}$ ), determined from the  $\alpha$ Glc 1-*P* released at steady state under standard microreactor conditions (25 °C, pH 7.0, [substrate] = 50 mM substrate, flow rate  $F = 5 \mu\text{L min}^{-1}$ ). Notably,  $E_{app} = [\alpha\text{Glc 1-}P] \times F$ . As the substrate conversion was typically below 50% and diffusional limitations were also absent (see later),  $E_{app}$  was an appropriate value of the immobilized enzyme activity.

Static immobilization in which the plate was soaked with enzyme solution for a certain time (1–24 h) was superior to immobilization under flow in which the enzyme solution was recirculated over the microplate at a low  $F$  of  $1 \mu\text{L min}^{-1}$ . The monovalent enzyme showed weak immobilization under recirculation conditions (Figure S4). The immobilization was relatively slow, which suggests that specific interactions between the enzyme and the surface must be formed for tight binding. However, after approximately 2 h of static incubation, the immobilization appeared to be complete (Figure S4). Interestingly, the repeated immobilization under static conditions (three times), which offered  $\sim 1 \mu\text{g}$  of the target protein in each step with extensive washing of the plate between the steps, did not enhance the amount of immobilized enzymes. Based on these results (Figure S4), a comparison of the different  $Z_{\text{basic}2}$ -enzyme fusions (Scheme 1) was made after a static immobilization for 2 h. Significant differences were observed among the individual enzymes with regard to the  $E_{app}$  achieved (Figure 1).

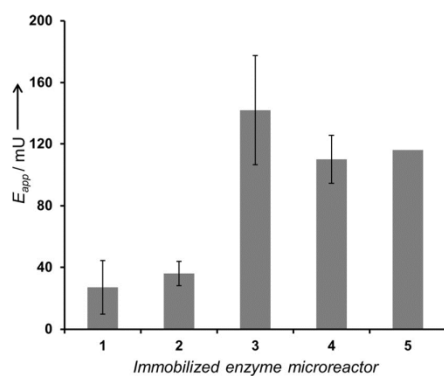


**Figure 1.** Comparison of sucrose phosphorylase constructs that harbor two  $Z_{\text{basic}2}$  modules to the monovalent  $Z_{\text{LmSPase}}$  reference in terms of  $E_{app}$ : 1,  $Z_{\text{LmSPase}}$ ; 2,  $Z\text{-}Z_{\text{LmSPase}}$ ; 3,  $Z_{\text{LmSPase}}\text{-}Z$ ; 4,  $Z_{\text{BiSPase}}$ ; and 5, purified  $Z_{\text{BiSPase}}$ . Error bars show standard deviations from four independent experiments.

The  $Z_{\text{LmSPase}}\text{-}Z$  and  $Z_{\text{BiSPase}}$  constructs reached a markedly high value of  $E_{app}$  which each exceeded the maximum level of the immobilized phosphorylase activity for an assumed protein monolayer adsorption on a flat microchannel surface (Table S1). The  $Z_{\text{LmSPase}}$  and  $Z\text{-}Z_{\text{LmSPase}}$  constructs fell

behind clearly (up to fivefold) in terms of  $E_{app}$ , the value of which was less than half of the calculated maximum (Table S1). A purified preparation of  $Z_{\text{BiSPase}}$  was also immobilized, which gave a value of  $E_{app}$  comparable to that obtained if the same enzyme was immobilized in an identical amount from the *E. coli* cell extract (Figure 1). This suggests that the immobilization of  $\text{BiSPase}$  was highly selective and not affected by impurities in the crude enzyme preparation.

We used a simple wash at a high ionic strength (4.75 M NaCl in 50 mM potassium phosphate buffer, pH 7.0; 0.5% Tween 20 added) to elute the immobilized phosphorylase constructs completely, and the microplate thus regenerated could be applied to a new immobilization without a loss of adsorption efficiency.

### Multivalency effects on the catalytic effectiveness of the immobilized enzymes

If we compare different phosphorylase constructs, differences in  $E_{app}$  could arise because of differences in the protein amount and/or the intrinsic activity of the enzymes immobilized. To determine effects in  $E_{app}$  caused by a change in the intrinsic activity of the immobilized relative to the free enzyme, we recovered the immobilized phosphorylases under elution conditions known to fully maintain their activity, measured the activity in the eluate ( $E_{\text{eluate}}$ ) and compared it to the  $E_{app}$  determined just before for the immobilized preparation. The ratio  $E_{app}/E_{\text{eluate}}$  is the effectiveness factor ( $\eta$ ) of the immobilized enzyme. Notably, the more common and simpler procedure to determine  $\eta$  by comparing the specific activities of immobilized and free enzyme was not applicable here as the amount of the protein attached to the microstructured plate was too small to be quantified by the assays used. The immobilized phosphorylases that contained two  $Z_{\text{basic}2}$  modules exhibited the same or greater  $\eta$  ( $0.67 \pm 0.05$ ;  $N=4$ ) within limits of the experimental error. The generally high value of  $\eta$  supports the notion that oriented immobilization on silica through the two  $Z_{\text{basic}2}$  modules succeeded in maintaining, to a large extent, the original phosphorylase activity in the immobilized preparations of these chimeric proteins. Additionally, the results show that the decreased  $E_{app}$  of  $Z\text{-}Z_{\text{LmSPase}}$  compared to  $Z_{\text{LmSPase}}\text{-}Z$  and  $Z_{\text{BiSPase}}$  was not because of an enzyme-construct-specific effect of the immobilization on the intrinsic activity. The binding of  $Z\text{-}Z_{\text{LmSPase}}$  apparently in a lower amount than that in the other two constructs was not pursued because the fine-tuned optimization of the immobilization conditions for each enzyme was not an immediate goal of this study. We also determined the  $\eta$  of each phosphorylase after different times of microreactor operation and found it to be constant.

The monovalent  $Z_{\text{LmSPase}}$  behaved differently to the other constructs in that its  $\eta$  varied in the range of 0.30–0.65. This might be the consequence of a heterogeneous population of immobilized enzymes, probably caused by different modes of  $Z_{\text{LmSPase}}$  binding to the silica surface.

The combined evidence from determination of  $E_{app}$  (Figure 1) and  $\eta$  shows that the multivalency derived from two  $Z_{\text{basic}2}$  modules instead of just one was highly beneficial for the

immobilization of sucrose phosphorylase in silica microchannels. Not only the quantity but also the catalytic “quality” of the immobilized enzyme could be enhanced in that way. The dimeric *Z\_BiSPase* had a natural advantage over the monomeric *LmSPase* in that  $Z_{\text{basic}2}$  multivalency was intrinsic to its protein structure. However, we show that the creation of functional multivalency from  $Z_{\text{basic}2}$  modules was also possible in the monomeric enzyme in which both *Z-Z\_LmSPase* and *Z\_LmSPase\_Z* constructs exhibited clearly elevated  $\eta$  compared to the monovalent *Z\_LmSPase* reference.

#### Multivalency effects on adsorption stability under continuous flow

To examine whether the multivalency in the enzyme–surface interaction derived from two  $Z_{\text{basic}2}$  modules would also boost the adsorption stability of the immobilized phosphorylases under conditions of fluid flow, we performed time-course experiments with each enzyme construct (Figure 2). To measure

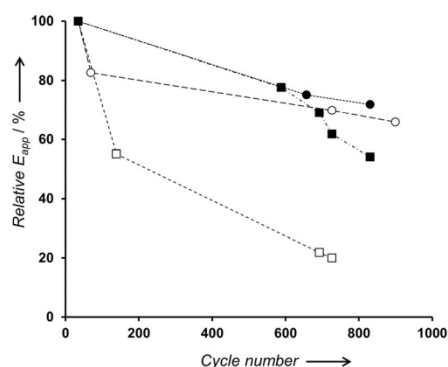


**Figure 2.** Dependence of  $E_{\text{app}}$  (normalized on the initial value) on the time of reactor operation, expressed as the number of operational cycles, is shown for the different enzyme constructs used. The symbols show *Z\_LmSPase* (□), *Z-Z\_LmSPase* (●), *Z\_LmSPase\_Z* (○) and *Z\_BiSPase* (■). The conditions used were:  $F = 5 \mu\text{L min}^{-1}$ , equivalent to  $\tau_{\text{res}} = 1.73 \text{ min}$ ; 50 mM of each sucrose and potassium phosphate; 25 °C, pH 7.0. The number of cycles is calculated dividing the actual time of operation by  $\tau_{\text{res}}$ .

the  $\alpha\text{Glc 1-P}$  concentration at steady state with respect to the time of reactor operation, the course of  $E_{\text{app}}$  was determined for each phosphorylase. Time was normalized to the average residence time used ( $\tau_{\text{res}} = \text{microreactor volume}/F$ ) to give a number of reactor operational cycles. The benefit of the presence of two  $Z_{\text{basic}2}$  modules instead of one in the enzyme is plainly evident from the results presented in Figure 2. The relative  $E_{\text{app}}$  of *Z\_LmSPase* decreased rapidly so that virtually 80% activity was lost after around 730 cycles. An operational half-life of around 200 cycles was calculated for *Z\_LmSPase* from the data. The loss in  $E_{\text{app}}$  was only apparent in that it reflected exclusively the washing out but it was not a real inactivation of the enzyme. *Z\_LmSPase* was completely stable in the time span of the experiment under the conditions used. The divalent phosphorylase constructs exhibited strongly improved

operational stability compared to *Z\_LmSPase*, which retained approximately 70% of the initial  $E_{\text{app}}$  even after 690 reactor cycles.

#### Visualization of enzymes immobilized on microchannel walls

*Z\_BiSPase* was immobilized on the microchannel plate, and the bound enzyme was labeled with fluorescein isothiocyanate (FITC). The protein wall coating was then visualized by using confocal laser scanning microscopy (CLSM). The images presented in Figure 3 A and C suggest a quite uniform distribution

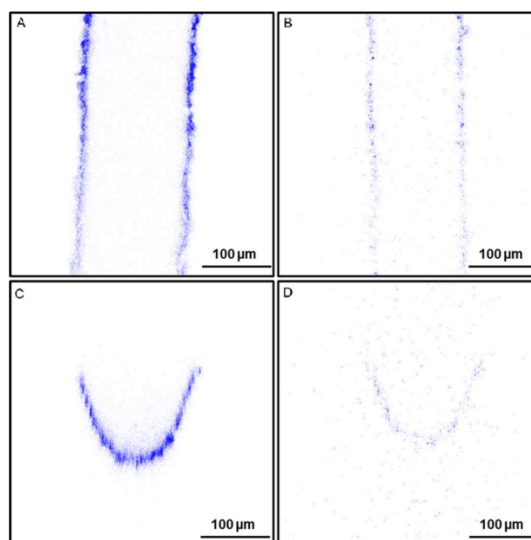


**Figure 3.** CLSM images recorded from the microstructured plate having *Z\_BiSPase* immobilized on the microchannel walls and subsequently labeled with FITC. Images from the horizontal section (A, B) and the cross-section (C, D) of the microchannel are shown. Images were recorded immediately after immobilization and labeling (A, C). The immobilized enzyme microreactor was continuously operated, and after approximately 1600 reactor cycles, when the relative  $E_{\text{app}}$  was already low ( $\leq 0.10$ ), the enzyme was labeled with FITC (B, D). Notably, because images analysis was done only qualitatively, possible effects from fluorescence saturation are not relevant.

of the enzyme on the channel walls. This was as expected from, and thus also provides support for, the proposed specific and oriented molecular interaction of the positively charged  $Z_{\text{basic}2}$  module with the negatively charged surfaces of the glass microchannel. To examine the decrease in the  $E_{\text{app}}$  of *Z\_BiSPase* (Figure 2) if the underlying cause is protein elution or enzyme inactivation, we subjected the immobilized enzyme to fluid flow, exactly as described in Figure 2. After approximately 1600 reactor cycles, if the relative  $E_{\text{app}}$  was already low ( $\leq 0.10$ ), the remaining enzyme was labeled with FITC and images were recorded (Figure 3 B and D). These images show a very low fluorescence intensity, which suggests that protein elution is still mainly responsible for the slow but gradual decrease in the  $E_{\text{app}}$  of the multivalent dimeric phosphorylase.

### Microreactor performance study and reaction–diffusion regime analysis

After we had shown that the divalent phosphorylases are promising catalysts to be used in an immobilized enzyme microreactor, the question about the actual performance characteristics of such a reactor in the synthesis of  $\alpha$ Glc 1-*P* arose. Therefore, we used *Z. B/SPase* as an example to analyze the dependence of  $[\alpha$ Glc 1-*P*] released at steady state on the  $\tau_{res}$  used.

The  $\tau_{res}$  was varied by ramping the *F* up and down in the range of 1–50  $\mu\text{L min}^{-1}$ , and the results are shown in Figure 4A. For conditions in which residual substrate (initial concentration: 50 mM) was still available at steady state, the relationship between  $[\alpha$ Glc 1-*P*] and  $\tau_{res}$  was linear, as expected for this type of reactor if the overall reaction rate is limited solely by the enzyme activity. At the highest  $\tau_{res}$  of 8.67 min used, substrate conversion was complete, and a productivity of 5.8  $\text{mM min}^{-1}$  was reached under these conditions. If we take 50% conversion as the target value, the productivity was more than doubled to 14  $\text{mM min}^{-1}$ . Notably, these are significant

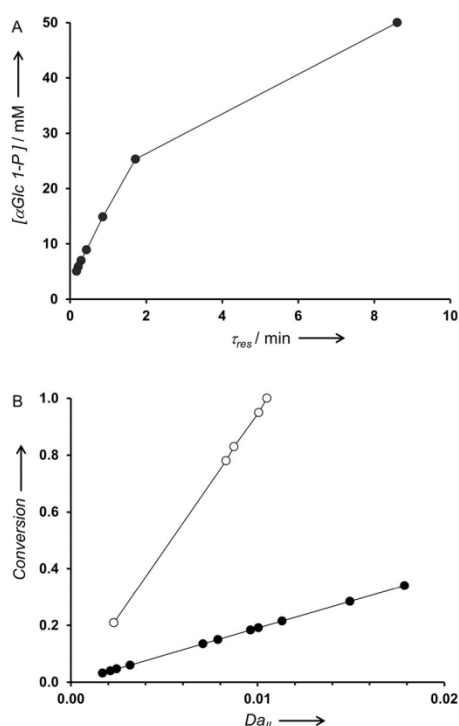


**Figure 4.** A) Performance characterization and B) reaction–diffusion regime analysis for the microreactor that contained immobilized *Z. B/SPase* are shown. In panel A, the results are from ramping up the *F* value from 1 to 50  $\mu\text{L min}^{-1}$  (●). In panel B, the conversion is  $[\alpha$ Glc 1-*P*] released divided by the initial [sucrose], which was 50 mM. Results are shown for *F* values of 1 (○) and 5  $\mu\text{L min}^{-1}$  (●) and an overall operation time of 48 h. The low value of  $Da_{II}$  indicates limitation of the overall conversion by the biocatalytic reaction.

productivities for an enzyme reactor. During flow rate excursion up and down, exactly the same steady-state concentrations of  $\alpha$ Glc 1-*P* were reached again on returning to the original *F* value, which thus provides a clear indication of a stably immobilized enzyme.

We applied reaction engineering analysis to the microreactor used to determine the dimensionless Reynolds number (*Re*).<sup>[32,33]</sup> This value varied between 0.26 and 12.81 dependent on *F*, which suggests the fully developed laminar conditions for the fluid flow (Figure S5 and Table S2). The Peclet number<sup>[32,33]</sup> and its dependence on *F* (Figure S6) indicates that the axial dispersion is controlled by convection. Reaction–diffusion regime analysis was performed in terms of the determination of the second Damköhler number ( $Da_{II}$ ),<sup>[32,33]</sup> which is defined as the ratio of characteristic time of diffusion ( $\tau_{diff}$ ) per characteristic time of reaction ( $\tau_{reac}$ ). The determination of  $\tau_{reac}$  and  $\tau_{diff}$  from the data presented here is shown in Table S3. Correlations between  $Da_{II}$  and the substrate conversion are shown for two representative values of *F* in Figure 4B. The results indicate that  $Da_{II}$  remained extremely low for the complete range of conversion up to a value of 1.0. In other words, the overall conversion was limited entirely by the enzyme-catalyzed reaction and the effect of diffusion was negligible. Under the conditions used, an *F* value of 5  $\mu\text{L min}^{-1}$  was already too high to attain full substrate conversion.

### Conclusions

This study reveals, and shows the practical use of, multivalency effects from two  $Z_{basic2}$  modules on enzyme immobilization in a glass microchannel flow reactor. The example of sucrose phosphorylase demonstrates the exploitation of the suggested general principle of protein design for effective immobilization for biocatalytic microreactor development. Compared to monovalent binding, the multivalent binding from two  $Z_{basic2}$  modules enhanced the binding affinity and stimulated the intrinsic activity of the immobilized phosphorylase. In particular, it boosted the operational stability of the biocatalytic microreactor significantly by reducing the wash-out of the reversibly immobilized enzyme activity under conditions of continuous operation. The microreactor showed excellent performance metrics with regard to the productivity as well as the utilization of the available enzyme activity in the absence of mass transfer limitations. The use of wall-coated enzyme microreactors in high-performance biocatalytic reaction engineering is, therefore, supported strongly. Glass microstructures that feature an enhanced internal surface area<sup>[25,34]</sup> might be even used to further increase the productivity. This could be relevant if enzymes of low specific activity are used.

### Experimental Section

#### Chemicals and materials

The glass microreactor (product code: FC\_R150.676.2\_PACK) and the Fluidic Connect PRO Chip Holder (product code: FC\_PRO\_CH4515) were from Micronit Microfluidics (Enschede, Netherlands).

Teflon tubing (250  $\mu\text{m}$  diameter) and connection parts were also from Micronit Microfluidics. Liquid flow was delivered by using a New Era NE-1000 syringe pump (Next Advance, Averill Park, NY) or a Smartline 1000 double-piston pump (Knauer, Berlin, GE). Chemicals and oligonucleotide primers were from Sigma-Aldrich (Vienna, Austria). DNA sequencing was performed at LGC Genomics (Berlin, Germany). Other reagents were of analytical grade and obtained as elsewhere reported.

### Enzymes

Cloning work, protein expression and purification, enzyme assays used and standard methods are described in the Supporting Information.

### Enzyme immobilization and operation of the microreactor under continuous flow

Enzyme immobilization utilized procedures described in earlier work.<sup>[27,29]</sup> Briefly, the plate was filled with an immobilization mix comprised of 0.5% Tween 20, the enzyme (loading more than the estimated binding capacity of the plain glass surface), and 0.25 M NaCl in potassium phosphate buffer (pH 8.0). Incubation was at 25 °C for 1–24 h, typically in the absence of liquid flow or agitation. Afterwards, the microreactor was washed with potassium phosphate buffer at 5  $\mu\text{L min}^{-1}$  flow rate (25 °C, pH 7.0). The enzyme immobilization (Figure S4) was evaluated from continuous microreactor experiments. To calculate  $E_{\text{ppp}}$ , the produced  $\alpha\text{Glc 1-P}$  was measured at different  $\tau_{\text{res}}$ . The reaction mixture that contained sucrose and potassium phosphate (50 mM each, 25 °C, pH 7.0) was flowed through the microreactor. The concentration of  $\alpha\text{Glc 1-P}$  in the outlet was measured by assays described in the Supporting Information.

### Confocal laser scanning microscopy

The labeling of surface immobilized enzyme with FITC was performed according to literature.<sup>[35]</sup> Briefly, 1  $\text{mg mL}^{-1}$  of FITC solution in DMSO was flowed through the microreactor that contained immobilized enzyme and incubated for 1 h in 25 °C followed by rinsing with 50 mM potassium phosphate (25 °C, pH 7.0). Images A and C in Figure 3 were recorded. A Leica TCS SPE confocal microscope (Mannheim, GE) was used for analysis. Confocal fluorescence images (excitation wavelength: 488 nm; emission wavelength: 500–600 nm) were recorded by using a Leica 20 $\times$ /0.5 water immersion objective. In another experiment, the immobilized enzyme microreactor was operated with substrates (50 mM each) at a flow rate of 5  $\mu\text{L min}^{-1}$  (25 °C, pH 7.0), and after approximately 1600 reactor cycles the remaining enzyme was labeled with FITC by the same procedure, and images B and D presented in Figure 3 were recorded.

### Acknowledgements

Financial support by Marie Curie ITN project EUROMBR (Grant Agreement Number 608104) is gratefully acknowledged. Dr. Zdenek Petrasek (Institute of Biotechnology and Biochemical Engineering) assisted with the CLSM experiments.

**Keywords:** biocatalysis · biotransformations · enzymes · immobilization · microreactors

- [1] A. Adamo, R. L. Beingsner, M. Behnam, J. Chen, T. F. Jamison, K. F. Jensen, J.-C. M. Monbaliu, A. S. Myerson, E. M. Revalor, D. R. Snead, T. Stelzer, N. Weeranoppanant, S. Y. Wong, P. Zhang, *Science* **2016**, *352*, 61–67.
- [2] H. P. L. Gemoets, Y. Su, M. Shang, V. Hessel, R. Luque, T. Noël, *Chem. Soc. Rev.* **2016**, *45*, 83–117.
- [3] B. Gutmann, D. Cantillo, C. O. Kappe, *Angew. Chem. Int. Ed.* **2015**, *54*, 6688–6728; *Angew. Chem.* **2015**, *127*, 6788–6832.
- [4] R. Ricciardi, J. Huskens, M. Holtkamp, U. Karst, W. Verboom, *ChemCatChem* **2015**, *7*, 936–942.
- [5] R. Munirathinam, J. Huskens, W. Verboom, *Adv. Synth. Catal.* **2015**, *357*, 1093–1123.
- [6] A. Günther, K. F. Jensen, *Lab Chip* **2006**, *6*, 1487–1503.
- [7] R. L. Hartman, K. F. Jensen, *Lab Chip* **2009**, *9*, 2495–2507.
- [8] B. Tomaszewski, R. C. Lloyd, A. J. Warr, K. Buehler, A. Schmid, *ChemCatChem* **2014**, *6*, 2567–2576.
- [9] R. Wohlgenuth, I. Plazl, P. Žnidaršič-Plazl, K. V. Gernaey, J. M. Woodley, *Trends Biotechnol.* **2015**, *33*, 302–314.
- [10] U. Novak, M. Lakner, I. Plazl, P. Žnidaršič-Plazl, *Microfluid. Nanofluid.* **2015**, *19*, 75–83.
- [11] J. M. Bolivar, J. Wiesbauer, B. Nidetzky, *Trends Biotechnol.* **2011**, *29*, 333–342.
- [12] S. Illner, C. Hofmann, P. Löb, U. Kragl, *ChemCatChem* **2014**, *6*, 1748–1754.
- [13] C. Garcia-Galan, A. Berenguer-Murcia, R. Fernandez-Lafuente, R. C. Rodrigues, *Adv. Synth. Catal.* **2011**, *353*, 2885–2904.
- [14] J. C. S. dos Santos, O. Barbosa, C. Ortiz, A. Berenguer-Murcia, R. C. Rodrigues, R. Fernandez-Lafuente, *ChemCatChem* **2015**, *7*, 2413–2432.
- [15] O. Barbosa, C. Ortiz, A. Berenguer-Murcia, R. Torres, R. C. Rodrigues, R. Fernandez-Lafuente, *Biotechnol. Adv.* **2015**, *33*, 435–456.
- [16] J. Rocha-Martin, A. Acosta, J. M. Guisan, F. López-Gallego, *ChemCatChem* **2015**, *7*, 1939–1947.
- [17] H. R. Luckarift, B. S. Ku, J. S. Dordick, J. C. Spain, *Biotechnol. Bioeng.* **2007**, *98*, 701–705.
- [18] H. Yamaguchi, T. Honda, M. Miyazaki, *J. Flow Chem.* **2016**, *6*, 13–17.
- [19] M. S. Thomsen, B. Nidetzky, *Biotechnol. J.* **2009**, *4*, 98–107.
- [20] S. Matosevic, G. J. Lye, F. Baganz, *Biotechnol. Prog.* **2010**, *26*, 118–126.
- [21] A. Schwarz, M. S. Thomsen, B. Nidetzky, *Biotechnol. Bioeng.* **2009**, *103*, 865–872.
- [22] A. A. Halim, N. Szita, F. Baganz, *J. Biotechnol.* **2013**, *168*, 567–575.
- [23] M. S. Thomsen, P. Pölt, B. Nidetzky, *Chem. Commun.* **2007**, 2527–2529.
- [24] M. S. Thomsen, B. Nidetzky, *Eng. Life Sci.* **2008**, *8*, 40–48.
- [25] J. M. Bolivar, B. Nidetzky, *Chim. Oggi* **2013**, *31*, 50–54.
- [26] J. M. Bolivar, C. E. M. Krämer, B. Ungerböck, T. Mayr, B. Nidetzky, *Biotechnol. Bioeng.* **2016**, *113*, 1862–1872.
- [27] J. M. Bolivar, M. A. Tribulato, Z. Petrasek, B. Nidetzky, *Biotechnol. Bioeng.* **2016**, *113*, 2342–2349.
- [28] J. Wiesbauer, J. M. Bolivar, M. Mueller, M. Schiller, B. Nidetzky, *ChemCatChem* **2011**, *3*, 1299–1303.
- [29] J. M. Bolivar, B. Nidetzky, *Langmuir* **2012**, *28*, 10040–10049.
- [30] J. M. Bolivar, S. Schelch, T. Mayr, B. Nidetzky, *ACS Catal.* **2015**, *5*, 5984–5993.
- [31] C. Goedel, A. Schwarz, A. Minani, B. Nidetzky, *J. Biotechnol.* **2007**, *129*, 77–86.
- [32] M. P. C. Marques, P. Fernandes, *Molecules* **2011**, *16*, 8368–8401.
- [33] T. Van Daele, D. F. del Pozo, D. Van Hauwermeiren, K. V. Gernaey, R. Wohlgenuth, I. Nopens, *Chem. Eng. J.* **2016**, *300*, 193–208.
- [34] K. F. Schilke, K. L. Wilson, T. Cantrell, G. Corti, D. N. McIlroy, C. Kelly, *Biotechnol. Prog.* **2010**, *26*, 1597–1605.
- [35] X. Wu, C. Yang, J. Ge, Z. Liu, *Nanoscale* **2015**, *7*, 18883–18886.

Received: August 17, 2016  
Published online on November 10, 2016



## Supporting Information

### **Multivalency Effects on the Immobilization of Sucrose Phosphorylase in Flow Microchannels and Their Use in the Development of a High-Performance Biocatalytic Microreactor**

Donya Valikhani,<sup>[a]</sup> Juan M. Bolivar,<sup>[a]</sup> Martin Pfeiffer,<sup>[a]</sup> and Bernd Nidetzky<sup>\*,[a, b]</sup>

cctc\_201601019\_sm\_miscellaneous\_information.pdf

## S1. Cloning of the chimeric enzymes, their expression and purification, and enzyme assays

### S1.1. Enzyme cloning

Using the monomeric sucrose phosphorylase from *Leuconostoc mesenteroides* (*LmSPase*) as the "monovalent reference", two approaches of inducing  $Z_{\text{basic2}}$  multivalency were pursued. One was to append  $Z_{\text{basic2}}$  to the N-terminus of the homodimeric sucrose phosphorylase from *Bifidobacterium longum* (*BSPase*). Another was to incorporate two  $Z_{\text{basic2}}$  modules in tandem repeat at the N-terminus of the *LmSPase*. Effect of having two  $Z_{\text{basic2}}$  modules separated from each other in the *LmSPase* structure was examined with a fusion protein containing  $Z_{\text{basic2}}$  both at the N- and the C-terminus.

For preparing *Z\_BSPase*, the *SPase* gene was amplified from pUC57-*BSPase* by PCR using Phusion DNA polymerase (Thermo Scientific, Waltham, USA) and the following pair of oligonucleotide primers: 5'-CGCTCTATATCTTTGATGGATCCAAAAACAAAG-3' and 5'-cagccaactcagctcAAGCTTTTAGTCGATA-3'. The resulting PCR product comprised 5'- and 3'-overhangs (shown in lower case letters) complementary to the target sequence of the pT7ZbHAD4 destination vector.<sup>[1]</sup> Vector pT7ZbHAD4 was amplified by PCR using Phusion DNA polymerase and the following pair of oligonucleotide primers: 5'-TATCGACTAAAAGCTTgaagctgagtggtg-3' and 5'-CTTTGTTTTGGATCCATCAAAGATA TAGAGCG-3'. The resulting construct encodes a fusion protein where the small module  $Z_{\text{basic2}}$  is joined by a flexible linker (11 amino acids) to the N-terminus of *BSPase*. Sequenced plasmid vector encoding the *Z\_BSPase* fusion protein was transformed into electrocompetent cells of *E. coli* BL21-Gold (DE3), and single-colony transformants were selected on agar plates containing 50  $\mu\text{g mL}^{-1}$  kanamycin.<sup>[2,3]</sup>

*Z\_LmSPase* was produced in *E. coli* by subcloning in plasmid vector pT7ZbQGKlenow (including the 3C protease cleavage site) to achieve fusion of  $Z_{\text{basic2}}$  at the N-terminus.<sup>[4-7]</sup>

The *Z\_LmSPase\_Z* expression vector was created by insertion of a second copy of the  $Z_{\text{basic2}}$  module preceded by an 24 amino acid linker to the C-terminal end of the coding sequence of *Z\_LmSPase* encoded by pT7ZLmSPase. The  $Z_{\text{basic2}}$  sequence was amplified using following set of primers: 5'-GATCCGTAGACAACAAATTCAACAAAG-3'; 5'-CAATAACTCGAGTTTCGGCGCCTGAG-3' and fused to the linker sequence by PCR using following set of primers: 5'-GTTATTAAGCTTCCAGATATGTTGTCTATATCTCGCGTC AGGTCCTGTCTCGAATTGAATCCGATGGGTCGCGGATCCGTAGACAACAAATTC-3', 5'-CAATAACTCGAGTTTCGGCGCCTGAG-3'. XhoI and HindIII restriction sites were introduced into the vector backbone using the following set of primers: 5'-

## Multivalency Effects on the Immobilization of Sucrose Phosphorylase in Flow Microchannels and Their Use in the Development of a High-Performance Biocatalytic Microreactor

GTTATTCTCGAGCACCACCACC-3' and 5'- CAATAAAAGCTTGTCTGAGTCAAATTATC-3'. PCR products were digested with XhoI and HindIII, ligated with T4-ligase and transformed into *E. coli* XL-1 Blue. Transformants were selected on LB-agar plates containing 50  $\mu\text{g mL}^{-1}$  kanamycin. Isolated vector was sequenced and transformed into the *E. coli* BL21 DE3 expression strain. Please note that as consequence of the subcloning procedure, a hexahistidine tag is found at the N-terminus  $Z_{\text{basic2}}$  module. Due to the deletion of the natural stop codon in the gene, the translation continued into the hexahistidine tag present in the vector coding the  $Z_{\text{basic2}}$ . Nevertheless, based on our earlier experiments,<sup>[4]</sup> His\_ *LmSPase* binds only very weakly to negatively activated surfaces so that the presence of the his-tag is unlikely to have affected the immobilization of the *Z\_ LmSPase\_ Z* construct. *Z-Z\_ LmSPase* was created by insertion of a second copy of the  $Z_{\text{basic2}}$  module into the pT7*ZLmSPase* vector. Therefore the  $Z_{\text{basic2}}$  sequence was amplified using the following set of primers: 5'-ATTATTATTATTGGATCCGTAGACAACAAATTC-3'; 5'-TTTATTATAGAGCTCATTCGGACCCTGGAA-3. SacI and EcoRI restriction sites were introduced into the vector backbone using following set of primers: 5'-AGGTTATTAGAGCTCGTAGACAACAAATTCAACAAAG-3' and 5'-TTATTTATTGGATCCGCGACCCATTTGCTG-3'. PCR products were digested with SacI and EcoRI, ligated with T4-ligase and transformed into *E. coli* XL-1 Blue. Transformants were selected on LB-agar plates containing 50  $\mu\text{g mL}^{-1}$  of kanamycin. The isolated vector was sequenced and transformed into the *E. coli* BL21 DE3 expression strain.

# Multivalency Effects on the Immobilization of Sucrose Phosphorylase in Flow Microchannels and Their Use in the Development of a High-Performance Biocatalytic Microreactor

## S1.2. Schematic representation of the created Z\_SPase fusion proteins

All created fusion proteins contain at least one Z<sub>basic2</sub> module connected to the SPase via a short linker are shown in Figure S1.

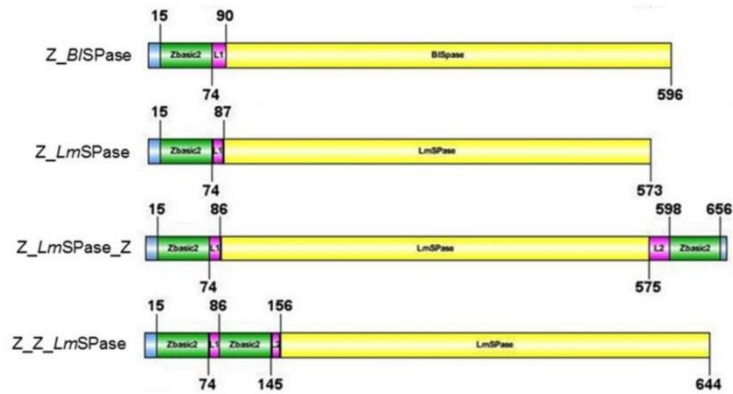


**Figure S1.** Module organisation of the enzyme constructs used.

# Multivalency Effects on the Immobilization of Sucrose Phosphorylase in Flow Microchannels and Their Use in the Development of a High-Performance Biocatalytic Microreactor

## S1.3. Amino acids sequences of the Z\_SPase constructs

The amino acids sequences of Z\_SPases defined by colors are shown below. The Z<sub>basic2</sub> module is always shown in green color. The linkers used to fuse the Z<sub>basic2</sub> module to the N-terminus of the enzyme are shown in purple color. The linker used to fuse the Z<sub>basic2</sub> module to the C-terminus of the enzyme is shown in blue. The enzymes are shown in orange (B/SPase) or red (LmSPase) color.

### Z\_B/SPase

```
MASMTGGQQMGRGSVDNKFNKERRRRARREIRHLPNLNREQRRAFIRSLRDDPSQSANLLAEAKKLND  
QAPKPNLEALFQGPPLYIFDGSKNKVQLITYADRLGDGTLSSMADILRTRFDGVYDGVHILPFFTFPDG  
ADAGFDPIDHTKVDERLGSWDDVAELSKTHNIMVDIVNHMSWESKQFQDVLEKGESEYYPMFLTMS  
SVFPNGATEEDLAGIYRPRPGLPFFTHYKFAGKTRLVWVSFTPQQVDIDTSDDKGWEYLMSIFDQMAAS  
HVSYIRLDAVGYGAKEAGTSCFMTPKTFKLI SRLREEGVKRGLEILIEVHSYKKQVEIASKVDRVYD  
FALPPLLLHSLFTGHVEPVAHWTEIRPNNAVTVLTDTHDGI GVIDIGSDQLDRSLKGLVPDEDVDNLVN  
TIHANTHGESQAATGAAASNLDLYQVNSTYYSALGCNDQHYLAARAVQFFLPQVPPVYVYGALAGRND  
MELLRRTNNGRDINRHYYSTAEIDENLERPVVKALNALAKFRNELPAFDGEFSEYVDGDTSI TFRWTA  
ADGTSTAALTFEPGRGLGTDNATPVASLAWSDAAGDHETRDLLANPPIADID
```

### Z\_LmSPase

```
MASMTGGQQMGRGSVDNKFNKERRRRARREIRHLPNLNREQRRAFIRSLRDDPSQSANLLAEAKKLND  
QAPKPNLEALFQGPNSEIQNKAMLIYADSLGKNLKDQVHLKEDIGDAIGGVHLLPFFPSTGDRGFA  
PADYTRVDAAFGDWADVEALGEEYYLMFDFMINHISRESVMYQDFKKNHDDSKYKDFFI RWEKFWAKA  
GENRPTQADVLIYKRKDKAPTQEITFDGDTTENLWNTFGEEQIDIDVNSAIAKEFIKTLEDVMKKG  
ANLIRLDAFAYAVKKVDTNDFVPEIWDTLNEVREILTPLKAEILPEIHEHYSIPKKINDHGYFTYD  
FALPMTTLYTLYSGKTNQLAKWLKMSPMKQFTTLDTHDGI GVV DARDILT DDEIDYASEQLYKVGANV  
KKTYSASYNLDIYQINSTYYSALGNDDAAYLLSRVFQVFAPGIPQIYYVGLLAGENDIALLESTKE  
GRNINRHYYT TREEVKSEVKRPVVANLLKLSWRNESPAFDLAGSITVDTPD TTIIVVTRQDENGQNK  
VLTADAANKTFEIVENGQTMSSDNL TQN
```

### Z\_LmSPase\_Z

```
MASMTGGQQMGRGSVDNKFNKERRRRARREIRHLPNLNREQRRAFIRSLRDDPSQSANLLAEAKKLND  
QAPKPNLEALFQGPNSEIQNKAMLIYADSLGKNLKDQVHLKEDIGDAIGGVHLLPFFPSTGDRGFA  
PADYTRVDAAFGDWADVEALGEEYYLMFDFMINHISRESVMYQDFKKNHDDSKYKDFFI RWEKFWAKA  
GENRPTQADVLIYKRKDKAPTQEITFDGDTTENLWNTFGEEQIDIDVNSAIAKEFIKTLEDVMKKG  
ANLIRLDAFAYAVKKVDTNDFVPEIWDTLNEVREILTPLKAEILPEIHEHYSIPKKINDHGYFTYD  
FALPMTTLYTLYSGKTNQLAKWLKMSPMKQFTTLDTHDGI GVV DARDILT DDEIDYASEQLYKVGANV  
KKTYSASYNLDIYQINSTYYSALGNDDAAYLLSRVFQVFAPGIPQIYYVGLLAGENDIALLESTKE  
GRNINRHYYT TREEVKSEVKRPVVANLLKLSWRNESPAFDLAGSITVDTPD TTIIVVTRQDENGQNK  
VLTADAANKTFEIVENGQTMSSDNL TQNKL PDMLSISRVRSCLELNP MGRGSVDNKFNKERRRRARRE  
IRHLPNLNREQRRAFIRSLRDDPSQSANLLAEAKKLNDQAPKLEHHHHHH
```

# Multivalency Effects on the Immobilization of Sucrose Phosphorylase in Flow Microchannels and Their Use in the Development of a High-Performance Biocatalytic Microreactor

## Z-Z\_LmSPase

MASMTGGQQMGRGSDVDNKFNKERRRRARREIRHLPNLNREQRRAFIRSLRDDPSQSANLLAEAKKLND  
QAPKPNLEALFQGPNELVDNKFNKERRRRARREIRHLPNLNREQRRAFIRSLRDDPSQSANLLAEAKKL  
NDAQAPKPNLEALFQGPNSEIQNKAMLI TYADSLGKNLKDVBHQVLKEDIGDAIGGVHLLPFFPSTGDR  
GFAPADYTRVDAAFGDWADVEALGEEYYLMFDFMINHISRESVYQDFKKNHDDSKYKDFRWEKFW  
AKAGENRPTQADVLDIYKRKDKAPTQEIFDGDGTENLWNTFGEEQIDIDVNSAIAKEFIKTTLEDMV  
KHGANLIRLDAFAYAVKKVDTNDFVPEIWDTLNEVREILTPLKAEILPEIHEHYSIPKINDHGYF  
TYDFALPMTTLYTLYSGKTNQLAKWLKMSPMKQFTTLDTHDGIGVVDARDILTDDEIDYASEQLYKVG  
ANVKKTYSSASYNNDIYQINSTYYALGNDDAAYLLSRVQVFAPGIPQIYYVGLLAGENDIALLES  
TKEGRNINRHYYTREEVKSEVKRPVVANLLKLLSWRNESPAFDLAGSITVDTPTDTTIVVTRQDENGQ  
NKAVLTADAANKTFEIVENGQTMSSDNLTON

## S1.4. Enzyme expression

Enzyme expression was done recombinantly in *E. coli* as described in earlier work.<sup>[4,8]</sup> *E. coli* cell extract containing the relevant enzyme was obtained by disrupting the cells, suspended in a 2-fold volume of 50 mM potassium phosphate buffer (pH 7.0), in a French press at 150 bar. After centrifugation (13200 rpm, 15 min, 4 °C), the clear supernatant was used further. Protein was determined with the Bio-Rad Protein Assay referenced against BSA.

## S1.5. Enzyme purification

Protein was purified at 25 °C using pre-packed (1.6 cm × 2.5 cm; 5 mL) HiTrap SP FF columns (GE Healthcare Life Sciences) fitted on a ÄKTA prime plus system. The column was equilibrated with buffer A (50 mM potassium phosphate buffer, pH 7.0) and 8 mL of the cell extract were loaded onto the column. Protein elution was performed using a continuous salt gradient from 0 to 100% of buffer B (50 mM potassium phosphate buffer containing 2 M NaCl, pH 7.0) in 75 mL at a flow rate of 3 mL min<sup>-1</sup>. The target protein (all constructs) eluted at around 40-50% buffer B. Pooled fractions were collected and buffer was exchanged to buffer A. Protein purification was monitored by SDS-PAGE, as shown in Figure S2.

## Multivalency Effects on the Immobilization of Sucrose Phosphorylase in Flow Microchannels and Their Use in the Development of a High-Performance Biocatalytic Microreactor

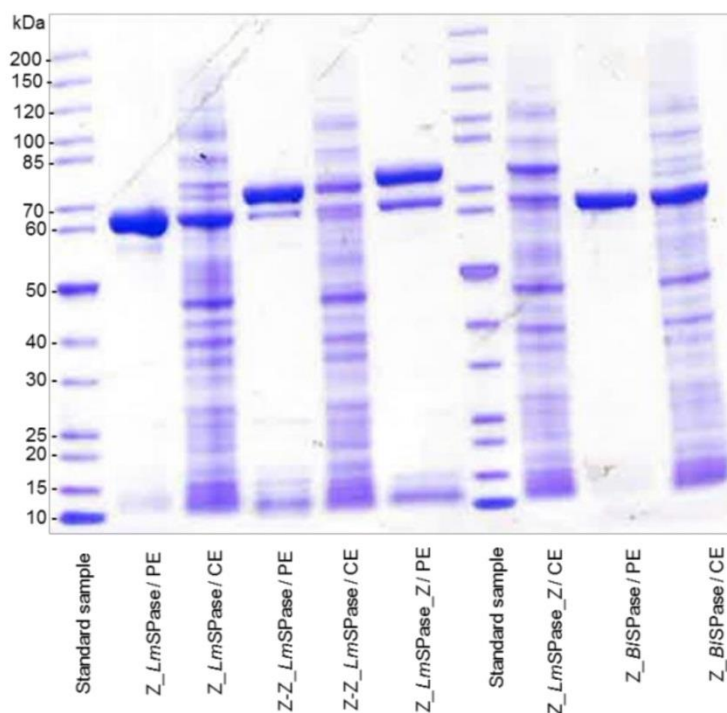


**Figure S2.** Purification of Z\_SPase constructs analyzed by SDS PAGE, comparing the purified enzyme (PE) and the corresponding cell extract (CE). Thermo Scientific PageRuler™ Unstained Protein Ladder was used as the size standard. The purified samples of *LmSPase* migrated as one major protein band of the expected mass plus an additional band of smaller size. The slight heterogeneity of the preparations is explainable by a small amount of degradation whereby one  $Z_{\text{basic}2}$  module was likely cleaved off from the doubly tagged fusion protein. Note, however, that because all immobilizations were performed by offering the enzyme in suitable excess (~40%) over the estimated maximum binding capacity of the plain glass surface available on the microplate, the relatively small extent of protein cleavage could not have affected the results of the binding study.

### S1.6. Enzyme assay

Phosphorylase activity was measured in an assay performed at 30 °C and pH 7.0. A previously reported continuous coupled enzyme assay was used.<sup>[4,8]</sup> The reaction mixture contained 250 mM sucrose and 50 mM potassium phosphate. The  $\alpha\text{Glc 1-P}$  released by the action of the phosphorylase was determined in the presence of phosphoglucomutase (PGM) and glucose 6-phosphate dehydrogenase (G6P-DH) as the formation of NADH (measured at 340 nm). Note: one unit (U) of enzyme activity is defined as the amount of enzyme that produces 1  $\mu\text{mol}$  of  $\alpha\text{Glc 1-P}$  per minute.

## S2. Immobilization in the glass microreactor

### S2.1. Estimating the theoretical maximum loading of Z\_SPase on the microchannel plate

A completely flat microchannel wall surface was assumed. From the geometry of the microchannel (based on technical drawing provided by Micronit Microfluidics, Chip Drawing R150.676.2) a total surface area of 374 mm<sup>2</sup> was calculated as follows. The cross section of the microchannel (Figure S3) was approximated as a triangle and the perimeter was calculated. By using the reported length of meander channel (771 mm) the surface area was calculated to 374 mm<sup>2</sup>.

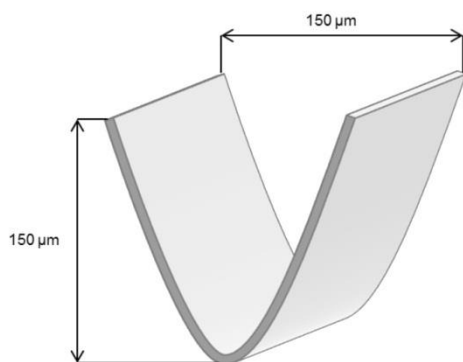


**Figure S3.** The cross-section of flow channel

The overall dimension of the *BSPase* molecule (Uniprot entry: Q84BY1) was assessed from the crystal structure of the homologous *SPase* from *Bifidobacterium adolescentis* (Uniprot entry: Q84HQ2, PDB code 1R7A). Both enzymes are functional homodimers and have subunits consisting of similar amino acids (*BSPase*: 508 amino acids, 56.414 kDa; *BaSPase*: 504 amino acids, 56.190 kDa). The program PyMOL 0.99rc6 was used for protein structure visualization. The largest footprint of the enzyme was taken from an orthogonal rectangle projection and determined to be 64.31 nm<sup>2</sup>. Regarding the variant of *Z\_LmSPase* (*LmSPase* Uniprot entry: Q59495) the same crystal structure was used in which one subunit was removed prior to determining the dimensions of the remaining subunit. The footprint was 40.5 nm<sup>2</sup>. The plain area of the plate divided by the enzyme area gave the maximum number of enzyme molecules immobilizable per plate which was transferred with Avogadro's constant, the size of the *Z\_SPase* and the specific activity of the enzyme into the theoretical activity loading per plate. Estimated data and basic properties of *Z<sub>basic2</sub>*-enzyme fusions are reported in Table S1.

# Multivalency Effects on the Immobilization of Sucrose Phosphorylase in Flow Microchannels and Their Use in the Development of a High-Performance Biocatalytic Microreactor

**Table S1.** Basic properties and estimated theoretical maximum loading of Z<sub>basic2</sub>-enzyme fusions on the microchannel plate.

Z <sub>basic2</sub> -enzyme fusion	Z_BSPase	Z_LmSPase	Z_LmSPase_Z	Z-Z_LmSPase
<b>Specific activity<sup>a</sup></b> (U mg <sup>-1</sup> )	77	75	90	69
<b>Expression level<sup>b</sup></b> (%)	23	10	11	14
<b>Total mass<sup>c</sup></b> (Da)	132834	65151	75749	73465
<b>Monolayer enzyme adsorption<sub>max</sub><sup>d</sup></b> (μg)	1.28	1.00	1.16	1.13
<b>Monolayer apparent enzyme activity<sub>max</sub><sup>e</sup></b> (mU)	99	75	104	78
<b>Volumetric rate<sub>max</sub><sup>f</sup></b> (mM min <sup>-1</sup> )	11.42	8.65	12.00	9.00

<sup>a</sup>The specific activities of the purified Z<sub>basic2</sub>-enzyme fusions are comparable within a factor of 2 or less to the specific activities of the corresponding "native" (untagged or His-tagged) enzymes, indicating that the module has no major influence of the enzymes' catalytic performance. <sup>b</sup>Specific activity of *E. coli* crude extract/specific activity of purified enzyme. <sup>c</sup>Total mass is calculated from the aminoacids sequence of Z\_SPase constructs with ProtParam tool. <sup>d</sup>The amount of enzyme required to form an adsorbed protein monolayer on the microreactor's surface with an internal surface area of 374 mm<sup>2</sup>. <sup>e</sup>Specific activity × monolayer enzyme adsorption. <sup>f</sup>Monolayer apparent enzyme activity/microreactor volume.

## S2.2. Enzyme immobilization procedure

### S2.2.1. Determination of [ $\alpha$ Glc 1-P]

The immobilization was evaluated based on the *apparent* enzyme activity bound to the plate ( $E_{app}$ ), determined from the [ $\alpha$ Glc 1-P] released at steady state under standard microreactor conditions. Samples from the microreactor outlet were collected and the concentration of  $\alpha$ Glc 1-P was measured by the application of reported coupled assays<sup>[1,4,8]</sup> in which  $\alpha$ Glc 1-P was measured as the NADH produced in a reaction by phosphoglucomutase and glucose 6-phosphate dehydrogenase. Concentration of reagents were identical to the phosphorylase activity assay with the modifications that sucrose phosphorylase was not present, sucrose and potassium phosphate were not added, 50 mM Tris/HCl buffer (pH 7.7) was used and final concentration of NAD<sup>+</sup> was 0.7 mM. Formation of NADH was monitored at 340 nm and

# Multivalency Effects on the Immobilization of Sucrose Phosphorylase in Flow Microchannels and Their Use in the Development of a High-Performance Biocatalytic Microreactor

the NADH end concentration was used to calculate the corresponding  $\alpha\text{Glc 1-}P$  concentration. Suitable calibration using  $\alpha\text{Glc 1-}P$  using standard was performed.

## S2.2.2. Evaluation of flow conditions and times on the immobilization

$Z\_LmSPase$  and  $Z\_BSPase$  were used to optimize the enzyme immobilization in the microreactor. Results are shown in Figure S4. Note:  $E_{app}$  is defined as  $[\alpha\text{Glc 1-}P] \times F$  under standard microreactor conditions (25 °C, pH 7.0, [substrate] = 50 mM,  $F = 5 \mu\text{L min}^{-1}$ ).

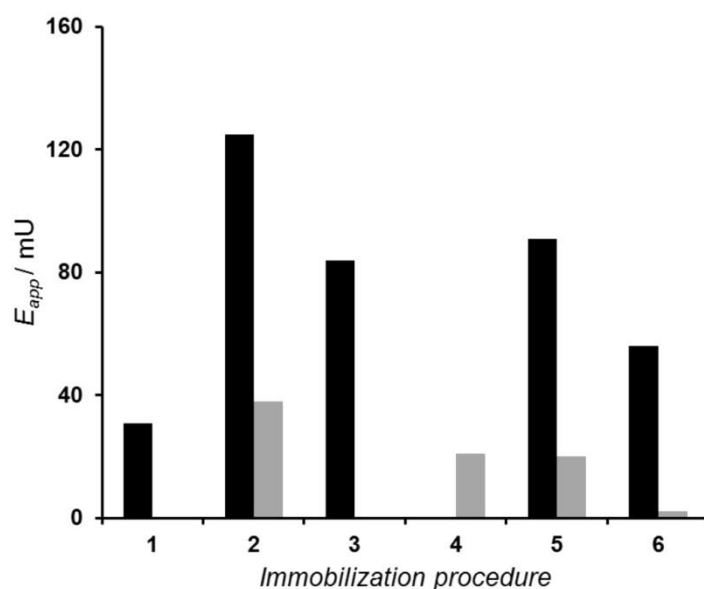


**Figure S4.** Evaluation of immobilization procedures of  $Z\_BSPase$  (black bars) and  $Z\_LmSPase$  (gray bars) in terms of *apparent* enzyme activity bound to the plate,  $E_{app}$ , under standard conditions of microreactor operation. 1, 1 h static incubation; 2, 2 h static incubation; 3, 4 h static incubation; 4, 24 h static incubation; 5, 3-times repeated static incubation (each time 2 h); 6, 24 h recirculation with  $1 \mu\text{L min}^{-1}$ .

## S3. Characterization of the performance of the enzymatic microreactor

The Reynolds number ( $Re$ ) was calculated with Equation S1 in which  $\mu$  is the dynamic viscosity,  $u_m$  is the mean velocity,  $\rho$  is the density of liquid and  $d_h$  is the hydraulic diameter.<sup>[9-11]</sup>

# Multivalency Effects on the Immobilization of Sucrose Phosphorylase in Flow Microchannels and Their Use in the Development of a High-Performance Biocatalytic Microreactor

$$Re = \frac{\rho d_h u_m}{\mu}$$

Equation S1

Calculations are based on a cross sectional area of  $1.125 \times 10^{-2} \text{ mm}^2$  and a hydraulic diameter of  $9.27 \times 10^{-5} \text{ m}$ .<sup>[9]</sup> The density and a dynamic viscosity of water at 25 °C were used (Note that the substrate solution contains only 1.7 % w/v of sucrose), the values were  $997.04 \text{ kg m}^{-3}$  and  $8.9 \times 10^{-4} \text{ Pa.s}$ , respectively.<sup>[9,12]</sup> The calculated data (Figure S5) indicate laminar flow under all  $F$  conditions used ( $Re < 2100$  is laminar). The parameters used in the calculations are shown in Table S2.

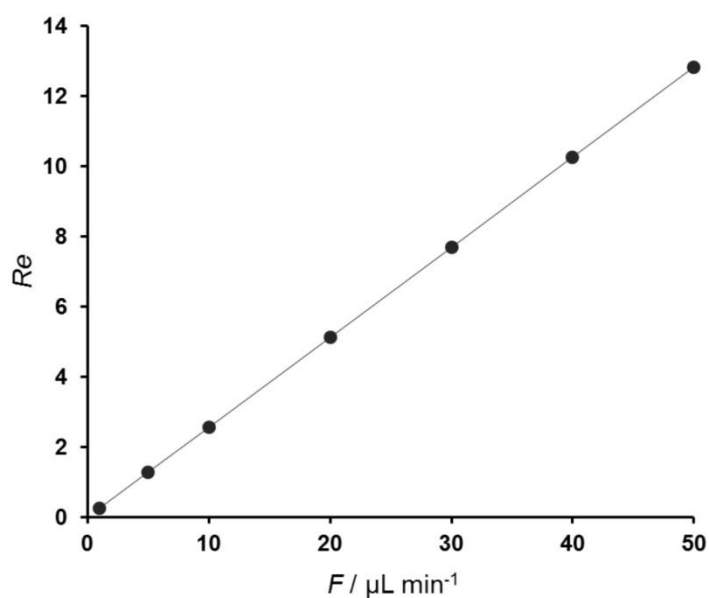


**Figure S5.** The Reynolds number is shown for fluid flow in the microreactor for the range of flow rates used.

**Table S2.** The related parameters for Reynolds number calculations

$F$ ( $\mu\text{L min}^{-1}$ )	$u_m$ ( $\text{m s}^{-1}$ )	$Re$
1	0.002	0.26
5	0.012	1.28
10	0.025	2.56
20	0.049	5.12
30	0.074	7.68
40	0.099	10.24
50	0.123	12.81

## Multivalency Effects on the Immobilization of Sucrose Phosphorylase in Flow Microchannels and Their Use in the Development of a High-Performance Biocatalytic Microreactor

The radial diffusive Peclet number<sup>[9-11]</sup> ( $Pe_D$ ) is shown in Figure S6 and defined in Equation S2 where  $D$  is the coefficient of diffusion of sucrose which is  $5.15 \times 10^{-10} \text{ m}^2 \text{ s}^{-1}$  at 25 °C in water.<sup>[13]</sup>

$$Pe_D = \frac{u_m d_h}{D} \quad \text{Equation S2}$$

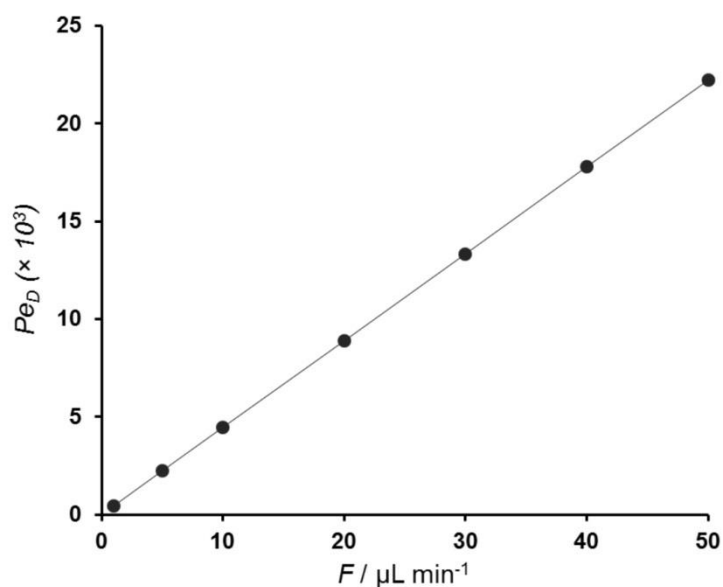


**Figure S6.** The radial diffusive channel Peclet number is shown for the range of applied flow rates in the microreactor.

The second Damköhler number ( $Da_{II}$ ) was calculated by Equation S3.<sup>[9-11]</sup>

$$Da_{II} = \frac{\tau_{diff}}{\tau_{reac}} \quad \text{Equation S3}$$

In Equation S3,  $\tau_{reac}$  is the characteristic reaction time and  $\tau_{diff}$  is the characteristic diffusion time.  $\tau_{diff}$  was calculated by Equation S4 for diffusive mass transfer and  $\tau_{reac}$  was calculated by Equation S5.

$$x^2 = 2 D \tau_{diff} \quad \text{Equation S4}$$

$$\tau_{reac} = \frac{60 [\text{sucrose}] Vol}{E_{app}} \quad \text{Equation S5}$$

## Multivalency Effects on the Immobilization of Sucrose Phosphorylase in Flow Microchannels and Their Use in the Development of a High-Performance Biocatalytic Microreactor

In Equation S4,  $x$  is the diffusional distance (= 75  $\mu\text{m}$ ; half of the flow channel width and height).<sup>[9]</sup> In Equation S5 [sucrose],  $Vol$ , and  $E_{app}$  are used in mM, mL and U respectively. The  $\tau_{\text{reac}}$  and the  $\tau_{\text{diff}}$  for the flow rate of 5  $\mu\text{L min}^{-1}$  are shown in Table S3.

**Table S3.** Reaction-diffusion regime analysis of the microreactor operation based on  $Da_{II}$  is shown. The flow rate was 5  $\mu\text{L min}^{-1}$ .

Conversion <sup>a</sup>	$E_{app}$ (mU)	$\tau_{\text{reac}}$ (s)	$\tau_{\text{diff}}$ (s)	$Da_{II}$
0.34	85	306	5.46	0.0179
0.28	71	365	5.46	0.0149
0.22	54	482	5.46	0.0113
0.19	48	543	5.46	0.0101
0.18	46	567	5.46	0.0096
0.15	38	692	5.46	0.0079
0.14	34	771	5.46	0.0071
0.06	15	1721	5.46	0.0032
0.05	12	2223	5.46	0.0025
0.04	10	2596	5.46	0.0021
0.03	8	3211	5.46	0.0017

<sup>a</sup> Conversion is the ratio of the concentrations of  $\alpha\text{Glc 1-}P$  (product) and sucrose (substrate). The different conversions were obtained during the operation of microreactor for a total time of 48 h.

## Supporting references

- [1] M. Pfeiffer, P. Wildberger, B. Nidetzky, *J. Mol. Catal. B: Enzym.* **2014**, *110*, 39-46.
- [2] J. Quan, J. Tian, *PLoS One* **2009**, *4*, e6441.
- [3] J. Quan, J. Tian, *Nat. Protoc.* **2011**, *6*, 242–251.
- [4] J. Wiesbauer, J. M. Bolivar, M. Mueller, M. Schiller, B. Nidetzky, *ChemCatChem* **2011**, *3*, 1299–1303.
- [5] T. Gräslund, M. Ehn, G. Lundin, M. Hedhammar, M. Uhlén, P. A. Nygren, S. Hober, *J. Chromatogr. A.* **2002**, *942*, 157–166.
- [6] M. Hedhammar, S. Hober, *J. Chromatogr. A.* **2007**, *1161*, 22–28.
- [7] T. Gräslund, G. Lundin, M. Uhlén, P. A. Nygren, S. Hober, *Protein Eng.* **2000**, *13*, 703–709.
- [8] C. Goedel, A. Schwarz, A. Minani, B. Nidetzky, *J. Biotechnol.* **2007**, *129*, 77-86.
- [9] J. M. Bolivar, M. A. Tribulato, Z. Petrasek, B. Nidetzky, *Biotechnol. Bioeng.* **2016**, in press (doi: 10.1002/bit.26011).
- [10] M. P. C. Marques, P. Fernandes, *Molecules* **2011**, *16*, 8368–8401.
- [11] T. Van Daele, D. Fernandes del Pozo, D. Van Hauwermeiren, K. V. Gernaey, R. Wohlgemuth, I. Nopens, *Chem. Eng. J.* **2016**, *300*, 193–208.
- [12] J. C. Crittenden, R. R. Trussell, D. W. Hand, K. J. Howe, G. Tchobanoglous, *MWH's Water Treatment: Principles and Design* John Wiley & Sons, Inc., Hoboken, **2012**.
- [13] P.W. Linder, L. R. Nassimbeni, A. Polson, A.L. Rodgers, *J. Chem. Educ.* **1976**, *53*, 330-332.

## **A Spring in Performance: Silica Nanosprings Boost Enzyme Immobilization in Microfluidic Channels**

## A Spring in Performance: Silica Nanosprings Boost Enzyme Immobilization in Microfluidic Channels

Donya Valikhani,<sup>†</sup> Juan M. Bolivar,<sup>†</sup> Martina Viehues,<sup>‡,¶,Ⓢ</sup> David N. McLroy,<sup>§</sup> Elwin X. Vrouwe,<sup>‡</sup> and Bernd Nidetzky<sup>\*,†,Ⓢ,Ⓣ</sup>

<sup>†</sup>Institute of Biotechnology and Biochemical Engineering, Graz University of Technology, NAWI Graz, Petersgasse 12, 8010 Graz, Austria

<sup>‡</sup>Micronit Microtechnologies B.V., Colosseum 15, 7521 PV, Enschede, The Netherlands

<sup>§</sup>Department of Physics, Oklahoma State University, Stillwater, Oklahoma 74078-3072, United States

<sup>Ⓣ</sup>Austrian Centre of Industrial Biotechnology, Petersgasse 14, 8010 Graz, Austria

**S** Supporting Information

**ABSTRACT:** Enzyme microreactors are important tools of miniaturized analytics and have promising applications in continuous biomanufacturing. A fundamental problem of their design is that plain microchannels without extensive static internals, or packings, offer limited exposed surface area for immobilizing the enzyme. To boost the immobilization in a manner broadly applicable to enzymes, we coated borosilicate microchannels with silica nanosprings and attached the enzyme, sucrose phosphorylase, via a silica-binding module genetically fused to it. We showed with confocal fluorescence microscopy that the enzyme was able to penetrate the  $\sim 70$   $\mu\text{m}$ -thick nanospring layer and became distributed uniformly in it. Compared with the plain surface, the activity of immobilized enzyme was enhanced 4.5-fold upon surface coating with nanosprings and further increased up to 10-fold by modifying the surface of the nanosprings with sulfonate groups. Operational stability during continuous-flow biocatalytic synthesis of  $\alpha$ -glucose 1-phosphate was improved by a factor of 11 when the microreactor coated with nanosprings was used. More than 85% of the initial conversion rate was retained after 840 reactor cycles performed with a single loading of enzyme. By varying the substrate flow rate, the microreactor performance was conveniently switched between steady states of quantitative product yield (50 mM) and optimum productivity (19  $\text{mM min}^{-1}$ ) at a lower product yield of 40%. Surface coating with silica nanosprings thus extends the possibilities for enzyme immobilization in microchannels. It effectively boosts the biocatalytic function of a microstructured reactor limited otherwise by the solid surface available for immobilizing the enzyme.

**KEYWORDS:** surface modification, silica nanosprings, microreactor, biocatalysis, enzyme immobilization



### 1. INTRODUCTION

Continuous-flow microfluidics is the key enabling technology for many important applications, from the lab-on-the-chip implementations in analytics, cell biology, and medicine<sup>1–5</sup> to the advanced tools of microprocess engineering in chemistry and biotechnology.<sup>6–13</sup> Microfluidic biocatalysis plays a central role in biochips for DNA sequencing, proteomic analysis, and clinical metabolite detection.<sup>13,14,15</sup> It has furthermore aroused significant interest for use in various flow chemistry applications. The idea in general is that by combining the high selectivity of enzymes with the efficient fluidics of a microstructured flow reactor, the performance characteristics of certain chemical transformations can be enhanced substantially. Fundamental problem of all microfluidic biocatalysis in continuous flow is, however, that irrespective of the enzyme's actual use for sample pretreatment, analytical detection, or organic synthesis, the enzyme must be applied in a form that

prevents it from being washed away.<sup>10–13,16</sup> Immobilizing the enzyme on the wall surface of the microchannels presents the most straightforward solution.<sup>10,17–22</sup> Doing so, however, demands a strongly integrated development of the microfluidic system considered. The flow channels must be designed to accommodate a suitable amount of active enzyme immobilized on their solid walls because the conversion rate scales directly with that amount.<sup>19,20,23,24</sup> The contrast to enzyme immobilization in conventional reactors is immediately noted. Bulk-scale immobilization is usually done on porous particles and so represents a task of the overall bioprocess development that is pursued somewhat independently of the actual bioreactor design.<sup>25–29</sup>

Received: July 7, 2017

Accepted: September 18, 2017

Published: September 18, 2017

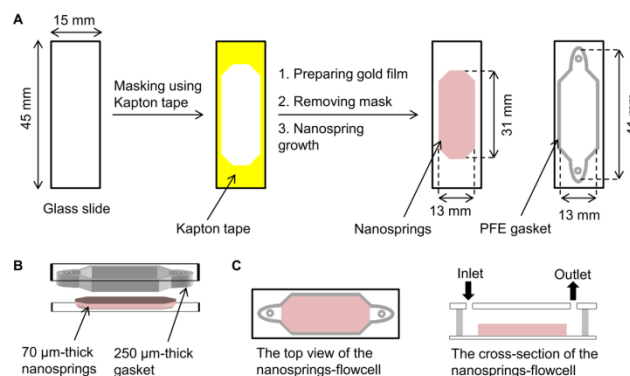


**Figure 1.** Preparation of the nanosprings-flowcell is shown. Panel A shows fabrication of the nanosprings glass slide. The gasket glass slide is also shown. Panel B illustrates stacking of the two glass slides on each other. Panel C shows the assembled nanosprings-flowcell (not to scale).

Microchannel design for efficient immobilization needs to join aspects of overall geometry and internal structure of the microchannels with those of the material used for microfabrication. The core problem is that plain microchannels, lacking extensive static internals or packings, offer only a limited amount of solid surface for immobilizing the enzyme. Because microparticle packings result in large pressure drops, and static internals alter the liquid flow pattern<sup>12,30</sup> usually more than they help increase the surface area, enhancement of the enzyme-accessible surface directly on the microchannel walls remains the most promising option. Among the materials widely used in microfluidics, silica has excellent properties, including high compatibility with enzymes, substrates, and solvents.<sup>26</sup> Immobilization technology based on silica-binding modules (SBMs) enables convenient immobilization of enzymes on plain silica (e.g., borosilicate glass). The SBM is a small three-helical protein, often referred to also as  $Z_{\text{basic2}}$ , that is highly positively charged on one protein face due to multiple Arg residues pointing outward.<sup>19–21,27</sup> The SBM is genetically fused to the enzyme of interest, and the resulting enzyme chimera becomes attached to underivatized silica surfaces via the SBM. Under conditions in which the silica material is negatively charged, binding occurs with high affinity and selectivity. Immobilization likely involves a high degree of molecular alignment of the enzyme via its SBM toward the silica surface. In contrast to silica, polymeric materials also popular in microreactor development, polydimethylsiloxane, for instance, is not directly accessible and so requires extensive surface derivatization for enzyme immobilization.<sup>5,11,15,31</sup> In the current study, therefore, we made an effort to bring surface engineering for efficient SBM-enzyme immobilization into the design of silica microchannel reactors.

Coating the microchannel walls with a suitably porous silica microstructure represents a promising approach to increase the enzyme-available surface for immobilization. Among different options available, silica nanosprings represent a well-characterized type of nanomaterial and have recently gained attention in particular.<sup>32,33</sup> Nanospring coatings provide a high solvent-accessible surface area, and their Darcy permeability ( $\sim 3 \times 10^{-6} \text{ cm}^2$ ) indicates low resistance to fluid flow.<sup>32</sup>

Their specific surface is extremely large ( $\sim 300 \text{ m}^2 \text{ g}^{-1}$ ) and fully accessible, and many surface silanol groups are available for chemical functionalization. Similarly, these silanol groups

present surface sites for enzymes to become anchored via their SBM. Using a modified vapor-liquid-solid (VLS) process, nanosprings can be deposited on essentially any solid surface able to tolerate a growth temperature of  $370^\circ \text{C}$ , thus making their applications quite versatile.<sup>34</sup> Nanosprings were previously used as a support in immobilized enzyme microreactors.<sup>32,33</sup> However, lacking the advantages of SBM technology, the overall immobilization required multiple steps, including enzyme purification and surface functionalization, and involved 87% loss of active enzyme in the process. Nanospring layers of different thickness were compared, but the enzyme distribution within was not clarified.<sup>33</sup>

We show here that the major performance characteristics of a biocatalytic microreactor were consistently improved in immediate consequence of immobilizing the SBM-enzyme on microchannel walls coated with silica nanosprings compared to immobilizing the same enzyme on plain silica walls. The immobilized enzyme activity was enhanced, and the obtainable productivity was boosted accordingly. Due to increased retention of the enzyme into the nanospring layer, the operational stability of the microreactor increased. We did our evaluation using sucrose phosphorylase, a well-known transglucosidase that has important applications in glycoside and sugar phosphate synthesis.<sup>35</sup> We present evidence that surface coating with silica nanosprings extends the current possibilities significantly and so addresses relevant limitations of enzyme immobilization in microchannels. Combined with immobilization technology based on SBM, it appears broadly useful in microfluidic systems limited otherwise by the solid surface available for immobilizing the enzyme.

## 2. EXPERIMENTAL SECTION

**2.1. Materials used.** Resealable flowcells made of borosilicate glass were used.<sup>36</sup> Their design, fabrication and use are described elsewhere in detail.<sup>36</sup> The complete flowcell consists of a microstructured element placed into a suitably interfaced and conveniently opened and closed chip holder. Fluidic Connect Pro Resealable flowcell 4515 holder, Teflon tubings, and connection parts were from Micronit Microtechnologies B.V (Enschede, NL). A New Era NE-1000 syringe pump (Next Advance, Averill Park, NY) was used to deliver the liquid flow. All chemicals were of analytical grade and reported elsewhere.<sup>19,35</sup>

**2.2. Fabrication of the Nanosprings-Flowcell.** **2.2.1. Integration of the Nanosprings in the Resealable Flowcell.** Fabrication of

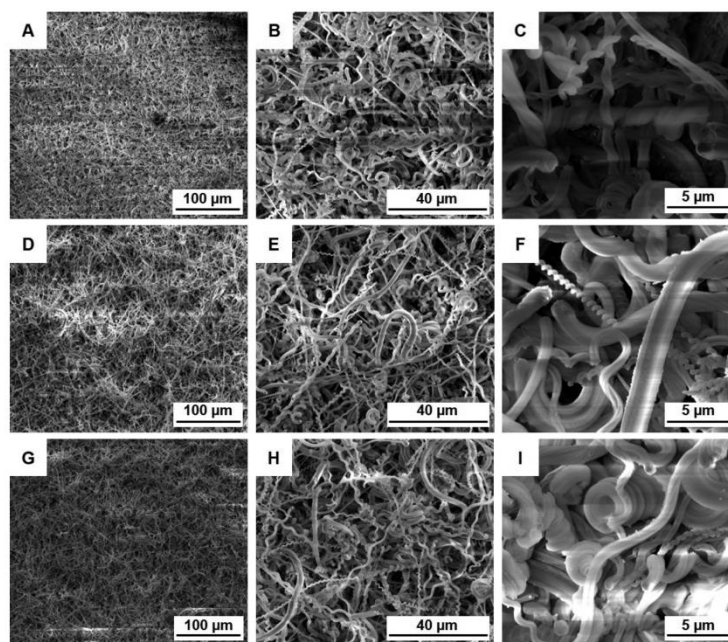


**Figure 2.** SEM images of the nanosprings coating are shown from three different positions on the glass slide. Each row shows one position at different magnifications.

the plain flowcell was by an established standard process.<sup>36</sup> Design of the flowcell implied that the bottom glass slide was conveniently usable for surface derivatization. The procedure applied to attach nanosprings onto the glass surface is summarized in Figure 1. The surface was masked with Kapton tape, thus ensuring that only the center area (i.e., the area eventually exposed to liquid flow inside the fully assembled flowcell) was used for growth of the nanosprings (Figure 1). The process of nanosprings growth on glass slides was described in detail before.<sup>34</sup> Synthesis was performed in a furnace operated at atmospheric pressure. A thin gold film prepared by sputtering on glass was used as catalyst. Nanosprings were formed by exposure to constant flows of a proprietary silicon precursor and oxygen in a nitrogen atmosphere. About 9 mg of the nanosprings, covering a surface area of  $\sim 3$  cm<sup>2</sup> and forming a layer of 70  $\mu$ m thickness, was grown on the glass slide. The coated area was then enclosed with a gasket made of perfluorinated elastomer. As shown in Figure 1, the gasket was present on a second glass slide, which also contained the fluidic channel pattern. The glass slides were inserted into the flowcell holder and connected with Teflon tubings (250  $\mu$ m inner diameter). The gasket had a thickness of 250  $\mu$ m, which was compressed by about 10% on usage in the flowcell holder.

**2.2.2. Functionalization of the Nanosprings–Flowcell.** The nanosprings glass slide was functionalized with sulfonic acid groups ( $-\text{SO}_3\text{H}$ ) using a procedure from the literature.<sup>37</sup> The glass slide was immersed in 1 M sodium hydroxide for 30 min followed by rinsing with deionized water. It was incubated in 10% (v/v) aqueous solution of 3-(trihydroxysilyl)-1-propane-sulfonic acid for 3 h (80 °C, pH 8.0) and after that washed extensively with 50 mM potassium phosphate, pH 7.0.

**2.3. Enzyme Immobilization in the Flowcell.** **2.3.1. Enzyme Immobilization Procedure.** A chimeric form of sucrose phosphorylase from *Bifidobacterium longum* (BSPase) was used that had the binding module  $Z_{\text{basic}2}$  fused to its N-terminus. BSPase is a functional homodimer, so each enzyme chimera used here contained two  $Z_{\text{basic}2}$  modules. The enzyme is referred to as  $Z_{\text{BSPase}}$  throughout.

$Z_{\text{BSPase}}$  was produced in *Escherichia coli* BL21(DE3) as reported elsewhere.<sup>19</sup> Unless mentioned otherwise, bacterial cell extract containing  $Z_{\text{BSPase}}$  was used for immobilization. The general procedure was described in earlier papers.<sup>19,20,27</sup> For reference from pure  $Z_{\text{BSPase}}$ , the enzyme was isolated according to a reported protocol<sup>19</sup> and shown to exhibit a specific activity of 77 U mg<sup>-1</sup> of protein. One unit (U) of enzyme activity is the enzyme amount producing 1  $\mu$ mol  $\alpha$ -D-glucose 1-phosphate ( $\alpha$ Glc 1-p) min<sup>-1</sup> under assay conditions (25 °C, pH 7.0). The immobilization described here only briefly involved filling of the flowcell with immobilization mixture, which comprised the enzyme in 50 mM potassium phosphate, pH 8.0, supplemented with 0.25 M sodium chloride. After incubation for 2 h, the flowcell was washed with 50 mM potassium phosphate (25 °C, pH 7.0) at a flow rate ( $F$ ) of 50  $\mu$ L min<sup>-1</sup>. We note, because it will be important for the discussion later, that by washing with the same phosphate buffer containing 2 M sodium chloride, it was possible to elute the immobilized enzyme from the plain glass without causing any inactivation. Enzyme still bound to the nanosprings matrix after elution at high salt concentration (5 M sodium chloride) was removed from the nanosprings–flowcell by rinsing with 1 M hydrochloric acid and then with deionized water.

**2.3.2. Measurement of the Enzyme Activity in Solution and Immobilized in the Flowcell.** The activity of  $Z_{\text{BSPase}}$  in solution and immobilized on the glass slide was measured by a spectrophotometric assay described elsewhere.<sup>19</sup> Briefly, the  $\alpha$ Glc 1-p released on conversion of sucrose (50 mM) and potassium phosphate (50 mM) by  $Z_{\text{BSPase}}$  was measured as the reduced form of nicotinamide adenine dinucleotide (NADH) formed in a coupled enzymatic reaction (25 °C, pH 7.0). The NADH was determined from absorbance at 340 nm. To obtain the apparent activity ( $E_{\text{app}}$ ) of immobilized  $Z_{\text{BSPase}}$ , a continuous reaction was performed in which solution of sucrose and potassium phosphate (50 mM each, 25 °C, pH 7.0) was delivered to the microreactor at different flow rates. The  $\alpha$ Glc 1-p produced at steady state was measured dependent on  $F$ .  $E_{\text{app}}$  was calculated from the relationship,  $E_{\text{app}} = [\alpha\text{Glc 1-p}] \times F$ . It is reported in U.

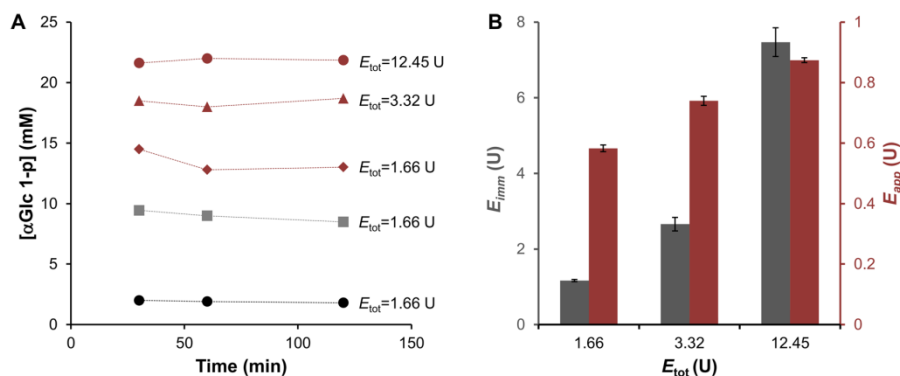


**Figure 3.** An analysis of immobilization in different flowcells is shown. Panel A shows the [ $\alpha$ Glc 1-p] at steady state produced in continuous reactions in different flowcells (black, plain flowcell; gray, nanosprings-flowcell; red, nanosprings-SO<sub>3</sub><sup>-</sup>-flowcell). Panel B shows the effect of increasing the  $E_{\text{tot}}$  on the performance of the nanosprings-SO<sub>3</sub><sup>-</sup>-flowcell in terms of  $E_{\text{imm}}$  and  $E_{\text{app}}$ . Data in panel A are used to calculate  $E_{\text{app}}$ . The conditions used were:  $F = 40 \mu\text{L min}^{-1}$ , 50 mM of each sucrose and potassium phosphate, 25 °C, and pH 7.0. Results in panel A are from three independent experiments. Average values are shown with a standard deviation of 5%.

**2.3.3. Immobilization Efficiency.** Immobilization yield ( $Y$ ) and catalytic effectiveness of immobilized enzyme ( $\eta$ ) were used to characterize the efficiency of *Z\_BIS*Pase immobilization in the nanosprings-SO<sub>3</sub><sup>-</sup>-flowcell.  $Y$  is the ratio of the enzyme activity immobilized on the surface ( $E_{\text{imm}}$ ) to the total enzyme activity offered in solution ( $E_{\text{tot}}$ ).  $E_{\text{imm}}$  is the difference in  $E_{\text{tot}}$  and the enzyme activity left in solution after the immobilization. An alternative way of determining  $E_{\text{imm}}$  was to elute the immobilized enzyme from the glass surface and measure its activity in solution. The latter approach was useful when activity differences in solution were too small for a reliable determination; hence, when  $Y$  is very low,  $\eta$  is the ratio of  $E_{\text{app}}$  to  $E_{\text{imm}}$ .

**2.4. Fluorescence Labeling of the Immobilized Enzyme.** Protocol from literature was used.<sup>29</sup> A solution of fluorescein isothiocyanate (FITC) was prepared in dimethyl sulfoxide and diluted in 50 mM potassium phosphate, pH 7.0. The FITC solution (20 mol FITC/mol enzyme) was passed through the nanosprings-SO<sub>3</sub><sup>-</sup>-flowcell containing immobilized enzyme and incubated for 1 h at 25 °C. Afterward, the flowcell was washed extensively with 50 mM potassium phosphate, pH 7.0.

**2.5. Material Characterization.** Scanning electron microscopy (SEM) was performed with an FEI NOVA 200 dual beam system (Thermo Fisher) using secondary electron imaging at 10 keV and 130 pA with the lowest possible doses unless otherwise specified. The samples were covered with a 20 nm-thick carbon layer prior to scanning.

Confocal laser scanning microscopy (CLSM) was performed using a Leica TCS SPE confocal microscope (Mannheim, Germany). The samples were excited at 488 nm, and the emission was detected in the range of 500–700 nm. A water immersion objective HCX APO LU-VI 20 × /0.50 W was used, and a drop of glycerol was placed onto the nanosprings before covering the sample with a microscope coverslip. This was done to improve the match in refractive index between the medium and the nanosprings layer.

The surface area of nanosprings was determined by the Brunauer–Emmett–Teller (BET) gas adsorption method.<sup>34</sup>

### 3. RESULTS AND DISCUSSION

The shown data are from multiple independent experiments, typically three or more. Mean values were calculated from the data and are given together with the corresponding standard deviation in text.

**3.1. Characteristics of the Nanosprings-Flowcell.** The plain flowcell offered a total wall surface area of 740 mm<sup>2</sup>, which was contributed from the top and bottom glass slides.

The calculated internal volume of the flow channel was  $\sim 83 \mu\text{L}$  (Figure 1C). Note that the effect of the nanosprings layer on reduction of internal volume was not considered in that value. On the basis of the nanosprings surface area determined by gravimetric BET (300 m<sup>2</sup> g<sup>-1</sup>), the extra surface area introduced with the nanosprings was estimated as  $\sim 2.7 \text{ m}^2$ .

The structure of the nanosprings coating was characterized by SEM. Analysis was performed at different positions along the glass slide using varied magnification. The complete set of SEM images recorded is given in Figure S1. SEM images from three different positions are shown in Figure 2. The overall structure of the nanosprings coating was best described as a highly irregular network of fibers arranged into a fine-mesh heterogeneous layer of material. Irregularity persisted at the level of individual nanosprings in terms of both size and shape. Nanosprings generally had strongly elongated form but differed widely in their length and thickness. Certain nanosprings had a strongly strung-out shape and appeared almost linear in shape, exhibiting only a slight internal twist. Others adopted spiral-wound conformations, differing widely, however, in the size of the individual coils forming the spiral. Nanosprings often displayed helicoidal shape of varying diameter (0.3–3  $\mu\text{m}$ ). The overall nanosprings layer exhibited nonuniform density and hence surface area, as shown in a representative cross-section image in Figure S2.

Density increased from the surface to the bottom of the nanosprings matrix. The overall solid layer did not contain defined pores but featured multiple interstices of variable size (from nm to  $\mu\text{m}$  scale). In principle, these interstices were sufficiently large to enable the enzyme (10.9 × 5.9 × 5 nm; deduced from the crystal structure of the highly similar enzyme from *Bifidobacterium adolescentis*) to penetrate the matrix by diffusion. The nanosprings layer, therefore, seemed promising for use as a densely woven, three-dimensional scaffold for *Z\_BIS*Pase immobilization. Besides offering a substantially enlarged surface area for the enzyme to become attached to, as compared to the plain surface, we also considered that the nanosprings layer might help improving the immobilization efficiency through effect on  $E_{\text{app}}$ . Although immobilization of *Z\_BIS*Pase is steered mainly by the  $Z_{\text{basic2}}$  module, nonspecific

protein adsorption on the solid surface might occur to a limited degree, as shown in our earlier study.<sup>19</sup> A fibrous layer of solid material could be useful to avoid nonspecific binding of the enzyme and, in consequence, help to maximize  $E_{app}$ . We finally considered that adsorption stability of immobilized Z\_BSPase might be increased on entrapment of the enzyme in the nanosprings matrix. Experiments were performed to explore these possibilities.

**3.2. Performance Analysis of Immobilized Enzyme Flowcell.** **3.2.1. Enzyme Immobilization in Nanosprings-Flowcells.** Nanosprings-flowcells were prepared with and without surface functionalization by sulfonate groups. The surface sulfonate groups were introduced because they could potentially enhance enzyme immobilization via the Z<sub>basic2</sub> module. The plain flowcell was used as reference. Immobilization involved offering Z\_BSPase in an amount that was the same for each flowcell and exceeded by a factor of 9 the estimated maximum binding capacity of the plain surface for that enzyme ( $B_{max} = 2.54 \mu\text{g}$ ). The Supporting Information describes the assumptions and calculations used in binding capacity assessment. It was thus ensured that enzyme in solution was not limiting the immobilization. From continuous reactor experiments performed as described in the Experimental Section, we determined the concentration of  $\alpha\text{Glc 1-p}$  released at steady state (Figure 3A). Results show that the plain flowcell exhibited an  $E_{app}$  of  $83 \pm 3 \text{ mU}$ . From the value of  $B_{max}$  and the specific activity of purified Z\_BSPase ( $77 \text{ U mg}^{-1}$ ), we calculated that the observed  $E_{app}$  corresponded to 40% of the  $E_{app}$  expected for maximum monolayer adsorption of the enzyme on the microchannel wall under the condition that all of the immobilized Z\_BSPase was fully active ( $\eta = 1$ ). The flowcell containing nanosprings exhibited an increase in  $E_{app}$  to  $378 \pm 8 \text{ mU}$ . The presence of sulfonate groups gave a further increase in  $E_{app}$  ( $583 \pm 11 \text{ mU}$ ), thus boosting the immobilization 7-fold compared to the plain reference.

Effect of varying the amount of enzyme offered ( $E_{tot}$ ) on the performance of nanosprings flowcell containing sulfonate groups was studied at conditions of reactor steady state (Figure 3A). The conversions reached were up to 10-fold higher compared to the plain flowcell. Critical parameters of the immobilization of Z\_BSPase ( $E_{imm}$ ,  $Y$ ,  $\eta$ ) were also determined from these experiments. Figure 3B shows that  $E_{imm}$  increased steadily on raising  $E_{tot}$ , indicating that the surface area available for immobilization was not saturated under the conditions used. Interestingly, therefore,  $Y$  was always below a value of unity ( $\leq 0.80$ ) that would indicate incomplete adsorption of the  $E_{tot}$  present. Further,  $Y$  did not have a pronounced dependent change on  $E_{tot}$  in the range used. The result suggests that, for reasons not known at the time, irrespective of  $E_{tot}$  a certain portion ( $\geq 20\%$ ) of the Z\_BSPase present as active enzyme in solution was unable to bind to the solid surface. Considering the large increase in  $E_{imm}$  dependent on  $E_{tot}$  it was important to determine what the corresponding change in  $E_{app}$  would be. Somewhat to our surprise, a 6-fold enhancement in  $E_{imm}$  due to increase in  $E_{tot}$  was reflected in only a 1.5-fold gain in  $E_{app}$ . Therefore, this implies a dramatic decrease in  $\eta$ , from a value of 0.52 to one of just 0.11 in response to the increase in  $E_{tot}$ .

In the ideal case of oriented immobilization via the Z<sub>basic2</sub> module in which becoming attached to the solid surface did not interfere with enzyme function in any way,  $\eta$  would have a value of unity, for the immobilized enzyme ( $E_{app}$ ) had exactly the same activity as the identical amount of enzyme would have in solution ( $E_{imm}$ ). We showed in earlier studies using different

Z<sub>basic2</sub> chimeras of sucrose phosphorylase, including Z\_BSPase, that the practical upper limit of  $\eta$  for these enzymes immobilized on silica surface was consistently lower than 1, typically in the range 0.45–0.65.<sup>19</sup> Molecular account of  $\eta$  is notoriously difficult to give for immobilized enzymes, but suffice it to say that the  $\eta = 0.52$  at low  $E_{tot}$  of Z\_BSPase was in good agreement with literature.<sup>19</sup> To the extent that different enzymes and different methods of immobilization can be compared directly, oriented immobilization via the Z<sub>basic2</sub> module enhanced the efficiency of the immobilized enzyme up to fourfold compared to random enzyme immobilization in the nanosprings.<sup>33</sup> Substantial drop in  $\eta$  at high  $E_{tot}$  was unexpected, however, and only a very tentative explanation can be offered at this point. It must be emphasized for the sake of clarity that a decrease in  $E_{app}$ , and hence  $\eta$ , was not caused by substrate depletion or any other limitation in the experiment. At the highest  $E_{app}$  we were able to reach in continuous flow reactions ( $\sim 880 \text{ mU}$ ), the substrate conversion was just around 40% when up to 90% conversion would have been possible at thermodynamic equilibrium. However, given the structure of the nanosprings matrix (Figure 2), it is conceivable that by increasing the enzyme loading, the portion of Z\_BSPase localized at nanointerstices within the matrix might also increase. Due to the highly irregular network of nanowires present at these interstices, it may no longer be possible for the immobilized enzyme to have a well-defined orientation toward, and interaction with, the solid material, contrary to the more compactly organized surfaces of plain glass, like those in plates and porous beads, that exhibit a moderate or even a null curvature.<sup>19,20,27,37</sup> An immobilization of Z\_BSPase in the nanosprings matrix that is not any more steered by the Z<sub>basic2</sub> module might be responsible for the decrease in  $\eta$  dependent on  $E_{tot}$ . In addition, the extreme irregularity of the solid matrix and the variation in local density associated with it might hinder, more strongly than anticipated, the diffusion of even small molecules. The possibility of diffusional limitations in supplying substrates to the immobilized enzyme could therefore not be excluded.

Using again the specific activity of the purified Z\_BSPase, we calculated from the values of  $E_{imm}$  that between 15 and 100  $\mu\text{g}$  of enzyme was bound onto the nanosprings- $\text{SO}_3^-$ -flowcell. These loadings are equivalent to an immobilization of 1.7–11 mg of protein/g of nanosprings. Compared to the  $B_{max}$  (calculated with the assumption of a strictly two-dimensional adsorption of the enzyme) normalized on the unit surface area ( $3.43 \text{ ng mm}^{-2}$ ), these amounts of immobilized enzyme represent a 6- to 40-fold enhancement over immobilization on the plain surface. These results show that nanosprings significantly increased the enzyme-loading capacity of the microchannel surface. There are, of course, other methods of surface modification to enhance the amount of immobilized enzyme. Layer-by-layer immobilization and surface-anchored polymer brushes are two interesting examples. However, in each case, the surface functionalization requires multiple steps.<sup>38–40</sup> It is evident from the considerations just made that immobilization of Z\_BSPase in the nanosprings- $\text{SO}_3^-$ -flowcell must have involved enzyme adsorption in all three dimensions of the nanosprings matrix. However, distribution of Z\_BSPase within the nanosprings layer was unknown, and visualization experiments were performed for clarification.

**3.2.2. Visualizing Enzymes Immobilized in the Nanosprings- $\text{SO}_3^-$ -Flowcell.** Z\_BSPase (15  $\mu\text{g}$ ) was immobilized in the nanosprings- $\text{SO}_3^-$ -flowcell, labeled fluorescently with

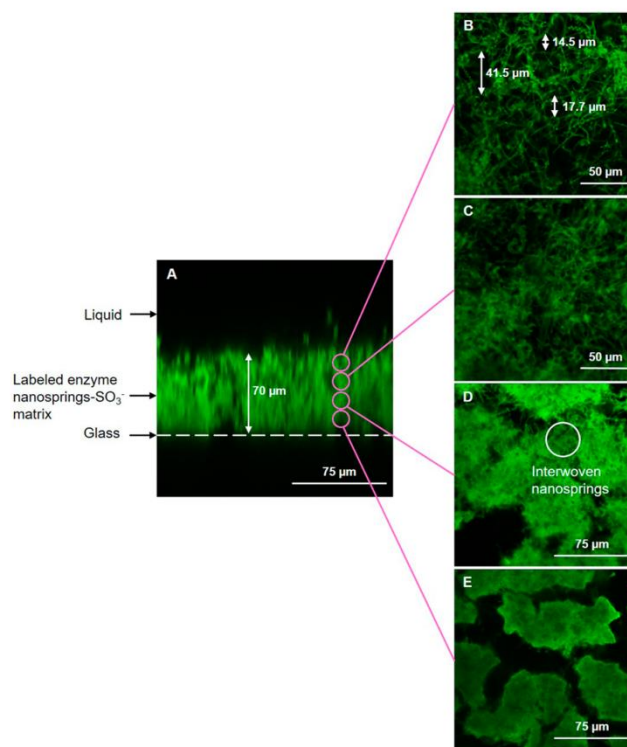


Figure 4. CLSM images of the nanosprings- $\text{SO}_3^-$ -glass slide containing FITC-labeled  $Z\_BISPase$  are shown.

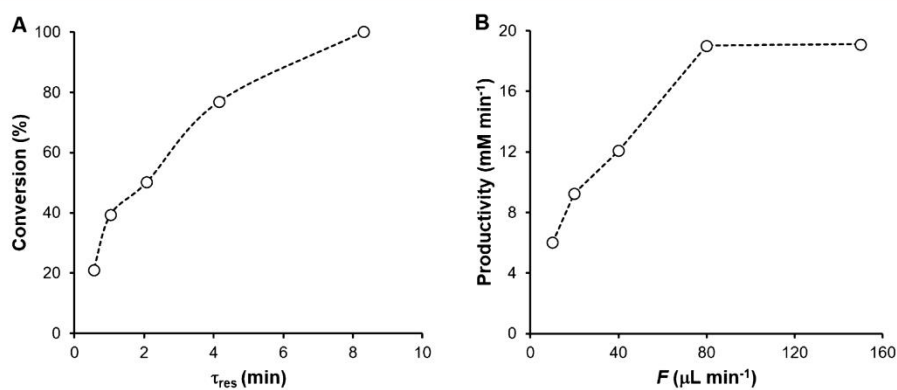


Figure 5. Performance analysis of the nanosprings- $\text{SO}_3^-$ -flowcell containing immobilized  $Z\_BISPase$  (100  $\mu\text{g}$ ) is shown. The substrate solution contained sucrose and phosphate (50 mM of each). The concentration of  $\alpha\text{Glc 1-p}$  released at steady state was measured. Conversion and productivity were calculated from the data.  $F$  was varied as indicated, and  $\tau_{res}$  was calculated with a volume  $V$  of 83  $\mu\text{L}$ . Results are from three independent experiments. Average values are shown with a standard deviation of 5%.

FITC, and analyzed with CLSM. Results are shown in Figure 4. A vertical cross-section image in panel A shows the nanosprings layer of about 70  $\mu\text{m}$  thickness (height) on the glass surface. Close-up images (panels B–E) from different points between top and bottom of the layer are also shown. The control was a

nanosprings- $\text{SO}_3^-$ -flowcell labeled with FITC but lacking the enzyme. It did not show fluorescence, thus validating the evidence in Figure 4. One recognizes immediately from Figure 4 that fluorescence was present all through the nanosprings layer, indicating that the enzyme was able to penetrate laterally

and vertically and so became distributed broadly across the solid matrix. Images in Figure 4 (panels B–E) reveal the increase in solid matrix density on moving from top to bottom of the nanosprings layer. The nanosprings material located closer to the glass surface exhibited areas in which nanosprings were extremely strongly interwoven with relatively large interstice in between (see Figure 4E). To the extent that fluorescence intensity informs about the amount of labeled protein present locally,  $Z\_BISPase$  seemed to be distributed somewhat uniformly in the nanosprings matrix irrespective of local differences in material density. The results in Figure 4 are from an immobilization of  $Z\_BISPase$  that used enzyme directly from the crude *E. coli* cell extract. To exclude the possibility of artifact, namely that FITC fluorescence in the nanosprings matrix was not from  $Z\_BISPase$  but actually from another *E. coli* protein, we repeated the experiment under exactly comparable conditions but used purified  $Z\_BISPase$  instead. The results are shown in Figure S3. Ability of  $Z\_BISPase$  to penetrate the nanosprings layer and become immobilized in it was confirmed unambiguously.

**3.2.3. Substrate Conversion in the Biocatalytic Microreactor Dependent on Liquid Flow Rate.** Flow chemistry involves the liquid flow rate  $F$  as a key process variable.  $F$  determines the average residence time ( $\tau_{res}$ ) via the relationship  $\tau_{res} = V/F$ , where  $V$  is liquid volume of reactor. Using  $Z\_BISPase$  immobilized in the nanosprings– $SO_3^-$ –flowcell, effect of  $F$  on substrate conversion at steady state was analyzed. Note that microreactor steady state implies time invariance of the substrate conversion at constant  $F$ . For each  $F$  used, therefore, it was ensured that steady state was maintained for a reaction time equivalent to 10 times the  $\tau_{res}$ . The change in  $F$  was achieved via ramp-up and ramp-down of the flow rate in the range  $10$ – $150 \mu L min^{-1}$ . Direction of the  $F$  excursion, up or down, did not affect the conversions obtained. Results are summarized in Figure 5.

The conversion increased dependent on  $\tau_{res}$  as expected from conventional fluidic behavior of a tubular reactor, and full conversion was reached within about 8 min. The productivity increased dependent on  $F$  to reach a maximum at  $80 \mu L min^{-1}$  or greater. Figure 5 shows that through systematic variation of  $F$ , the microreactor performance was switched between steady states of quantitative product yield ( $50 mM$ ; 100% conversion) and optimum productivity ( $19 mM min^{-1}$ ) at a lower product yield of about 40%. We previously showed a productivity of  $14 mM min^{-1}$  at a product yield of 50% when the same enzymatic conversion was performed in a meander-shaped fluid microchannel.<sup>19</sup> Increased productivity of the nanosprings– $SO_3^-$ –flowcell, even at a lower degree of miniaturization compared to the previously used microchannel reactor, emphasizes the efficiency of the nanosprings coating for enzyme immobilization.

**3.2.4. Enhanced Operational Stability of Enzyme Immobilized in Nanosprings Layer.** Operational stability represents a critically important parameter of efficiency of the enzymatic microreactor applied to continuous flow synthesis. Enzyme immobilization via the  $Z_{basic2}$  module is readily reversible by its design. However, lacking the high endurance of enzyme immobilization via covalent fixation, its stability under continuous operation is a problem requiring special attention. Besides actual loss of enzyme activity due to denaturation under conditions of use, limited operational stability might involve effect of washing out of the enzyme. We evaluated the operational stability of immobilized  $Z\_BISPase$  in time-course

experiments comparing the nanosprings– $SO_3^-$ –flowcell to the plain flowcell. The reaction setup ( $F = 40 \mu L min^{-1}$ ) was selected such that the  $\alpha Glc 1-p$  released at steady state was an immediate measure of  $E_{app}$ . The initial  $E_{app}$  was  $874 \pm 8 mU$  for the nanosprings– $SO_3^-$ –flowcell, while it was  $83 \pm 3 mU$  for the plain flowcell. The actual reaction time was normalized on  $\tau_{res}$  ( $= 2.08 min$ ) to show the number of reactor cycles run through. The results are shown in Figure 6.

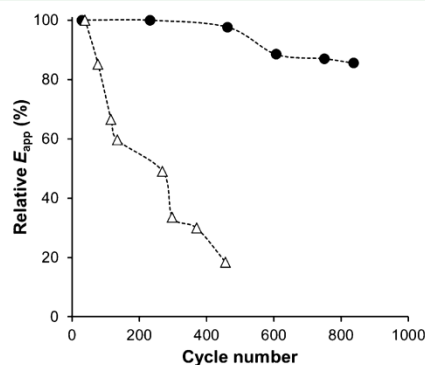


**Figure 6.** Comparison of nanosprings– $SO_3^-$ –flowcell (●) and plain flowcell (Δ) in terms of their operational stability is shown. Operational stability was evaluated as decrease in  $E_{app}$  over time. The total reaction time is expressed relative to the  $\tau_{res}$  of 2.08 min and given as number of reactor cycles. The conditions used were:  $F = 40 \mu L min^{-1}$ , 50 mM of each sucrose and potassium phosphate, 25 °C, and pH 7.0. Results are from three independent experiments. Average values are shown with standard deviation of 8%.

Using the nanosprings– $SO_3^-$ –flowcell, about 85% of the initial  $E_{app}$  was retained after 840 reactor cycles. Using the plain flowcell, by contrast,  $E_{app}$  decreased continuously to just 20% of the initial value after 450 reactor cycles. An operational half-life of about 269 cycles, equivalent to 560 min, was determined for  $Z\_BISPase$  immobilized in the plain flowcell. The corresponding half-life of enzyme immobilized in the nanosprings– $SO_3^-$ –flowcell was approximately 6160 min, representing a substantial 11-fold enhancement of stability. Because  $Z\_BISPase$  does not lose activity in the timespan of these experiments under the conditions used, the decrease in  $E_{app}$  solely reflects washing out of the immobilized enzyme. Enhanced operational stability of immobilized  $Z\_BISPase$  is therefore ascribed to the incorporation of the enzyme into the solid matrix of nanosprings of the glass surface. This is consistent with evidence obtained with other silica-based microreactors lacking the coating with nanosprings.<sup>19,36</sup>

#### 4. CONCLUSION

The current study demonstrates significant advance in enzyme immobilization in flow microchannels through well-coordinated designs of the enzyme and the material used. Design of the enzyme's molecular structure as to promote efficient "affinity-like" binding to silica surfaces involved fusion to the silica-binding module  $Z_{basic2}$ . Evidence for the  $Z_{basic2}$  fusion of *Bifidobacterium longum* sucrose phosphorylase herein obtained revealed that surface coating with a layer of silica nanosprings boosted the immobilization in flow microchannels in two important ways. First, enzyme binding was enhanced by an

order of magnitude or more as compared to binding to the plain wall surface of uncoated microchannels. Second, resistance of the (noncovalently) bound enzyme to washing out under conditions of continuous liquid flow was also enhanced compared to the plain surface reference, likewise by an order of magnitude or more. The surface layer of nanosprings was characterized in its morphology as a fibrous network of material that was readily penetrated by the enzyme. The enzyme efficiency factor, which is typically quite good ( $\geq 0.5$ ) for immobilizations to silica steered by the  $Z_{\text{basic}2}$  module, decreased to an unusually low value of 0.11 at high enzyme loadings into the silica nanosprings matrix. While the effect must wait further study for deeper understanding, a nanosprings synthesis mainly via lateral growth on the surface so as to lower the thickness of the final layer might help to increase the efficiency of the immobilized enzyme. Evidence from continuous reaction studies suggested that the microchannel reactor, containing enzyme immobilized on nanosprings-coated wall surface, is a flexible and powerful tool for both chemistry and chemical engineering to characterize and optimize biocatalytic transformations in flow. The operational stability of the continuous  $Z_{\text{BSPase}}$  reactor would enable over 1000 cycles (reactor volumes processed) to be performed with only a single load of enzyme. In summary, therefore, surface coating with silica nanosprings extends the possibilities for enzyme immobilization in flow microchannels. It effectively boosts the performance in biocatalytic synthesis of a microstructured reactor limited otherwise by the solid surface available for immobilizing the enzyme. The approach appears to be broadly applicable to different enzymes as well as microreactor designs.

### ■ ASSOCIATED CONTENT

#### 🔗 Supporting Information

The Supporting Information is available free of charge on the ACS Publications website at DOI: 10.1021/acsami.7b09875.

Evaluation of the theoretical maximum loading of enzyme on the plain microchannel, SEM images of the nanosprings-coated glass slide (Figure S1), SEM image of the cross-section of the nanosprings-coated glass slide (Figure S2), CLSM images showing purified enzyme immobilized in the nanosprings- $\text{SO}_3^-$  matrix (Figure S3) (PDF)

### ■ AUTHOR INFORMATION

#### Corresponding Author

\*Phone: +43 316 873 8400; Fax: +43 316 873 8434; E-mail: bernd.nidetzky@tugraz.at

#### ORCID

Martina Viehues: 0000-0002-7644-640X

Bernd Nidetzky: 0000-0002-5030-2643

#### Present Address

<sup>†</sup>M.V.: Experimental Biophysics and Applied Nanoscience, Faculty of Physics, Bielefeld University, 33615 Bielefeld, Germany.

#### Author Contributions

The manuscript was written through contributions of all authors. All authors have given approval to the final version of the manuscript. D.V., J.M.B. and B.N. designed the research. D.V. performed experiments and analyzed data. M.V. and E.X.V. designed and fabricated the flowcells. D.N.M. prepared

the nanosprings glass slide. D.V., J.M.B., and B.N. wrote the paper.

#### Notes

The authors declare no competing financial interest.

### ■ ACKNOWLEDGMENTS

Dr. Zdenek Petrasek (Institute of Biotechnology and Biochemical Engineering) assisted with the CLSM experiments. Financial support from the European Commission is gratefully acknowledged (Marie Curie ITN project EUROMBR, Grant 608104). D.N.M. acknowledges support of the United States Office of Naval Research (Grant N00014-16-1-2277).

### ■ ABBREVIATIONS

BET, Brunauer–Emmett–Teller  
 BSPase, sucrose phosphorylase from *Bifidobacterium longum*  
 CLSM, confocal laser scanning microscopy  
 FITC, fluorescein isothiocyanate  
 $\alpha\text{Glc 1-p}$ ,  $\alpha\text{-D-glucose 1-phosphate}$   
 PFE, perfluorinated elastomer  
 SBM, silica binding modules  
 SEM, scanning electron microscopy  
 $Z_{\text{BSPase}}$ , BSPase containing  $Z_{\text{basic}2}$  fused as SBM to the enzyme's *N*-terminus

### ■ REFERENCES

- (1) Liu, D.; Zhang, H.; Fontana, F.; Hirvonen, J. T.; Santos, H. A. Microfluidic-Assisted Fabrication of Carriers for Controlled Drug Delivery. *Lab Chip* **2017**, *17*, 1856–1883.
- (2) Mauk, M.; Song, J.; Bau, H. H.; Gross, R.; Bushman, F. D.; Collman, R. G.; Liu, C. Miniaturized Devices for Point of Care Molecular Detection of HIV. *Lab Chip* **2017**, *17*, 382–394.
- (3) Duncombe, T. A.; Tentori, A. M.; Herr, A. E. Microfluidics: Reframing Biological Enquiry. *Nat. Rev. Mol. Cell Biol.* **2015**, *16*, 554–567.
- (4) Lei, K. F.; Huang, C.-H. Paper-Based Microreactor Integrating Cell Culture and Subsequent Immunoassay for the Investigation of Cellular Phosphorylation. *ACS Appl. Mater. Interfaces* **2014**, *6*, 22423–22429.
- (5) Bhatia, S. N.; Ingber, D. E. Microfluidic Organs-on-Chips. *Nat. Biotechnol.* **2014**, *32*, 760–772.
- (6) Elvira, K. S.; i Solvas, X. C.; Wootton, R. C. R.; deMello, A. J. The Past, Present and Potential for Microfluidic Reactor Technology in Chemical Synthesis. *Nat. Chem.* **2013**, *5*, 905–915.
- (7) Adamo, A.; Beingessner, R. L.; Behnam, M.; Chen, J.; Jamison, T. F.; Jensen, K. F.; Monbaliu, J.-C. M.; Myerson, A. S.; Revalor, E. M.; Snead, D. R.; Stelzer, T.; Weeranoppanant, N.; Wong, S. Y.; Zhang, P. On-Demand Continuous-Flow Production of Pharmaceuticals in a Compact, Reconfigurable System. *Science* **2016**, *352*, 61–67.
- (8) Gemoets, H. P. L.; Su, Y.; Shang, M.; Hessel, V.; Luque, R.; Noël, T. Liquid Phase Oxidation Chemistry in Continuous-Flow Microreactors. *Chem. Soc. Rev.* **2016**, *45*, 83–117.
- (9) Wohlgenuth, R.; Plazl, I.; Žnidaršič-Plazl, P.; Gernaey, K. V.; Woodley, J. M. Microscale Technology and Biocatalytic Processes: Opportunities and Challenges for Synthesis. *Trends Biotechnol.* **2015**, *33*, 302–314.
- (10) Bolivar, J. M.; Wiesbauer, J.; Nidetzky, B. Biotransformations in Microstructured Reactors: More than Flowing with the Stream? *Trends Biotechnol.* **2011**, *29*, 333–342.
- (11) Laurenti, E.; dos Santos Vianna, A., Jr. Enzymatic Microreactors in Biocatalysis: History, Features, and Future Perspectives. *Biocatalysis* **2016**, *1*, 148–165.
- (12) Matosevic, S.; Szita, N.; Baganz, F. Fundamentals and Applications of Immobilized Microfluidic Enzymatic Reactors. *J. Chem. Technol. Biotechnol.* **2011**, *86*, 325–334.

- (13) Asanomi, Y.; Yamaguchi, H.; Miyazaki, M.; Maeda, H. Enzyme-Immobilized Microfluidic Process Reactors. *Molecules* **2011**, *16*, 6041–6059.
- (14) Luka, G.; Ahmadi, A.; Najjaran, H.; Alocilja, E.; DeRosa, M.; Wolthers, K.; Malki, A.; Aziz, H.; Althani, A.; Hoorfar, M. Microfluidics Integrated Biosensors: A Leading Technology towards Lab-on-a-Chip and Sensing Applications. *Sensors* **2015**, *15*, 30011–30031.
- (15) Sims, P. A.; Greenleaf, W. J.; Duan, H.; Xie, X. S. Fluorogenic DNA Sequencing in PDMS Microreactors. *Nat. Methods* **2011**, *8*, 575–580.
- (16) Kuchler, A.; Bleich, J. N.; Sebastian, B.; Dittrich, P. S.; Walde, P. Stable and Simple Immobilization of Proteinase K Inside Glass Tubes and Microfluidic Channels. *ACS Appl. Mater. Interfaces* **2015**, *7*, 25970–25980.
- (17) Bolivar, J. M.; Nidetzky, B. Smart Enzyme Immobilization in Microstructured Reactors. *Chim. Oggi Chem. Today* **2013**, *31*, 50–54.
- (18) de León, A. S.; Vargas-Alfredo, N.; Gallardo, A.; Fernández-Mayoralas, A.; Bastida, A.; Muñoz-Bonilla, A.; Rodríguez-Hernández, J. Microfluidic Reactors Based on Rechargeable Catalytic Porous Supports: Heterogeneous Enzymatic Catalysis via Reversible Host–Guest Interactions. *ACS Appl. Mater. Interfaces* **2017**, *9*, 4184–4191.
- (19) Valikhani, D.; Bolivar, J. M.; Pfeiffer, M.; Nidetzky, B. Multivalency Effects on the Immobilization of Sucrose Phosphorylase in Flow Microchannels and Their Use in the Development of a High-Performance Biocatalytic Microreactor. *ChemCatChem* **2017**, *9*, 161–166.
- (20) Bolivar, J. M.; Tribulato, M. A.; Petrasek, Z.; Nidetzky, B. Let the Substrate Flow, Not the Enzyme: Practical Immobilization of D-Amino Acid Oxidase in a Glass Microreactor for Effective Biocatalytic Conversions. *Biotechnol. Bioeng.* **2016**, *113*, 2342–2349.
- (21) Bolivar, J. M.; Krämer, C. E. M.; Ungerböck, B.; Mayr, T.; Nidetzky, B. Development of a Fully Integrated Falling Film Microreactor for Gas–liquid–solid Biotransformation with Surface Immobilized O<sub>2</sub>-Dependent Enzyme. *Biotechnol. Bioeng.* **2016**, *113*, 1862–1872.
- (22) Thomsen, M. S.; Nidetzky, B. Coated-Wall Microreactor for Continuous Biocatalytic Transformations Using Immobilized Enzymes. *Biotechnol. J.* **2009**, *4*, 98–107.
- (23) Tang, C.; Saquing, C. D.; Morton, S. W.; Glatz, B. N.; Kelly, R. M.; Khan, S. A. Cross-Linked Polymer Nanofibers for Hyperthermophilic Enzyme Immobilization: Approaches to Improve Enzyme Performance. *ACS Appl. Mater. Interfaces* **2014**, *6*, 11899–11906.
- (24) Betancor, L.; Luckarift, H. R.; Seo, J. H.; Brand, O.; Spain, J. C. Three-Dimensional Immobilization of Beta-Galactosidase on a Silicon Surface. *Biotechnol. Bioeng.* **2008**, *99*, 261–267.
- (25) dos Santos, J. C.; Barbosa, O.; Ortiz, C.; Berenguer-Murcia, A.; Rodrigues, R. C.; Fernandez-Lafuente, R. Importance of the Support Properties for Immobilization or Purification of Enzymes. *ChemCatChem* **2015**, *7*, 2413–2432.
- (26) Hartmann, M.; Kostrov, X. Immobilization of Enzymes on Porous Silicas – Benefits and Challenges. *Chem. Soc. Rev.* **2013**, *42*, 6277–6289.
- (27) Bolivar, J. M.; Nidetzky, B. Positively Charged Mini-Protein Z<sub>basic2</sub> As a Highly Efficient Silica Binding Module: Opportunities for Enzyme Immobilization on Unmodified Silica Supports. *Langmuir* **2012**, *28*, 10040–10049.
- (28) Jiang, Y.; Shi, L.; Huang, Y.; Gao, J.; Zhang, X.; Zhou, L. Preparation of Robust Biocatalyst Based on Cross-Linked Enzyme Aggregates Entrapped in Three-Dimensionally Ordered Macroporous Silica. *ACS Appl. Mater. Interfaces* **2014**, *6*, 2622–2628.
- (29) Rocha-Martín, J.; de las Rivas, B.; Muñoz, R.; Guisán, J. M.; López-Gallego, F. Rational Co-Immobilization of Bi-Enzyme Cascades on Porous Supports and Their Applications in Bio-Redox Reactions with In Situ Recycling of Soluble Cofactors. *ChemCatChem* **2012**, *4*, 1279–1288.
- (30) Denčić, I.; de Vaan, S.; Noël, T.; Meuldijk, J.; de Croon, M.; Hessel, V. Lipase-Based Biocatalytic Flow Process in a Packed-Bed Microreactor. *Ind. Eng. Chem. Res.* **2013**, *52*, 10951–10960.
- (31) Zhou, J.; Ellis, A. V.; Voelcker, N. H. Recent Developments in PDMS Surface Modification for Microfluidic Devices. *Electrophoresis* **2010**, *31*, 2–16.
- (32) Schilke, K. F.; Wilson, K. L.; Cantrell, T.; Corti, G.; McIlroy, D. N.; Kelly, C. A Novel Enzymatic Microreactor with *Aspergillus Oryzae*  $\beta$ -Galactosidase Immobilized on Silicon Dioxide Nanosprings. *Biotechnol. Prog.* **2010**, *26*, 1597–1605.
- (33) Fu, H.; Dencic, I.; Tibbe, J.; Sanchez Pedraza, C. A.; Wang, Q.; Noel, T.; Meuldijk, J.; de Croon, M.; Hessel, V.; Weizenmann, N.; Oeser, T.; Kinkeade, T.; Hyatt, D.; Van Roy, S.; Dejonghe, W.; Diels, L. Threonine Aldolase Immobilization on Different Supports for Engineering of Productive, Cost-Efficient Enzymatic Microreactors. *Chem. Eng. J. (Amsterdam, Neth.)* **2012**, *207–208*, 564–576.
- (34) Kengne, B.-A. F.; Alayat, A. M.; Luo, G.; McDonald, A. G.; Brown, J.; Smotherman, H.; McIlroy, D. N. Preparation, Surface Characterization and Performance of a Fischer–Tropsch Catalyst of Cobalt Supported on Silica Nanosprings. *Appl. Surf. Sci.* **2015**, *359*, 508–514.
- (35) Goedel, C.; Schwarz, A.; Minani, A.; Nidetzky, B. Recombinant Sucrose Phosphorylase from *Leuconostoc mesenteroides*: Characterization, Kinetic Studies of Transglucosylation, and Application of Immobilised Enzyme for Production of  $\alpha$ -D-Glucose 1-Phosphate. *J. Biotechnol.* **2007**, *129*, 77–86.
- (36) Viehues, M.; Sun, S.; Valikhani, D.; Nidetzky, B.; Vrouwe, E. X.; Mayr, T.; Bolivar, J. M. Tailor-Made Resealable Micro(bio)reactors Providing Easy Integration of in Situ Sensors. *J. Micromech. Microeng.* **2017**, *27*, 065012.
- (37) Bolivar, J. M.; Nidetzky, B. Oriented and Selective Enzyme Immobilization on Functionalized Silica Carrier Using the Cationic Binding Module Z<sub>basic2</sub>: Design of a Heterogeneous D-Amino Acid Oxidase Catalyst on Porous Glass. *Biotechnol. Bioeng.* **2012**, *109*, 1490–1498.
- (38) Bi, Y.; Zhou, H.; Jia, H.; Wei, P. A Flow-through Enzymatic Microreactor Immobilizing Lipase Based on Layer-by-Layer Method for Biosynthetic Process: Catalyzing the Transesterification of Soybean Oil for Fatty Acid Methyl Ester Production. *Process Biochem.* **2017**, *54*, 73–80.
- (39) Cullen, S. P.; Mandel, I. C.; Gopalan, P. Surface-Anchored Poly(2-Vinyl-4,4-Dimethyl Azlactone) Brushes as Templates for Enzyme Immobilization. *Langmuir* **2008**, *24*, 13701–13709.
- (40) Feng, Q.; Hou, D.; Zhao, Y.; Xu, T.; Menkhaus, T. J.; Fong, H. Electrospun Regenerated Cellulose Nanofibrous Membranes Surface-Grafted with Polymer Chains/Brushes via the Atom Transfer Radical Polymerization Method for Catalase Immobilization. *ACS Appl. Mater. Interfaces* **2014**, *6*, 20958–20967.

## Supporting Information

# A Spring in Performance: Silica Nanosprings Boost Enzyme Immobilization in Microfluidic Channels

*Donya Valikhani,<sup>‡</sup> Juan M. Bolivar,<sup>‡</sup> Martina Viefhues,<sup>§,†</sup> David N. McIlroy,<sup>⊥</sup> Elwin X.  
Vrouwe<sup>§</sup> and Bernd Nidetzky<sup>\*,‡, ¶</sup>*

<sup>‡</sup>Institute of Biotechnology and Biochemical Engineering, Graz University of Technology,  
NAWI Graz, Petersgasse 12, 8010 Graz, Austria

<sup>§</sup>Micronit Microtechnologies B.V., Colosseum 15, 7521 PV Enschede, The Netherlands

<sup>†</sup>Experimental Biophysics and Applied Nanoscience, Faculty of Physics, Bielefeld  
University, 33615 Bielefeld, Germany

<sup>⊥</sup>Department of Physics, Oklahoma State University, Stillwater, OK, 74078-3072, United  
States

<sup>¶</sup>Austrian Centre of Industrial Biotechnology, Petersgasse 14, 8010 Graz, Austria

Corresponding Author

\*Prof. Bernd Nidetzky, Institute of Biotechnology and Biochemical Engineering, Graz  
University of Technology, NAWI Graz, Petersgasse 12, A-8010 Graz, Austria; phone: +43  
316 873 8400; fax: +43 316 873 8434; e-mail: bernd.nidetzky@tugraz.at

## Supporting methods

### Evaluation of the theoretical maximum loading of enzyme on the plain microchannel

From the geometry of the microchannel patterned by the gasket, the plain flowcell is calculated to have a total surface area of 740 mm<sup>2</sup>. The overall dimension of the *B*/SPase molecule (Uniprot entry: Q84BY1) was assessed from the crystal structure of the homologous SPase from *Bifidobacterium adolescentis* (Uniprot entry: Q84HQ2, PDB code 1R7A). The total mass of the homodimeric *Z*\_B/SPase was calculated from the amino acid sequence using ProtParam tool. It was 132.83 kDa. The program PyMOL 0.99rc6 was used for protein structure visualization. The largest footprint of the enzyme was taken from an orthogonal rectangle projection and determined to be 64.31 nm<sup>2</sup>. The plain area of the plate divided by the enzyme area gave the maximum number of enzyme molecules immobilizable per plate ( $n = 1.15 \times 10^{13}$ ) which was transferred with Avogadro's constant ( $6.02 \times 10^{23}$ ), the size of the *Z*\_B/SPase and the specific activity of the enzyme ( $77 \text{ U mg}^{-1}$ ) into the theoretical activity loading per plate. Therefore, we calculated that  $B_{\max} = 2.54 \text{ } \mu\text{g}$  and  $\max_{E_{\text{app}}} = 0.19 \text{ U}$ .

Supporting Figures

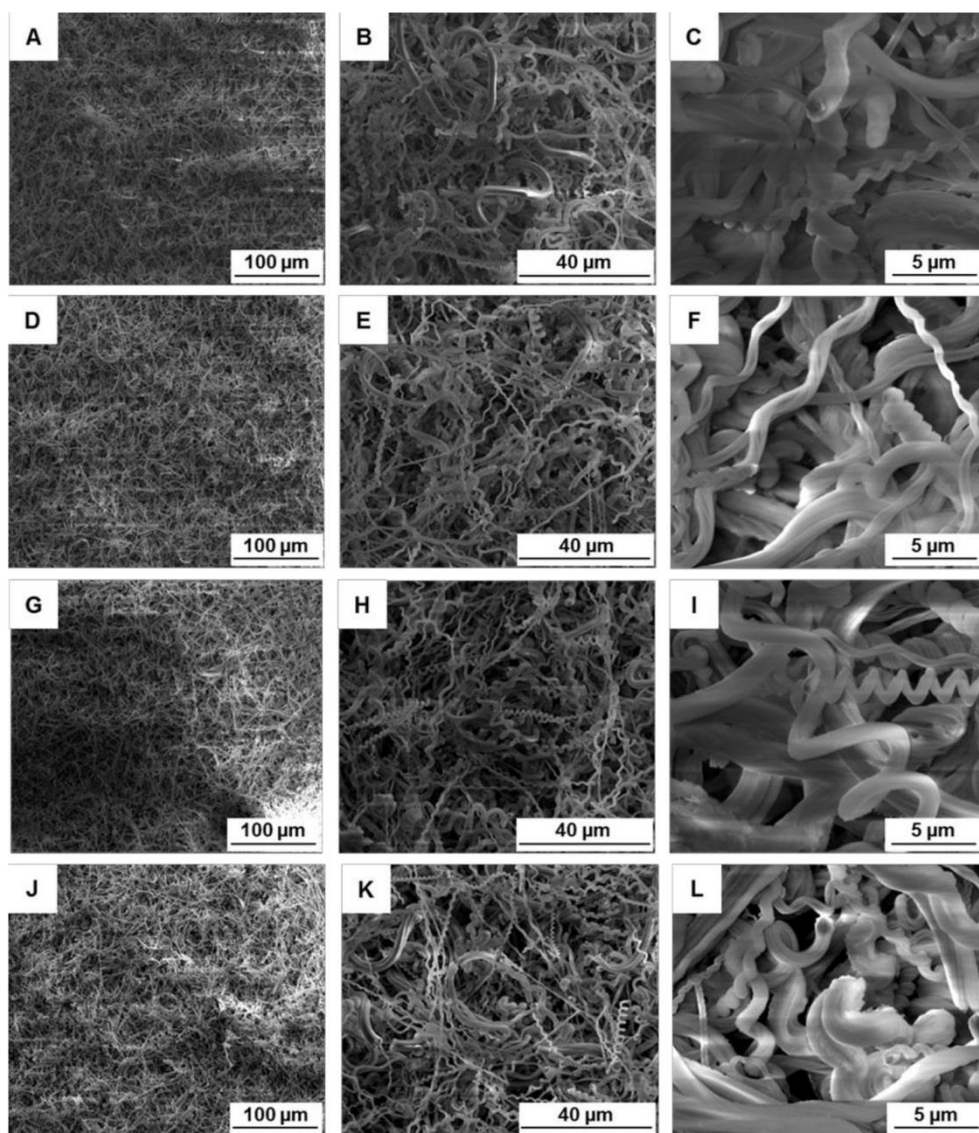


**Figure S1.** SEM images of the nanosprings-coated glass slide from different positions of the nanosprings matrix. Each row indicates one position at different magnifications.

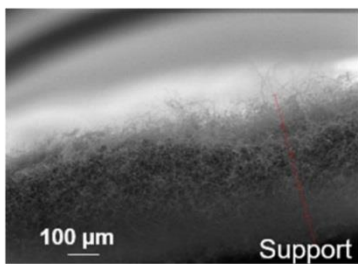


**Figure S2.** SEM image of the cross-section of the nanosprings-coated glass slide is shown. It is shown that the bottom areas of the nanosprings are denser than the top ones.

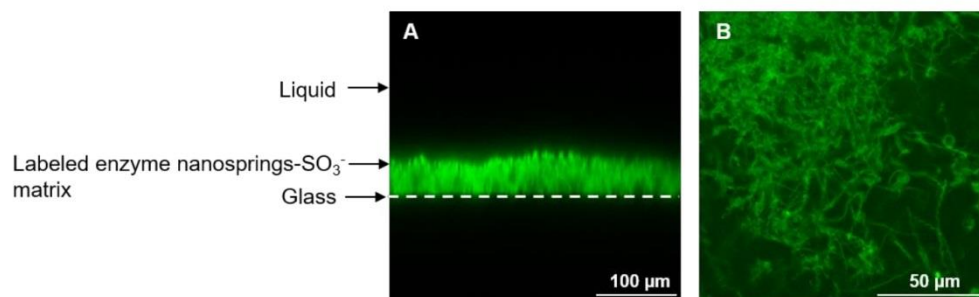


**Figure S3.** CLSM images showing purified enzyme immobilized in the nanosprings-SO<sub>3</sub><sup>-</sup> matrix.

**Tailor-made resealable micro(bio)reactors providing easy integration of *in situ* sensors**

# Tailor-made resealable micro(bio)reactors providing easy integration of *in situ* sensors

Martina Viefhues<sup>1,5</sup>, Shiwen Sun<sup>2</sup>, Donya Valikhani<sup>3</sup>, Bernd Nidetzky<sup>3,4</sup>,  
Elwin X Vrouwe<sup>1</sup>, Torsten Mayr<sup>2</sup> and Juan M Bolivar<sup>3</sup>

<sup>1</sup> Micronit Microtechnologies BV, 7521 PV Enschede, Netherlands

<sup>2</sup> Applied Sensors group, Institute of Analytical Chemistry and Food Chemistry, Graz University of Technology, 8010 Graz, Austria

<sup>3</sup> Institute of Biotechnology and Biochemical Engineering, Graz University of Technology, NAWI Graz, 8010 Graz, Austria

<sup>4</sup> Austrian Centre of Industrial Biotechnology, 8010 Graz, Austria

<sup>5</sup> Current address: Bielefeld University, Experimental Biophysics and Applied Nanosciences, Faculty of Physics, 33615 Bielefeld, Germany

E-mail: [elwin.vrouwe@micronit.com](mailto:elwin.vrouwe@micronit.com)

Received 6 February 2017, revised 20 April 2017

Accepted for publication 24 April 2017

Published 10 May 2017



CrossMark

## Abstract

Flow microreactors utilizing immobilized enzymes are of great interest in biocatalysis development. Most of the common devices are permanently closed, single-use systems, which allow limited physical and chemical surface modifications and evaluation methods. In this paper we will present resealable flowcells that overcome these limitations and moreover allow a quick and easy integration of sensor systems, because of the use of modular building blocks. The devices were utilized to study the enzyme activity of glucose oxidase immobilized on chemically modified glass surfaces under flow conditions, employing integrated optical oxygen sensors for on-line monitoring.

Keywords: micro(bio)reactor, glucose oxidase, modular system, oxygen sensor, resealable flowcell

 Supplementary material for this article is available [online](#)

(Some figures may appear in colour only in the online journal)

## 1. Introduction

One field of applications of microfluidic flowcells is the screening and characterization of biocatalytic processes at small scale. Microfluidic devices provide a huge surface area to volume ratio, thus they represent a clear opportunity for surface-immobilized enzyme microreactors [1–5]. The latter also can be used for continuous flow operations [2, 6–8]. In addition, the control over temperature and reaction time is improved compared to conventional batch reactors using enzymatic reactions. Also the diffusion distances are reduced, which provides a potentially better mixing and contact with the reaction substrates. Implementation of enzyme immobilization in microreactors still faces many drawbacks, especially when different approaches, e.g. surface functionalizations, are to be studied systemically [9–11].

The ideal micro(bio)reactors provide highly customizable flow paths and controlled surface modification, e.g. different enzymes can be immobilized at localized areas of the device. Most of the flowcells and micro(bio)reactors that are commercially available are made of glass, plastics, silicon or combinations of these materials [12]. The majority of the devices have in common that they consist of permanently closed systems and the only way to access the inside of the channels is through the inlet and outlet [11, 13–15]. Thus localized modifications are challenging and need a huge effort in order to develop surface modification processes and analysis tools. Additionally, those flowcells have a one directional, linear path from development to application in common, which is defined by the conception and design, the production and sensor integration followed by enzyme immobilization and characterization.

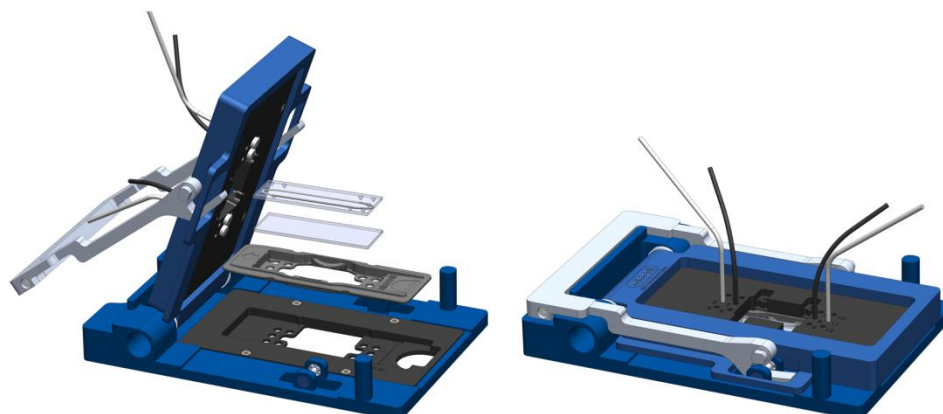


**Figure 1.** Drawing of the holder used for the experiments. (Left) exploded view of the resealable flowcell in the open holder with the tubings and optical fibers connected. (Right) drawing of the closed holder.

Resealable devices, thus, devices that could be sealed and reopened, are presented in [16–20]. Tkachento *et al* and Reichen *et al* used devices [16, 18] that were made of PDMS using soft lithography. Their master molds were made by means of either photo lithography or micromilling. Alam *et al* used PDMS as gasket material to form a flowcell that could be reopened [20]. However, PDMS is not compatible for many organic solvents as used for cleaning and sterilization [21]. The devices in [17, 19] were made by micromilling of PMMA and plastics and needed specific gaskets to form tight seals. The milling process enables easy adaptation of the device layout, but the need for separate gasket rings, of exact flowcell geometry, limits the flexibility. A new approach of fabricating microfluidic devices towards more flexible, modular systems can therefore improve biocatalysis studies fundamentally.

The goal was to develop a new fabrication strategy for highly customizable resealable flowcells for applications in enzyme reaction studies, with at the same time high reproducibility. The new flowcells constitute a modular system, since individually components can be suited independently and then assembled. The idea behind the modular system was that separate features can be optimized individually to build tailor-made layouts. This modular system in its current form was composed of two parts combining to form a resealable flowcell. One part forms the microfluidic structures utilizing chemically inert elastomers and the second part is used to close the system, see figure 1. Both parts can be designed and modified independently from each other, as long as the outer boundaries are identical. Thus, the inner surfaces of the flowcell could be functionalized for example with combinations of enzymes to study heterogeneous catalysis and with *in situ* sensor elements like electrodes or chemical sensing layers. The microfluidic structures were fabricated by dispensing onto the substrates a pre-polymer that is cured to form an elastomer. The new fabrication strategy offers great utility for many microfluidic users due to its ability for quick and easy adaptation of designs. Moreover, easy connecting and disconnecting of the modules enables effective characterization of modified surfaces.

The applicability of the resealable flowcells for enzyme studies was assessed using a heterogeneous biocatalysis with glucose oxidases (GOX) as a model system, which has an immediate need to have an *in situ* advanced sensing [22] due to the oxygen dependence. The new device provided easy integration of *in situ* sensor features. The modular approach makes it possible to decide for each experiment which type of sensor would be suitable. Super *et al* connected a separate oxygen probe device *via* Luer-lock adapters to their microfluidic cultivation chip to monitor the oxygen consumption [23]. Nevertheless, integration of the oxygen sensor directly in the reaction region would offer better control of processes. The impact of different surface activation methods on the enzyme immobilization was studied. The amount of immobilized activity and stability were the observed parameters for three surfaces with different surface modifications. The enzyme activity was determined using off-line and on-line methods.

In this work, integration of oxygen sensors is shown for prove of concept of easy surface modification. A luminescence lifetime measurement was used for accurate oxygen monitoring. The oxygen sensing layer was deposited in a well-controlled way in the area of interest for that purpose. With the integrated oxygen sensor the oxygen permeability of the resealable flowcells, which might impact oxygen sensitive reactions, was analyzed. Finally, integration of an oxygen sensor provided a better insight view of the enzymatic behavior with respect to substrate limitations as well as long-term stability measurements.

## 2. Materials and methods

### 2.1. Fabrication of resealable flowcells

The gasket was made by dispensing a liquid prepolymer onto a borosilicate glass (Schott, Germany) surface, which, when cured, forms an elastomer. The gasket was made from two types of material: perfluorinated elastomer (PFE) or medical grade silicone (MED). The pre-polymers were cured by heating the material for 10min on a hotplate set to 140

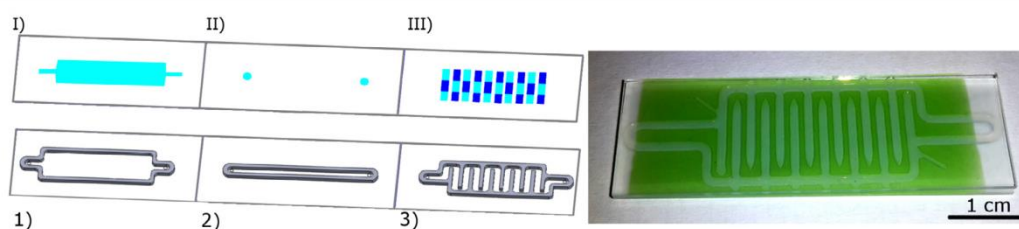


**Figure 2.** (Left) examples of various modules that could be combined to form a tailor-made flowcell. One module from section I–III and one from section 1–3 were selected and stacked. (I) Represents a homogeneous surface modification, e.g. with catalytic biomolecules or sensing layers. (II) Represents a modification for spot measurements. (III) Represents a heterogeneous surface modification, e.g. with two different enzymes. These modifications could also be applied to the fluidic part, i.e. 1–3. (Right) microfluidic chip with meandering channel and oxygen sensing layer (green) as used for the experiments. Please note, this example chip did not contain the access through holes.

°C. Both materials were tested with respect to the chemical resistance against organic solvents and mild acids and bases often used in biocatalytic and enzymatic reactions, i.e. ethanol, isopropanol, acetone, methanol, sodium hydroxide, and hydrochloric acid. Incubation of the flowcells in those chemicals for 60 min did not affect the size, shape or sealing ability of the gaskets.

The outer dimensions of the glass plates were 15 mm × 45 mm and the thickness was 1.1 mm for the top part and 0.7 mm for the bottom part. The top glass slide was equipped with through holes at well-defined positions with respect to the gasket structure forming the fluidic inlet and outlet.

The two modular parts were stacked, shown in figure 1, and placed into a fluidic connect pro chip holder (Micronit Microtechnologies, The Netherlands), which compressed the stack, resulting in a liquid tight seal. The 10 mm wide straight and the meandering channel (structures 1 and 3 in figure 2) were used in combination with either plain glass slides or slides covered with oxygen sensors, see section 2.4. The test setup for determining the leakage pressure of the resealable flowcells, was composed of the flowcell in the holder, a syringe pump with water connected to the flowcell, a pressure sensor connected in series to the flowcell, and a capillary downstream of the resealable flowcell to generate a back-pressure.

## 2.2. Surface functionalization

Before use, the surfaces of the top and bottom part could be functionalized with enzymes or sensing layers, see figure 2. Two surface activation protocols were used for the generation of an amino-activated surface on the glass. Glucose oxidase was subsequently immobilized on the modified surfaces by ionic adsorption.

**2.2.1. Surface functionalization with APTES and PEI.** The first step of the surface functionalization of the top part, containing the gasket, was to clean and remove organic residues. The disassembled flowcell was immersed in a mixture of methanol/HCl (1:1) for 30 min, rinsed with deionized water, immersed in sodium hydroxide solution (1 M in water) for 30 min and rinsed with deionized water again. Finally, the flowcell was rinsed with 50 mM potassium phosphate buffer

(PPB), pH 7.0. For the N-(2-aminoethyl)-3-aminopropyltriethoxysilane (APTES) functionalization the procedure described in [24] was followed.

The poly(ethyleneimine) (PEI) surface functionalization was started by incubating a cleaned disassembled flowcell in 5% (v v<sup>-1</sup>) solution of (3-glycidyloxypropyl)trimethoxysilane, pH 8.5, for 16 h at 25 °C as described in [24]. Afterward, the glass slides were rinsed with deionized water and incubated in a solution of 0.1 g ml<sup>-1</sup> PEI in water, pH 10.0, at room temperature while gently stirred in an end-over-end rotator. Finally, rinsing with ethanol and deionized water removed weakly bound residues. The surface functionalization also could be performed in an assembled flowcell if only specific regions should be modified, e.g. as shown in figure 2(I).

**2.2.2. Enzyme immobilization procedure.** Enzymes were immobilized on non-modified glass surfaces and surfaces with APTES or PEI functionalization. The flowcell part was placed into enzyme immobilization mixture (6 U ml<sup>-1</sup> GOX in 50 mM PPB, pH 7.0), and incubated for 2 h without agitation at room temperature. After that, the flowcell was assembled and flushed with 50 mM PPB, pH 7.0, at a flow rate of 50 μl min<sup>-1</sup> using a syringe pump to remove enzyme that was not strongly bound to the surface. The effluent was analyzed by a coupled peroxidase assay.

## 2.3. Determination of enzyme activity by colorimetric assay

The activity of GOX was analyzed by a coupled peroxidase assay, i.e. colorimetric assay, which was performed as described elsewhere [24]. A quinonediimine dye was used for the activity determination, see SI for more information.

The activity of GOX immobilized in the resealable flowcells was analyzed off-line by flushing the assay mixture through the flowcell, containing the immobilized enzyme, and collecting the effluent at the outlet. The collected samples were stored on ice to quench the reaction in case enzyme was eluted. Afterward, the collected volume was analyzed spectrometrically to determine off-line the hydrogen peroxide concentration. The hydrogen peroxide concentration formed was used to calculate the volumetric activity (U ml<sup>-1</sup>). The volumetric activity is defined as the amount of hydrogen peroxide produced (mM) per applied residence time. Note: one activity

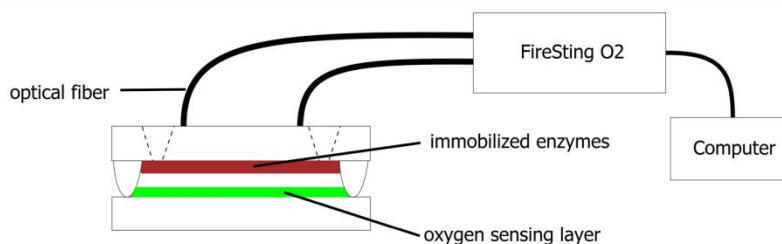


**Figure 3.** Setup for on-line spot oxygen consumption measurement. An oxygen sensitive layer was integrated into the resealable flowcell. Optical fibers were led to the spots of interest through the top of the holder and the signals were monitored in real-time.

unit (U) is the amount of GOX that produces  $1 \mu\text{mol min}^{-1}$  hydrogen peroxide or consumes  $1 \mu\text{mol min}^{-1}$  oxygen at the conditions used. This procedure is referred to as continuous coupled peroxidase assay.

#### 2.4. Oxygen sensing

On-line oxygen consumption monitoring and imaging was conducted by integrating oxygen sensor layers into the resealable flowcells. The resealable flowcell was disassembled and the oxygen sensor layer was deposited by spray coating an oxygen sensor cocktail on a roughened glass slide, to be used for closing the resealable flowcell. The oxygen sensor cocktail was made by dissolving the oxygen sensitive dye, platinum(II) meso-tetra(4-fluorophenyl)tetrabenzoporphyrin (PtTPTBP) [25], and silicone rubber adhesive E4 (DRAWIN Vertriebs-GmbH, Germany) in chloroform [26].

Spray coating was done with a custom built device as described in [26]. The airbrush was led over each substrate in spirals to cover the whole area inside the flowcell with sensor material. Adequate layer thickness was verified by checking the signal intensity.

An optical fiber (tip diameter 1 mm) was directed to the outer surface of the resealable flowcell, see figure 3. The optical fibers were led through access holes in the chip holder and connected to an oxygen meter 'FireStingO2' (PyroScience, Germany) for the spot on-line oxygen monitoring. The theory of optical oxygen sensing is described in the supplementary information ([stacks.iop.org/JMM/27/065012/mmedia](http://stacks.iop.org/JMM/27/065012/mmedia)).

Time-resolved oxygen imaging of a large area was performed using a PCO sensiCam (PCO, Kehlheim, Germany) for rapid lifetime determination (RLD) as described by Moser *et al* [27]. A blue ultra-bright LED with emission maximum at 450 nm (Luxeon Lambert emitter, 5 W, Germany) was applied as the triggered excitation light source for phosphorescence lifetime imaging and combined with a filter set consisting of Schott BG12 and Schott RG 9 (Schott, Germany) as the excitation filter and barrier filter, respectively.

Before starting the measurement the sensing system was calibrated using a two-point calibration. The flowcell, containing the sensing layer, was flushed with air-saturated buffer to determine the phase shift between excitation and emitted light. Afterward, the flowcell was flushed with deoxygenated buffer to again determine the phase shift.

The activity of immobilized enzyme was determined by flushing 100 mM glucose through the flowcell whilst monitoring the oxygen concentration near the inlet and outlet. The amount of oxygen consumed by the enzyme was calculated from the difference between the two signals and the volumetric activity was calculated by the consumed oxygen concentration per applied residence time.

**2.4.1. Long-term stability test of immobilized GOX-flowcell.** The long-term stability of GOX immobilized in a PEI functionalized resealable flowcell was studied by monitoring the oxygen consumption for 24 h. To decrease deactivation of the oxidase by hydrogen peroxide that is produced during the experiment  $0.01 \text{ mg ml}^{-1}$  catalase was added to the substrate solution, consisting of 100 mM glucose in 50 mM PPB, pH 7.0. This mixture was then pumped through the flowcell, whilst simultaneously monitoring the oxygen concentration. The mixture was recirculated for 24 h at a flow rate of  $20 \mu\text{l min}^{-1}$  with a HPLC pump.

### 3. Results

#### 3.1. Resealable flowcells

**3.1.1. Fabrication of resealable flowcells.** The goal was to produce a micro(bio)reactor that provides easy access to the inside surfaces during the pre- and post-processing steps. The sealing method needs to be compatible with biological materials when these are present on the surfaces before sealing, i.e. excluding the use of high temperatures and pressures or organic solvents. Additionally, the production should allow customization. Therefore, the concept of a resealable flowcell was developed where an elastomeric gasket on a glass slide defines the shape of the flow path and the flowcell is closed with a second glass slide, see figure 1. A leak tight sealing was achieved by mechanical compression using a holder (fluidic connect PRO), hence no permanent bonding of the layers was necessary.

In this work, we used the heat curing materials PFE and MED for the gaskets. Additionally, to heat curing elastomers also UV curing materials could be used easily, for example polyurethane methacrylate (PUMA).

The elastomeric gaskets were made by dispensing a prepolymer onto a glass slide, using a dispensing robot, and curing it. For instance, the programmed dispensing

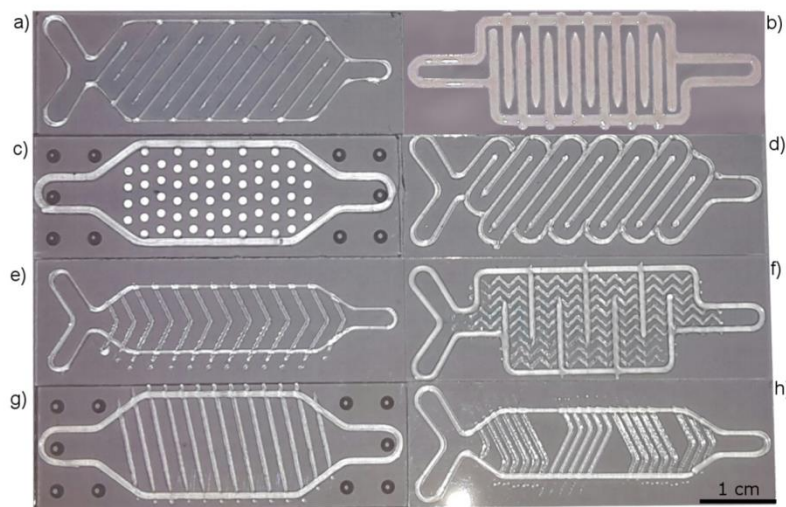


**Figure 4.** Various layouts of structured flowcells that have been successfully fabricated. The structures in (a)–(d) are all of the same height on a single device. In (e)–(f) the structures inside the outline are lower than the height of the outline.

path defines the final gasket layout, see also figure S11. Thus, no soft lithographic or casting steps were necessary. Moreover, this is a very efficient use of materials since almost no material is wasted. The gasket height was controlled by the dispensing parameters, like the *x/y*-writing velocity and the applied supply pressure.

The advantage of the production using a dispensing robot was that it allowed very fast prototyping since the layout of the part could be exported to the instrument directly. Figure 4 displays a few examples of layouts that have been fabricated successfully. The ease to adapt the fabrication to different layouts on demand is a powerful asset.

To prove the very good reproducibility of the dispensing production 425 PFE flowcells were made with a single loop, shown in figure 2(1), during a period of several months and the gasket height was measured. With the dispensing robot set to dispense a 355  $\mu\text{m}$  high gasket, the resulting mean height was 354  $\mu\text{m}$  with a standard deviation of 6  $\mu\text{m}$ , illustrated in figure S12. The total thickness variation for a single flowcell was within instrumental error. The final flowcell height strongly depended on the compression of the gasket. Measurements of 354  $\mu\text{m}$  gaskets revealed a compression of about 10% for usage of the Fluidic Connect Pro holder.

We achieved a minimum channel width of 450  $\mu\text{m}$  in a meandering channel with a PFE gasket, at a height of 354  $\mu\text{m}$ . However the minimum height strongly depends on the gasket material and the dispensing tip, see also SI. So far, the thinnest gasket that led to a sealing flowcell was 70  $\mu\text{m}$  in height.

More complex structures can be made as shown in figure 4 in order for example to elongate the path length through the flowcell or serve to assist in mixing or trapping microparticles.

Regarding resealable flowcells with inner structuring one can further distinguish between features that are all of the same height as the outer border, e.g. forming a meandering channel, and features that do not extend to the bottom of the

flowcell, e.g. forming ridges. For the latter ones it needed to be taken into account that the elastomeric gasket was compressed when placed inside the holder, thus, the compressed height of the flowcell structure had to be higher than the ridges in order not to block the fluidic path completely.

**3.1.2. Sealing performance under pressurized flow.** A reliable device has to be leak tight for the pressures used during the experiments. For applications with biological samples, e.g. cells, or with enzymes the shear stress and the maximum pressure have to be limited, the latter to about 0.3 bar, to not degrade the samples or destroy weak bindings.

Flowcells were fabricated using two different elastomers to form the gasket consisting of a single closed loop and the maximum operating pressure was determined. During the experiments it was found that the absolute height deviation along a single structure had to be less than 10  $\mu\text{m}$  to get a tightly sealing flowcell. Figure S13(a) depicts the results from 14 flowcells, all made of PFE and with a gasket height of 354  $\mu\text{m}$ . The leakage pressure of the flowcells was 0.7 bar  $\pm$  0.1 bar, which is higher than the typical maximum pressures used in biological or enzymatic applications [28–30]. Hence, a reliable and reproducible sealing performance of the resealable flowcells was observed proving the suitability for micro(bio) reactors.

Additional experiments using a higher clamping force revealed that the leakage pressure could be increased (results not shown here). The only limitation was the stability of the glass slides as they bent and broke for a too high clamping force. This might be prevented when using additional supporting layers.

Meandering channels, illustrated in figure 4(b), were tested as well and exhibited leakage pressures above 0.45 bar (figure S14), which was less than for straight flowcells of the same height but still sufficient for many applications. An

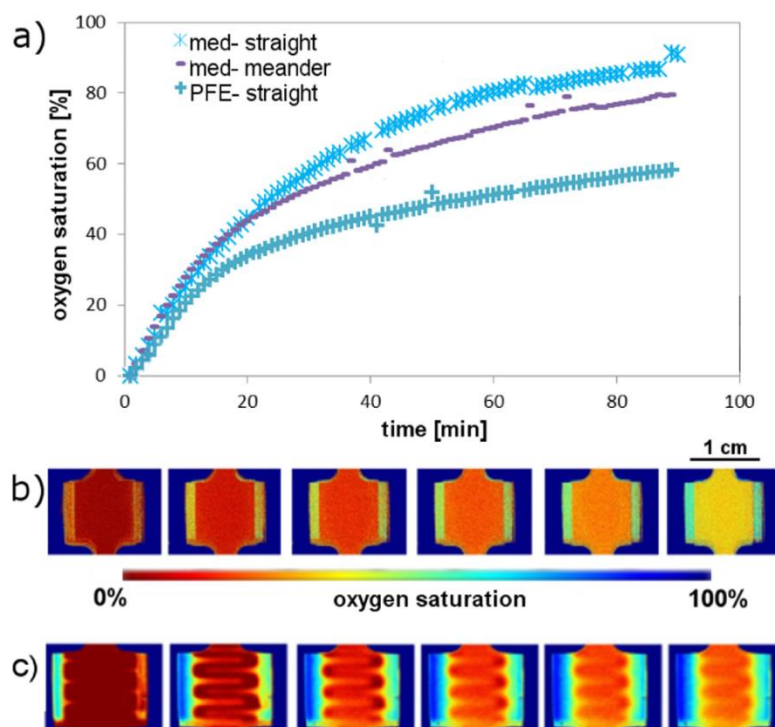


**Figure 5.** Evaluation of the oxygen transfer through the gasket. (a) Oxygen resaturation versus time in the gas phase, two different layouts, straight (figure 2(1)) and meandering (figure 2(3)), and two different materials, PFE and medical silicone. (b) Time-lapse pictures of the first 6 min, 1 per min, of resaturation in the gas phase for a meandering MED channel. A 8 pixel by 8 pixel region of interest was chosen in the center of the fluorescence lifetime image for the numerical evaluation in (a). (c) Time-lapse pictures of the first 6 min, 1 picture per minute, of resaturation in water for a meandering MED channel.

explanation of the reduced pressure resistance is that slight height variations were observed at the regions where two lines cross each other. This was also in accordance with the observation that the leakage pressure demonstrated poor correlation with the gasket height since the height deviation at the crossing points was almost independent from the total gasket height. In addition, the larger contact area between the gasket and cover resulted in less compression of the gasket. Instead the elastic ferrules connecting the tubing to the flowcell would be compressed more and the glass or support structure in the holder underneath the flowcell could bend.

Flow rates of  $8 \text{ ml min}^{-1}$  have been tested in a single loop flowcell without observing a leakage for a gasket height of  $355 \mu\text{m}$ . This was in good agreement with calculated flow rates of  $7 \text{ ml min}^{-1}$  for a hydrodynamic pressure of 0.7 bar and  $8 \text{ ml min}^{-1}$  for 0.8 bar. Since the devices are aimed at bio or enzymatic applications, no higher flow rates have been tested according to the very high shear stress that would apply to the surfaces of the bio or enzymatic samples. Moreover, the resulting residence time would be too short for oxygen consumption by immobilized enzymes. Nevertheless, with the right combination of gasket material and thickness a maximum operating pressure up to 2.4 bar was achieved.

### 3.2. Applications of surface modifications

So far the general concept of resealable flowcells and a characterization of them, with respect to production and sealing performance, have been presented. The results demonstrate the versatility of the production method to create customized devices. In the previous section this was shown for the fluidic path, but this also applies for surface modifications with enzymes or sensor layers.

**3.2.1. Oxygen transfer through the gasket.** The oxygen transfer through the gasket was determined in gas phase as well as in liquid phase. For the gas phase the flowcell with a meandering gasket made from MED and straight flowcells made of PFE and MED were tested. We flushed the flowcell with nitrogen until no oxygen was measured. Then the nitrogen flow was stopped and the connections were closed. Phosphorescence lifetime images were recorded every minute (demonstrated in figure 5(b)) and the oxygen saturation level was plotted versus time (figure 5(a)). To measure oxygen resaturation of an aqueous phase, de-oxygenated water was flushed through the flowcell. The flowcell was closed and phosphorescence lifetime images were taken, at an interval of one minute.

Figure 5(a) reveals that the oxygen transfer rate through the gasket was different for all configurations. The medical silicone exhibited a higher oxygen transfer rate than the PFE when comparing structures of the same gasket height. This is assumed due to the following reasons; first, the medical silicone had narrower gasket widths than the PFE reducing the diffusion distance, and second, the medical silicone could have a higher gas permeability. A comparison of the straight and meander channels made of MED revealed that the straight channel exhibited a faster resaturation. One reason for the faster resaturation of that channel was because the oxygen could diffuse more freely without the ridges.

Regarding the re-oxygenation of water, figure 5(c), it was significantly slower than in gas phase, figure 5(b). The MED resealable flowcells reached 50% oxygen saturation after thirty minutes in the gas phase, whereas in the liquid phase the mean oxygen saturation after thirty minutes was about 20%, see figure S15. In water there was a clear gradient visible from the channel wall to the center of the channel. In contrast, no gradient was visible for the gas phase, figure 5(b). This is assumed to be due to the much faster diffusion of oxygen in air versus water.

The results of the permeability test proved two things. First, the gaskets made of PFE and MED are oxygen permeable, but the re-oxygenation is very slow and in many applications the consumption of oxygen would be higher than the replenishing. Second, a concentration gradient over the flowcell will appear in oxygen consumption applications, which might not be desirable. Additionally, we have shown that integrating oxygen sensing layers inside of the flowcell is a powerful analytical tool. It provided information of the oxygen distribution over the whole chamber, as well as further information on oxygen related enzymatic reactions.

**3.2.2. Surface modifications for enzyme immobilization.** The modular concept of the resealable flowcells provides easy access to the internal surfaces of the devices. This feature was exploited to apply specific surface functionalization on the glass to increase the binding capacity and stability of enzymes.

The use of AAPTES- and PEI-linkers was investigated to functionalize the surface and introduce binding sites for the glucose oxidase. During surface modification the resealable flowcell was disassembled and the top parts were immersed in the functionalization mixture. This offered several advantages compared to closed systems. The first advantage was that by this procedure a homogeneous distribution of linker molecules could be achieved easily because the functionalization mixture was not flushed through a closed system, which could have led to different linker concentrations at the inlet compared to the outlet. Furthermore, several disassembled flowcells could be treated simultaneously in the same vessel whereas for closed systems that might be tedious because each cell needs to be connected to a pump.

During the PEI modification a precipitation was observed in some devices, which would lead to blockage in permanently closed channel systems. This can be very complicated if the device cannot be cleaned properly. In contrast, the resealable flowcells offer an easy access to the inner surfaces when

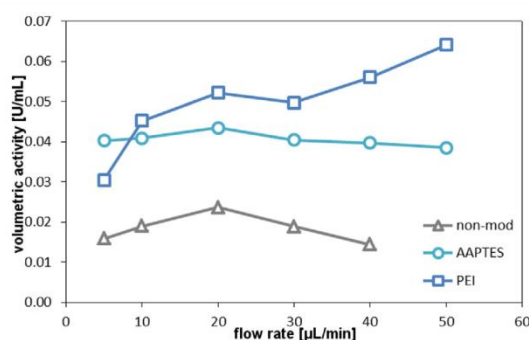


**Figure 6.** Volumetric activities of glucose oxidase modified flowcell as function of the flow rate with different activated surfaces -non-modified bare glass, AAPTES modified, and PEI modified. Assay mixture was flushed through the resealable flowcell and collected at the outlet. The volumetric activity was calculated via the hydrogen peroxide formed (see experimental information for more details, section 2.3).

disassembled. Thus, those could be cleaned thoroughly and even precipitated material could be removed.

GOX was subsequently adsorbed on bare glass surfaces activated with AAPTES or PEI. Increased binding capability and stability were expected for the linker functionalized surfaces. This was confirmed by performing a continuous coupled assay, figure 6. The volumetric activity was then calculated, section 2.3.

The enzyme activity was higher for surfaces with modification than for the bare glass surface and the PEI modification resulted in a higher activity than the AAPTES coating. The increased binding for the amino-linker functionalized surfaces compares well with literature [31, 32]. It was observed that the activity in the non-modified flowcell and AAPTES modified one significantly decreased for higher flow rates. The decreased activity can be explained via desorption of enzymes or inactivation. This behavior was not observed for the PEI modified flowcell. However, the off-line approach did not allow differentiating between these effects and the contribution of eluted enzyme to the detected hydrogen peroxide was unknown.

It is important to note that each flow cell was submitted to a wash-off procedure (see experimental section) to completely elute the bound enzyme. Hence, the flowcells could be used for several rounds of immobilization/elution without difference between the experiments. Results shown here are representative of multiple experiments.

### 3.3. Advanced characterization—on-line sensing

In the previous sections the modular feature of the resealable flowcells, the ease for tailor-made surface modifications, and the ability to perform enzymatic binding and activity studies have been shown. Beyond that all those features were combined, i.e. one surface of the resealable flowcell (meandering channel made of MED) has been modified with an amino functionalization followed by immobilization of

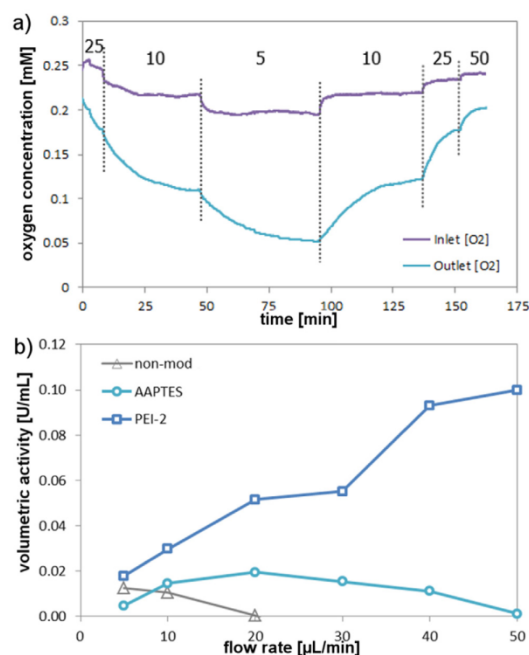


**Figure 7.** On-line monitoring with integrated oxygen sensor. (a) Two point on-line monitoring of oxygen concentration at the inlet and outlet. GOX was bound to a PEI modified surface and a glucose mixture was flushed at different flow rates through the resealable flowcell, whilst the oxygen consumption was monitored simultaneously. The vertical lines indicate changes of the flow rates in the range of 50 to 5  $\mu\text{L}/\text{min}$ . (b) Volumetric activity of GOX, bound to different modified surfaces, calculated from the oxygen consumption.

GOX on that surface and the second surface of the resealable flowcell has been modified with an oxygen sensing layer. This enabled an advanced characterization of the enzymatic microreactor.

In figure 7(a) the oxygen concentration is shown for a resealable flowcell with GOX immobilized on a PEI modified surface. The oxygen concentration has been monitored at the inlet and at the outlet of the flowcell. Via the on-line monitoring a change in the oxygen consumption depending on the flow rate became visible. The flow rate, thus, the residence time depending oxygen concentration at the inlet was due to GOX immobilized in the region between the inlet and the position of the optical fiber 5 mm downstream of the inlet.

The impact of various surface modification on the performance of immobilized enzyme reactor was monitored via on-line measurement exploiting the oxygen consumption as analytical parameter. Figure 7(b) shows the volumetric activity of different immobilized enzyme flowcells. The volumetric activity was very low for the non-modified flowcell, and it got lost when the flow rate increased. The volumetric activity was higher for the AAPTES-modified flowcell one but it also decreased when the flow rate increased. It seems that slightly elution of enzyme under continuous flow conditions caused the reduction of enzyme activity.

A quantitative comparison revealed that the volumetric activity of AAPTES- and non-modified flowcells were higher for the off-line method than for the on-line monitoring. It is plausible that, due to analytical limitations of the colorimetric assay, the enzyme elution was not observable with the off-line method.

Regarding the PEI-modified flowcell, which provided higher binding capacities to load enzymes, the volumetric activity was higher and increased with the flow rate. The dependence between apparent volumetric activity and residence time have been attributed to co-substrate (oxygen) limitation in oxidase immobilized microreactors [33] but it can be only probed via direct oxygen measurements. Measurement of the net oxygen consumption indicated that at long enough residence times, the oxygen concentration was depleted to a level of first-order dependency between reaction rate and concentration [33, 34]. Additionally, imaging of the oxygen concentration through the microchannel could be performed to support this continuous depletion.

As summary, the comparison between the two analytical methods demonstrated that the on-line monitoring provided a better insight view because the on-line monitoring was not affected by eluted enzymes since the product concentration was directly measured in the flowcell. Therefore, the product concentration in the flowcell was determined without the overestimation of the enzyme activity due to additional products by eluted enzymes. This highlights once again the advantage of the modular character of the resealable flowcell, enabling various modification scenarios and integration of *in situ* sensors.

For oxidase immobilized reactors, there is the hypothesis that, at long enough residence time, oxygen will limit and the calculate volumetric activity will be flow-dependent (the shorter the residence time, the higher the volumetric activity) [33]. On-line sensing provide an insight on that, whereas imaging the oxygen concentration along the whole fluidic path allows to overcome the restriction of using outlet-inlet data. Thus, in addition to the spot measurements near inlet and outlet also the oxygen concentration distribution was imaged. PEI modification was used because that led to the best binding stability of enzyme in the previous experiments. Pictures of the phosphorescence lifetime were taken, see figure 8. The oxygen concentration distribution was determined for six different flow rates between 5  $\mu\text{L}/\text{min}$  and 50  $\mu\text{L}/\text{min}$ . It is obvious that the oxygen concentration at the outlet dropped significantly for low flow rates of 5 and 10  $\mu\text{L}/\text{min}$ . This was due to the long residence time and led to an underestimated volumetric activity due to oxygen limitations. Thus, these results further explain and confirm the results that have been gained by the coupled assay and the on-line monitoring. For flow rates of 20  $\mu\text{L}/\text{min}$ –50  $\mu\text{L}/\text{min}$  the gradient of oxygen concentration along the fluidic path was significantly smaller compared to those with flow rates of 5  $\mu\text{L}/\text{min}$  and 10  $\mu\text{L}/\text{min}$ . Thus, it is assumed that for those flow rates no oxygen limitation would lead to underestimated volumetric activities [33], while at the same time an oxygen depletion by the immobilized enzymes could be observed. Previous systems with oxidases in microfluidic reactors have been limited

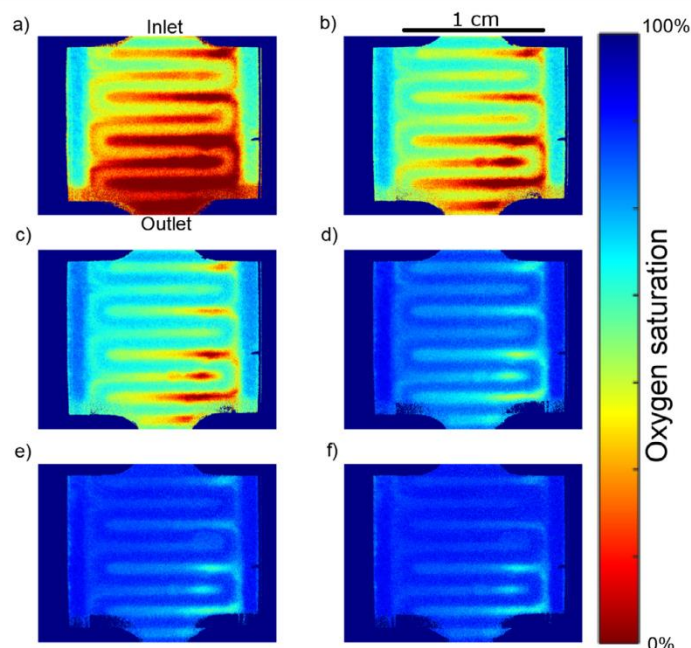


**Figure 8.** Oxygen consumption monitoring of GOX immobilized on a PEI functionalized surface. Images were taken for various flow rates after equilibrium was reached, checked with two point monitoring. Flow rates: (a)  $5 \mu\text{l min}^{-1}$ , (b)  $10 \mu\text{l min}^{-1}$ , (c)  $20 \mu\text{l min}^{-1}$ , (d)  $30 \mu\text{l min}^{-1}$ , (e)  $40 \mu\text{l min}^{-1}$ , and (f)  $50 \mu\text{l min}^{-1}$ .

to using oxygen imaging and free enzymes [26, 35] or surface-immobilized enzymes and inlet-outlet detection [33].

Finally, an on-line monitoring experiment was carried out to study the stability of the enzyme during constant perfusion at  $20 \mu\text{l min}^{-1}$ , to prevent oxygen limitation, over a period of 24 h. The results of the long-term measurement are depicted in figure 9. The volumetric activity at the beginning of the experiment was comparable to the previous experiments. The subsequent decrease of enzymatic activity could have two causes. First, the enzyme might desorb from the surface. Secondly, the enzymes might have degraded, for example due to the presence of hydrogen peroxide [36]. That effect could be reduced through the addition of catalase to the mixture. These results prove that the on-line monitoring via spot measurements was very effective in detecting slow changes over time as well as events.

In order to investigate the cause of the decay in enzymatic activity during long-term measurements, imaging analysis could be exploited, e.g. labeling the enzymes with a dye and performing surface scanning microscopy to check whether the enzymes detached from the surface. Beyond that in next studies the combined effect of the oxygen concentration and the pH of the substrate solution on the enzymatic conversion could be implemented in the presented devices.

An inspection of the oxygen sensing layer after the long-term measurement revealed that the experiment had no impact on the sensing layer. Furthermore, no changes were observed for the resealable flowcell, thus both, the sensing layer and the resealable flowcell could be reused, the latter was already

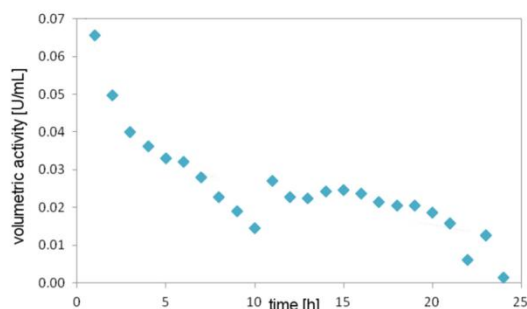


**Figure 9.** Enzyme volumetric activity monitored during a 24 h period. The flowcell surface was activated with PEI for stable binding during the test with a flow rate of  $20 \mu\text{l min}^{-1}$ .

proven to resist treatment with organic solvents, hydrochloric acid, or sodium hydroxide to remove organic residues if needed.

#### 4. Conclusion

In this work, we presented a new type of resealable micro(bio) reactors for biocatalysis studies. The device was based on modular building blocks. The idea behind the modular system was that microfluidic flow paths and surface functionalization, e.g. with sensor elements, can be adapted and combined individually to build a customized device. The device was easily closed and re-opened by stacking and un-stacking the two

parts and provided easy access to the inner surfaces before or after experiments.

The resealable flowcells were produced by a dispensing technique, which offered a quick and easy adaptation towards a tailor-made device. The production reproducibility and sealing performance was characterized and it was found that the production was very reliable with a relative standard deviation of the gasket height of approximately 1.7% for 355  $\mu\text{m}$  high gaskets. Those could be operated with pressures up to 0.7 bar  $\pm$ 0.1 bar. Flow tests revealed a correlation between the gasket height and the sealing performance. The burst pressure increased with height and was sufficiently high for use as a micro(bio)reactor. With the right combination of gasket material and thickness a maximum operating pressure up to 2.4 bar was achieved.

Optical oxygen sensing layers were integrated in the resealable flowcells. Oxygen concentration imaging was used to investigate the oxygen diffusion into the flowcell from the outside through the gasket. The experiments proved that the used gasket materials were permeable to oxygen, though only to a limited extent.

As a proof-of-concept of the applicability of the devices to enzyme studies, glucose oxidase was immobilized in the resealable flowcells and the enzymatic activity was determined by a well-established coupled assay. Additionally, the impact of surface activations on the binding stability and enzymatic activity was studied and the results were in good agreement with literature. An integrated oxygen sensor for on-line monitoring of the oxygen consumption of the enzyme was superior to the off-line coupled assay. There were indications that the latter method was biased due to enzyme leaching out of the reactor and contaminating the collected samples.

In conclusion, the most suitable device, regarding the flow path design and surface activations, could be tailor-made for enzymatic studies. The easy integration of the respective necessary sensing layers offers access to versatile applications.

## Acknowledgment

The research leading to these results has received funding from the People Program (Marie Curie Actions) of the European Union's Seventh Framework Program under REA grant agreement no 608104.

## References

- [1] Bolivar J M, Wiesbauer J and Nidetzky B 2011 Biotransformations in microstructured reactors: more than flowing with the stream? *Trends Biotechnol.* **29** 333–42
- [2] Wohlgemuth R, Plazl I, Žnidaršič-Plazl P, Gernaey K V and Woodley J M 2015 Microscale technology and biocatalytic processes: opportunities and challenges for synthesis *Trends Biotechnol.* **33** 302–14
- [3] Liu D-M, Chen J and Shi Y-P 2015 An online immobilized (small alpha)-glucosidase microreactor for enzyme kinetics and inhibition assays *RSC Adv.* **5** 56841–7
- [4] Fernandes P 2010 Miniaturization in biocatalysis *Int. J. Mol. Sci.* **11** 858–79
- [5] Matosevic S, Szita N and Baganz F 2011 Fundamentals and applications of immobilized microfluidic enzymatic reactors *J. Chem. Technol. Biotechnol.* **86** 325–34
- [6] Rodrigues R C, Ortiz C, Berenguer-Murcia A, Torres R and Fernández-Lafuente R 2013 Modifying enzyme activity and selectivity by immobilization *Chem. Soc. Rev.* **42** 6290–307
- [7] Laffleur J P, Senkbeil S, Novotny J, Nys G, Bøgelund N, Rand K D, Foret F and Kutter J P 2015 Rapid and simple preparation of thiol-ene emulsion-templated monoliths and their application as enzymatic microreactors *Lab Chip* **15** 2162–72
- [8] Matsuura S-I, Chiba M, Tomon E and Tsunoda T 2014 Synthesis of amino acid using a flow-type microreactor containing enzyme-mesoporous silica microsphere composites *RSC Adv.* **4** 9021–30
- [9] Munirathinam R, Huskens J and Verboom W 2015 Supported catalysis in continuous-flow microreactors *Adv. Synth. Catal.* **357** 1093–123
- [10] Bolivar J M and Nidetzky B 2013 Smart enzyme immobilization in microstructured reactors *Chim. Oggi Chem. Today* **31** 50–4
- [11] Asanomi Y, Yamaguchi H, Miyazaki M and Maeda H 2011 Enzyme-immobilized microfluidic process reactors *Molecules* **16** 6041–59
- [12] Ren K, Chen Y and Wu H 2014 New materials for microfluidics in biology *Curr. Opin. Biotechnol.* **25** 78–85
- [13] Haerberle S and Zengerle R 2007 Microfluidic platforms for lab-on-a-chip applications *Lab Chip* **7** 1094–110
- [14] Kim L 2013 Overview of the microfluidic diagnostics commercial landscape *Methods Mol. Biol.* **949** 65–83
- [15] Becker H and Gärtner C 2012 Microfluidics and the life sciences *Sci. Prog.* **95** 175–98
- [16] Tkachenko E, Gutierrez E, Ginsberg M H and Groisman A 2009 An easy to assemble microfluidic perfusion device with a magnetic clamp *Lab Chip* **9** 1085–95
- [17] Brevig T, Krühne U, Kahn R A, Ahl T, Beyer M and Pedersen L H 2003 Hydrodynamic guiding for addressing subsets of immobilized cells and molecules in microfluidic systems *BMC Biotechnol.* **3** 10
- [18] Reichen M, Veraitch F S and Szita N 2013 Development of a multiplexed microfluidic platform for the automated cultivation of embryonic stem cells *J. Lab. Autom.* **18** 519–29
- [19] Tamanaha C R, Malito M P, Mulvaney S P and Whitman L J 2009 Reusable, compression-sealed fluid cells for surface mounting to planar substrates *Lab Chip* **9** 1468–71
- [20] Alam M N H Z, Pinelo M, Samanta K, Jonsson G, Meyer A and Gernaey K V 2011 A continuous membrane microreactor system for development of integrated pectin modification and separation processes *Chem. Eng. J.* **167** 418–26
- [21] Lee J N, Park C and Whitesides G M 2003 Solvent compatibility of poly (dimethylsiloxane)-based microfluidic devices *Anal. Chem.* **75** 6544–54
- [22] Bolivar J M, Consolati T, Mayr T and Nidetzky B 2013 Shine a light on immobilized enzymes: real-time sensing in solid supported biocatalysts *Trends Biotechnol.* **31** 194–203
- [23] Super A, Jaccard N, Marques M P C, Macown R J, Griffin L D, Veraitch F S and Szita N 2016 Real-time monitoring of specific oxygen uptake rates of embryonic stem cells in a microfluidic cell culture device *Biotechnol. J.* **11** 1179–89
- [24] Bolivar J M and Nidetzky B 2012 Oriented and selective enzyme immobilization on functionalized silica carrier using the cationic binding module z basic2: design of a heterogeneous d-amino acid oxidase catalyst on porous glass *Biotechnol. Bioeng.* **109** 1490–8
- [25] Borisov S M, Nuss G, Haas W, Saf R, Schmuck M and Klimant I 2009 New nir-emitting complexes of platinum(ii)

- and palladium(ii) with fluorinated benzoporphyrins *J. Photochem. Photobiol. Chem.* **201** 128–35
- [26] Ehgartner J, Sulzer P, Burger T, Kasjanow A, Bouwes D, Krühne U, Klimant I and Mayr T 2016 Online analysis of oxygen inside silicon-glass microreactors with integrated optical sensors *Sensors Actuators B* **228** 748–57
- [27] Moser C, Mayr T and Klimant I 2006 Microsphere sedimentation arrays for multiplexed bioanalytics *Anal. Chim. Acta* **558** 102–9
- [28] Rupprecht P, Golé L, Rieu J-P, Vézy C, Ferrigno R, Mertani H C and Rivière C 2012 A tapered channel microfluidic device for comprehensive cell adhesion analysis, using measurements of detachment kinetics and shear stress-dependent motion *Biomicrofluidics* **6** 14107–12
- [29] Saïas L, Autebert J, Malaquin L and Viovy J-L 2011 Design, modeling and characterization of microfluidic architectures for high flow rate, small footprint microfluidic systems *Lab Chip* **11** 822–32
- [30] Tsukahara T, Mawatari K, Hibara A and Kitamori T 2008 Development of a pressure-driven nanofluidic control system and its application to an enzymatic reaction *Anal. Bioanal. Chem.* **391** 2745–52
- [31] dos Santos J C S, Barbosa O, Ortiz C, Berenguer-Murcia A, Rodrigues R C and Fernandez-Lafuente R 2015 Importance of the support properties for immobilization or purification of enzymes *Chem. Cat. Chem.* **7** 2413–32
- [32] Betancor L, López-Gallego F, Hidalgo A, Alonso-Morales N, Dellamora-Ortiz G, Guisán J M and Fernández-Lafuente R 2006 Preparation of a very stable immobilized biocatalyst of glucose oxidase from *aspergillus niger* *J. Biotechnol.* **121** 284–9
- [33] Bolivar J M, Tribulato M A, Petrasek Z and Nidetzky B 2016 Let the substrate flow, not the enzyme: Practical immobilization of d-amino acid oxidase in a glass microreactor for effective biocatalytic conversions *Biotechnol. Bioeng.* **113** 2342–9
- [34] Bolivar J M, Consolati T, Mayr T and Nidetzky B 2013 Quantitating intraparticle o<sub>2</sub> gradients in solid supported enzyme immobilizates: experimental determination of their role in limiting the catalytic effectiveness of immobilized glucose oxidase *Biotechnol. Bioeng.* **110** 2086–95
- [35] Sun S, Ungerböck B and Mayr T 2015 Imaging of oxygen in microreactors and microfluidic systems *Methods Appl. Fluoresc.* **3** 034002
- [36] Greenfield P F, Kittrell J R and Laurence R L 1975 Inactivation of immobilized glucose oxidase by hydrogen peroxide *Anal. Biochem.* **65** 109–24

**Supplementary information**

**Tailor-made resealable micro(bio)reactors providing easy integration of in-situ sensors**

Martina Viefhues,<sup>a‡</sup> Shiwen Sun,<sup>b</sup> Donya Valikhani,<sup>c</sup> Bernd Nidetzky,<sup>c,d</sup> Elwin Vrouwe,<sup>a\*</sup> Torsten Mayr,<sup>b</sup> and Juan Bolivar<sup>c</sup>

<sup>a</sup> Micronit Microtechnologies, 7521 PV Enschede, The Netherlands. E-mail: elwin.vrouwe@micronit.com

<sup>b</sup> Applied Sensors group, Institute of Analytical Chemistry and Food Chemistry, Graz university for Technology, 8010 Graz, Austria

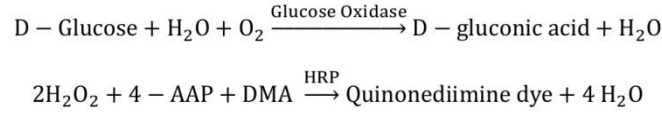
<sup>c</sup> Institute of Biotechnology and Biochemical Engineering, Graz university of Technology, NAWI Graz, 8010 Graz, Austria

<sup>d</sup> Austrian Centre of Industrial Biotechnology, 8010 Graz, Austria

<sup>‡</sup> Current address: Experimental Biophysics and Applied Nanoscience, Faculty of Physics, Bielefeld University, 33615 Bielefeld, Germany.

### Determination of enzyme activity by colorimetric assay

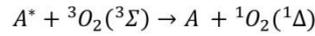
The dye was measured photometrically at 565 nm. For blanks the assay mixture plus 50  $\mu\text{L}$  of 50 mM PPB, pH 7.0, was used instead of the sample. The colorimetric dye, quinonediimine, was formed via the reaction



where 4-AAP, DMA, and HRP denote 4-aminoantipyrine, N,N-dimethylaniline, and horseradish peroxidase.

### Theory of oxygen sensing

The sensing mechanism of most optical oxygen sensors is based on collisional quenching. It requires the luminescent probe to be sensitive to quenching by the desired analyte [1, 2]. In the case of oxygen sensing, the excited oxygen sensitive probe gets quenched by molecular oxygen. And oxygen molecules at triplet state (ground state) get excited to singlet state (excited stated). This reaction is described by the equation below:



where  $A^*$  ( $A$ ) is the molecule of the oxygen sensitive probe at excited (ground) state;  ${}^3\text{O}_2$  ( ${}^1\text{O}_2$ ) is molecular oxygen at triplet (singlet) state.

The dynamic quenching of the oxygen indicator can be described theoretically by the two-side Stern-Volmer equation [3],

$$\frac{F_0}{F} = \frac{\tau_0}{\tau} = \left( \frac{f}{1 + K_{SV1} \cdot [O_2]} + \frac{1-f}{1 + K_{SV2} \cdot [O_2]} \right)^{-1}$$

where  $F_0$  ( $\tau_0$ ) and  $F$  ( $\tau$ ) are the luminescence intensities (lifetimes) in the absence and presence of the quencher, oxygen;  $K_{SV1}$  and  $K_{SV2}$  are the respective Stern-Volmer constants, which describe the quenching efficiency for two micro-environments;  $f$  is the distribution coefficient between the two media, and  $[O_2]$  is the oxygen concentration in the sample.

For the sensor read-out, a frequency-domain lifetime-based measurement was used. Different from time-domain lifetime measurement, the frequency-domain measurement utilizes a sinusoidal intensity-modulated light. The time delay between photon absorption and emission causes a measurable shift in the phase angle between the excitation light and emitted light. The relation between the phase angle shift and the lifetime of the oxygen sensitive dye can be written as

$$\tan(\varphi) = 2\pi\nu\tau$$

with  $\varphi$  the phase shift angle and  $\nu$  the modulation frequency of the excitation light source [4].

### Dispensing production of resealable flowcells

The resealable flowcells were produced by dispensing the prepolymer of the gasket onto a plain glass slide. Thus, no masks or soft lithographic steps are needed, which allows quick and easy in-process adaptation of the device layout. The dispensing process is shown in Figure S11. The final gasket height depended on various dispensing settings. For instance the supply pressure that is applied to the cartridge containing the prepolymer, thus, the higher the applied pressure was the thicker the dispensed line became. The diameter of the dispensing tip also had impact on the gasket height, so with smaller diameters the dispensed line became thinner. Finally, the gasket thickness could be adapted by tuning the writing velocity during dispensing.

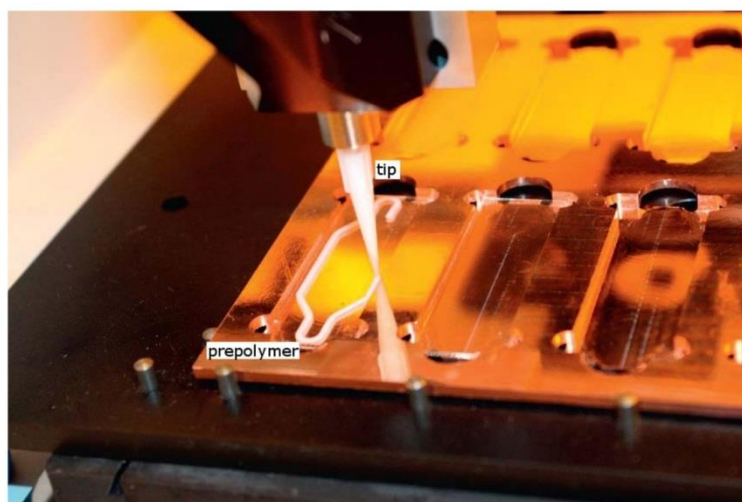


Figure S11: Dispensing of prepolymer of gasket onto glass slides. The gasket height depended on the dispensing settings and the respective polymer, e.g. its viscosity. The prepolymer was dispensed to the surface by applying a pressure to the prepolymer cartridge. By controlled movement in x,y,z-direction the flowcell boundary was made.

### Characterization of resealable flowcells

The production of resealable flowcells had to be reproducible with respect to the design, the shape, and the height of the gasket. The latter was measured for many flowcells that were produced over months. For the measurement a 6x25 mm<sup>2</sup> piece of a microscope cover slide with a thickness of 0.2 mm was placed on top of the gasket. Then the outer boundary of the contact area of gasket and cover slide was focused with a microscope. A Mitutoyo gauge was mounted to the microscope to measure differences in z-direction and set to zero. Then the boundary of the gasket was focused and the respective height of the gasket was read from the gauge. The instrumental tolerance was +/- 5  $\mu$ m. This was repeated at four different positions along the gasket.

The dispensing parameters were set to reach the desired value and then production was started. The height distribution of PFE flowcells (single loop design, i.e. figure 2.1 in main text) is shown in Figure S12. In case of fitting the distribution with a Gaussian distribution 95.44% would be in the range of 343  $\mu$ m and 365  $\mu$ m, thus within a range of 22  $\mu$ m, which is 6.2% of the total height.

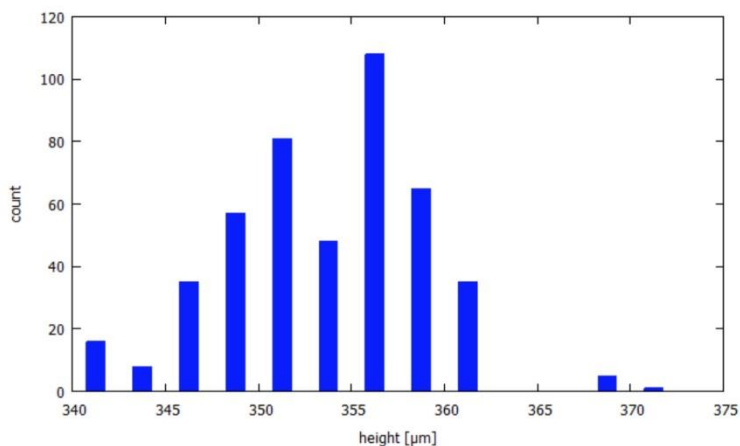


Figure S12: Height distribution for one set of dispensing parameters. The mean height is 354  $\mu\text{m}$  with a standard deviation of 6  $\mu\text{m}$ . If a normal distribution is fitted, 95.44 %, which is the definition of  $2\sigma$ , of the produced structures have a height in the range of 343  $\mu\text{m}$  and 365  $\mu\text{m}$ .

Besides characterization of the height reproducibility the sealing ability was tested as well. The test setup for determining the leakage pressure, i.e. the lowest pressure for which leakage was observed, was composed of the flowcell, assembled in a holder, a syringe pump with water connected to the flowcell, a pressure sensor connected in series to the flowcell, and a capillary downstream of the resealable flowcell to generate a backpressure. The results are shown in Figure S13.

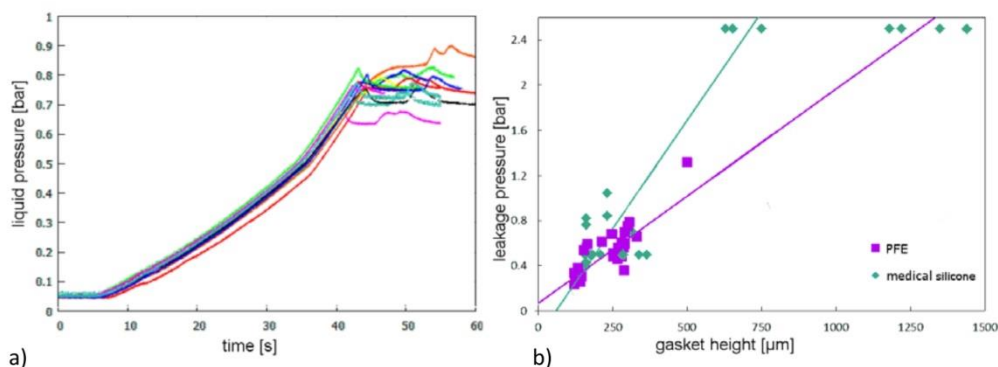


Figure S13: Sealing abilities of resealable flowcells. a) Sealing ability test results of 14 flowcells of same gasket height, 354  $\mu\text{m}$ , all with extended shape. A fixed pumping scheme was programmed starting at a flow rate of 0.1 ml/min and increasing the flow rate every 30 s by 0.1 ml/min. When leakage appeared the pressure did not increase further and the pump was stopped. b) Leakage pressures for different materials and gasket heights, the design was kept the same for all.

Figure S13 a) depicts the results from 14 flowcells, all made of the same material and with a gasket height of 354  $\mu\text{m}$ . The flow rates were stepwise increased with a repetition of 30 s and it is obvious that the behaviors were the same as well as the leakage pressure with 0.7 bar  $\pm$  0.1 bar. Hence, a reliable and reproducible sealing ability of the resealable flowcells was observed.

Two things became obvious from the sealing tests of various heights and gasket materials, Figure S13 b) . First, the leakage pressure was dependent on the gasket height, i.e. it increased linearly with the thickness over a certain range. That was due to the fact that the applied pressure onto the thicker

gaskets was higher. Additionally, their width increased and thereby the increased contact area between the gasket and the glass led to a higher leakage resistance. Thus, both effects combined led to better sealing abilities of thicker gaskets. The second observation was that the materials also affected the leakage pressures although of same gasket height. That was due to different durometer hardness's of the material. For instance, a softer material was deformed easier, thus was able to level out small height variations, whereas a harder material could not. A third observation was made for the medical silicone, whose leakage pressure reached a plateau at 2.5 bar. This is assumed to be related to the holder, which also has compressible parts.

The sealing ability of meandering channels was not directly dependent on the gasket height; see Figure S12 and Figure S14. When a leakage appeared that happened mostly at the crossing points of the ridges and the outer structure due to a tendency to small height variations at these points compared to the rest of the structure. This was independent from the total height of the gasket.

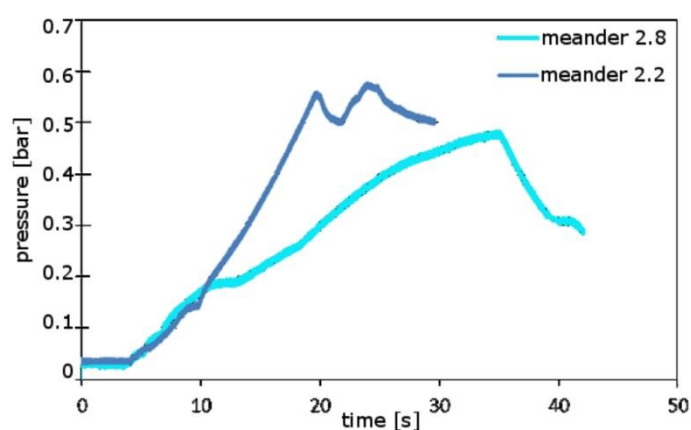


Figure S14: Sealing test of meandering channels of different height. Meander 2.8 had a height of 350  $\mu\text{m}$  and meander 2.2 had a height of 300  $\mu\text{m}$ .

An overview of the oxygen re-saturation in a water filled meandering channel is shown in Figure S15 in detail. It is clear that the re-saturation in the gasket was faster than in water. A close look revealed this tendency along the whole re-saturation process.

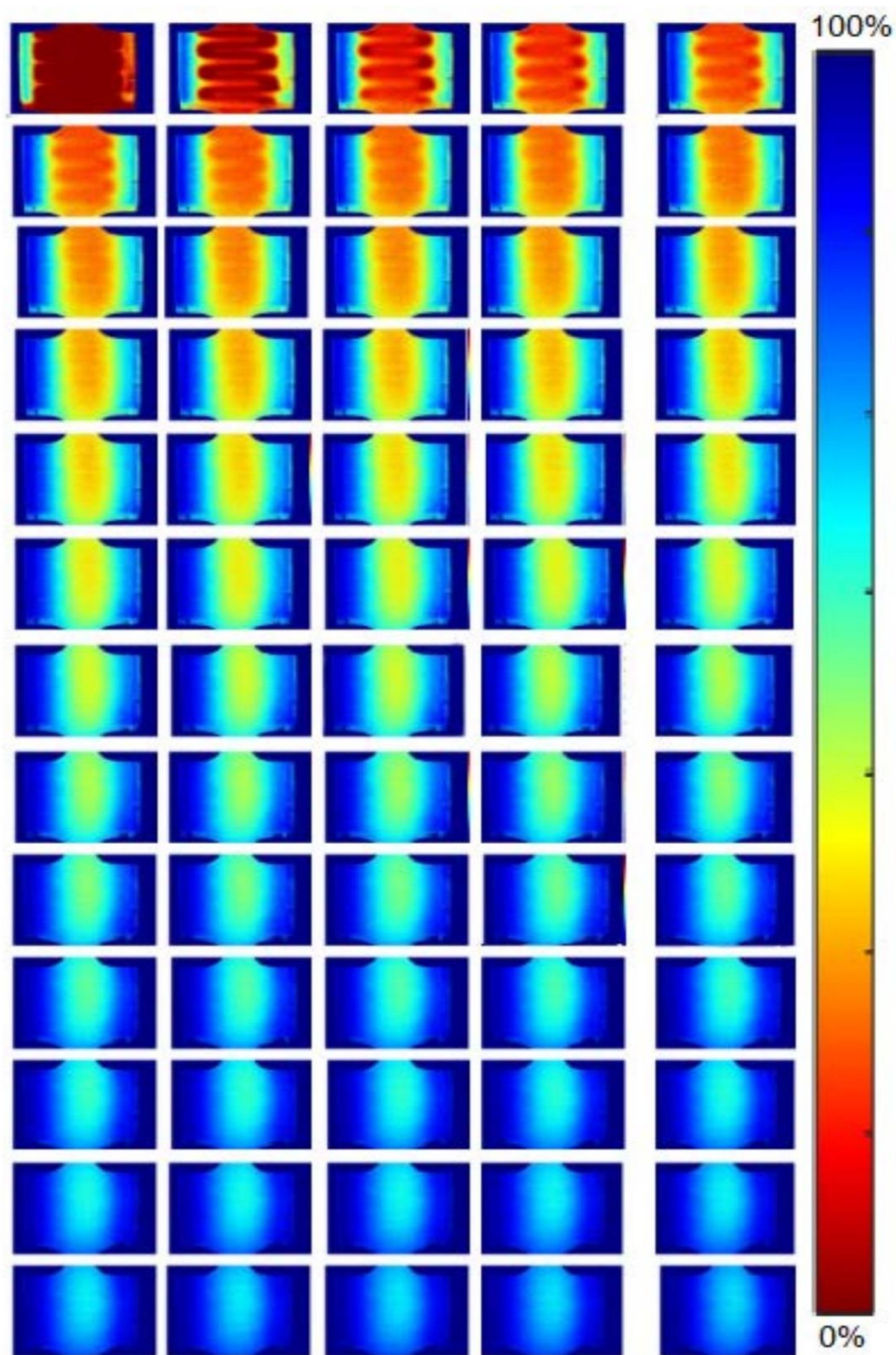


Figure S15: Time-lapse fluorescence life-time images, 1 per minute, of the re-oxygenation of water in a meandering MED channel. The oxygen concentration is color-coded from red, no oxygen, to dark blue, fully saturated.

### References

- [1] Sun, S., Ungerböck, B., and Mayr, T. *Methods and Applications in Fluorescence* **3**(3), 034002 (2015).
- [2] Pfeiffer, S. A. and Nagl, S. *Methods and Applications in Fluorescence* **3**(3), 034003 (2015).
- [3] Ehgartner, J., Sulzer, P., Burger, T., Kasjanow, A., Bouwes, D., Krühne, U., Klimant, I., and Mayr, T. *Sensors and Actuators B: Chemical* (2016).
- [4] Medina-Rodriguez, S., Marin-Suárez, M., Fernández-Sánchez, J. F., de la Torre-Vega, Á., Baranoff, E., and Fernández-Gutiérrez, A. *Analyst* **138**(16), 4607–4617 Aug (2013).

**Tailor-made, Self-sufficient and Recyclable  
Monooxygenase Catalyst Based on Co-immobilized  
Cytochrome P450 BM3 and Glucose Dehydrogenase**

Tailor-made, Self-sufficient and Recyclable Monooxygenase Catalyst Based on Co-immobilized Cytochrome P450 BM3 and Glucose Dehydrogenase

## **Tailor-made, Self-sufficient and Recyclable Monooxygenase Catalyst Based on Co-immobilized Cytochrome P450 BM3 and Glucose Dehydrogenase**

Donya Valikhani<sup>1</sup>, Juan M. Bolivar<sup>1</sup>, Alexander Dennig<sup>1</sup>, and Bernd Nidetzky<sup>1,2</sup>

<sup>1</sup>Institute of Biotechnology and Biochemical Engineering, Graz University of Technology, NAWI Graz, Petersgasse 12, 8010 Graz, Austria

<sup>2</sup>Austrian Centre of Industrial Biotechnology (acib), Petersgasse 14, 8010 Graz, Austria

Corresponding author (B.N.)

e-mail: bernd.nidetzky@tugraz.at; phone: +43 316 873 8400

**Abstract.** Cytochrome P450 monooxygenases (P450s) promote hydroxylations, via oxygen insertion from O<sub>2</sub>, in a broad variety of substrates. Their prowess in C-H bond functionalization renders P450s promising catalysts for organic synthesis. However, operating P450 reactions involves complex management of main substrates, O<sub>2</sub> and NADPH reducing equivalents against an overall background of low enzyme operational stability. Whole cell biocatalysis, although often used, offers no general solution to this problem. Herein, we present a tailor-made design of a self-sufficient, operationally stabilized and recyclable P450 catalyst on porous solid support. Using enzymes as fusion proteins with the positively charged binding module Z<sub>basic2</sub>, the canonical P450 monooxygenase (P450 BM3) was co-immobilized with glucose dehydrogenase (type IV; from *Bacillus megaterium*) on anionic sulfopropyl-activated carrier (ReliSorb SP). Affinity-like immobilization via Z<sub>basic2</sub> enabled each enzyme to be loaded in controllable amount, thus maximizing the relative portion of the limiting P450 M3 (90 nmol/g<sub>carriers</sub>) in total enzyme immobilized. Using lauric acid (2 mM) as a representative P450 substrate that is poorly accessible to whole-cell catalysts, we demonstrate complete hydroxylation of substrate under efficient coupling, inside of catalyst particle, to the regeneration of NADPH from glucose (20 cycles). The immobilized P450 BM3 showed a total turnover number of 11,000, thus allowing fully active catalyst to be recycled at least 10 times. This study therefore supports the idea of practical heterogeneous catalysis by P450 monooxygenase systems immobilized on solid support.

Keywords: Hydroxylation; Cytochrome P450; Glucose dehydrogenase; Immobilization; Heterogeneous biocatalysis

## Introduction

Cytochrome P450 monooxygenases (CYPs or P450s) are heme-containing enzymes that catalyze chemically challenging reactions such as the introduction of molecular oxygen into non-activated carbon atoms (Kang et al., 2014; O'Reilly, Kohler, Flitsch, & Turner, 2011; Ortiz de Montellano, 2010; Urlacher & Eiben, 2006; Urlacher & Girhard, 2012). P450 BM3 from *Bacillus megaterium*, a well-characterized and self-sufficient P450 monooxygenase (monooxygenase and reductase domains are fused via a short linker), hydroxylates a broad variety of substrates at high activity rates with NAD(P)H as electron source and O<sub>2</sub> (air) as oxidant (Munro et al., 2002; Whitehouse, Bell, & Wong, 2012).

Despite its large synthetic and industrial potential, the effective use of P450 BM3, especially in large-scale production processes, has been hindered since operating P450 reactions involves complex management of the target substrates, O<sub>2</sub> and NADPH reducing equivalents (Dennig, Lülldorf, Liu, & Schwaneberg, 2013; Schoemaker, Mink, & Wubbolts, 2003). In addition, low operational stability and high uncoupling efficiency (% NADPH that is oxidized but no product is formed) when converting non-natural substrates are usually found.

Whole cells catalysis solves some of the aforementioned limitations and they allow the successful use of P450s (Hernandez-Martin et al., 2014; Park et al., 2015). However, in some cases the activity is too low, or the reaction is not viable. For example, while using fatty acids as natural substrates, P450 BM3 displays a high activity (>1000 turnovers/min) and nearly 100% coupling efficiency (Di Nardo & Gilardi, 2012), medium and long chain fatty acids are notoriously challenging in whole cell catalysis due to their poor uptake and metabolizing activities in whole cells (Schewe, Holtmann, & Schrader, 2009).

## Tailor-made, Self-sufficient and Recyclable Monooxygenase Catalyst Based on Co-immobilized Cytochrome P450 BM3 and Glucose Dehydrogenase

To gain versatility, isolated enzymes can be used, but stability issues arise. When using cell-free P450 BM3 preparations the hydrophobicity of fatty acids, their low solubility in water and heterogeneous character at higher concentrations often impairs with the typically polar environment needed for efficient enzyme catalysis. At high substrate loading, further challenges become the efficient regeneration of NADPH and related pH changes as well as transfer of O<sub>2</sub> into water (Dennig, Busto, Kroutil, & Faber, 2015). The use of solid-supported immobilized enzymes proved to be a good strategy to address many of the mentioned challenges. Enzyme immobilizes generally further offer the significant advantages of facile re-use and clean separation from the liquid phase containing the product (López-Gallego, Jackson, & Betancor, 2017; Mateo, Palomo, Fernandez-Lorente, Guisan, & Fernandez-Lafuente, 2007; Santos et al., 2015; D. N. Tran & Balkus, 2011).

Compared to other enzyme families, there are only a few reports on the immobilization of monooxygenases and mainly P450 BM3 has been used due to its self-sufficient character that simplifies electron transfer (Ducharme & Auclair, 2018). For instance, the cross-linking-adsorption of P450 BM3 on Ni<sup>+2</sup>-functionalized magnetic nanoparticles via its His-tag succeeded in hydroxylation of 10-(4-nitro-phenoxy) decanoic acid (10-pNCA). The catalyst was used for six cycles and the corresponding TTN was reached 2983 (Bahrami et al., 2017). Through fusion with phasin, P450 BM3 was immobilized on biopolymer where using 7-ethoxycoumarin as a substrate, the catalyst showed the TTN of ~2400 (J. H. Lee et al., 2014). In another study, encapsulation of P450 BM3 in a sol-gel matrix obtained the TTN of 2460 for the oxidation of 10-pNCA (Maurer, Schulze, Schmid, & Urlacher, 2003). The immobilization of P450 BM3 on metal surface via binding peptide (Zernia et al., 2016) or using mesoporous molecular sieves to immobilize the isolated heme domain of P450 BM3 (Weber et al., 2010) showed other techniques of P450s immobilization. Reported concepts utilized colorimetric/fluorogenic substrates during development and characterization (robustness and rapid development), however, examples for conversion of relevant

## Tailor-made, Self-sufficient and Recyclable Monooxygenase Catalyst Based on Co-immobilized Cytochrome P450 BM3 and Glucose Dehydrogenase

industrial substrates and/or relevant product titers are often lacking. Consequently, there is a clear demand to develop robust and practical methods of immobilized preparations involving monooxygenases.

In P450 catalysis, NAD(P)H needs to be recycled in-situ ideally from a renewable and cheap electron sources such as glucose or formate by a dehydrogenase (Lu & Mei, 2007; Maurer et al., 2003; Nagao et al., 1992). Alternatively electrons can be supplied/regenerated by chemical, electrochemical or photochemical setups (Hollmann, Hofstetter, & Schmid, 2006; S. H. Lee, Kwon, Kim, & Park, 2013; N. H. Tran et al., 2013; Wang et al., 2017; Wu et al., 2013) and non-natural cofactor mimics (Nowak, Pick, Lommes, & Sieber, 2017). However, enzymatic approaches for cofactor regeneration provide noticeable highest compatibility as NAD(P)H is universally accepted in Nature and mild reaction conditions are used that are favored by most enzymes. Glucose dehydrogenase (GDH) from *Bacillus megaterium* is widely applied and highly active enzyme that catalyzes the oxidation of glucose to gluconolactone with participant reduction of  $\text{NAD}^+$  and/or  $\text{NADP}^+$  (Müller et al., 2013; Nagao et al., 1992; Nowak et al., 2017). Although, there are some reports on the co-expression of GDH and P450 monooxygenase in *E. coli*, the low amount of product remained as the main challenge (Lu & Mei, 2007; Pham, Gao, & Li, 2013). As the example of cofactor regeneration system,  $\text{NADP}^+$ -dependent formate dehydrogenase co-immobilized with P450 BM3 in a sol-gel matrix showed the TTN of 235 increased to 630 using immobilized single enzymes for the oxidation of 10-pNCA (Maurer et al., 2003). An ideal immobilization procedure for P450 BM3 should provide conditions to load P450 BM3 and the regeneration enzyme in one platform which can offer the “self-sufficient” system only requires substrate,  $\text{O}_2$  and source of reducing equivalents.

A well-established immobilization technology based on cationic binding via  $Z_{\text{basic2}}$ , would suggest a novel, mild and selective method for immobilization of P450 BM3 WT and the regeneration enzyme on solid carriers.  $Z_{\text{basic2}}$ , a 7 kDa protein containing three  $\alpha$ -helices with clustered positive charges

from multiple arginine residues, allows creating protein chimeras that bind very tightly to negatively charged surfaces at physiological pH. Due to the high pI of  $Z_{\text{basic2}}$  (~10), the immobilized enzyme can be applied over a broad range of pH values, which is relevant in particular for pH sensitive/changing reactions by oxidoreductases (one mol  $H^+$  released per mol NAD(P)H regenerated). The immobilization with  $Z_{\text{basic2}}$  is highly selective, most likely because it appears to occur in a well-defined orientation via the cationic residues. It is stable under operation, yet readily reversible which allows reusability of carriers (Bolivar, Gascon, Marquez-Alvarez, Blanco, & Nidetzky, 2017; Bolivar & Nidetzky, 2012a, 2012b; Wiesbauer, Bolivar, Mueller, Schiller, & Nidetzky, 2011).

Here, we show the development of an efficient and re-usable heterogenous P450 BM3 WT monooxygenase co-immobilized with a GDH. We use lauric acid and anisole as the two model substrates both having a specific challenge due to their low solubility in water. The co-immobilized system serves as off-the-shelf-catalyst to catalyze hydroxylation of industrially relevant substrates.

## **Materials and Methods**

### **Materials**

ReliSorb SP400/SS was a gift from Resindion (Milano, Italy) with the following specifications: 50-150  $\mu\text{m}$  diameter and 80-100 nm pore size. Unless stated otherwise, chemicals were of the highest available purity and obtained from Sigma-Aldrich (Vienna, Austria) or Carl Roth (Karlsruhe, Germany). Catalase bovine liver (2000-5000 U/mg) was from Sigma-Aldrich (Steinheim, Germany). DNA sequencing was done at LGC Genomics (Berlin, Germany).

## Molecular cloning and expression of enzymes

### *Enzyme cloning*

The plasmids containing either GDH or P450 BM3 WT fused at the N-terminal part with Z<sub>basic2</sub> (Z\_P450 BM3, Z\_GDH) were constructed by using a modified the megaprimer/megawoop protocol approach (Miyazaki, 2011). For this, a pT7ZbQGKlenow plasmid (Wiesbauer et al., 2011) containing the N-terminal Z<sub>basic2</sub> was used as recipient vector. DNA amplifications by PCR were done using Q5 high-fidelity DNA polymerase (New England Biolabs, U.S.) and following the producer's manual. Underlined letters in primer sequences indicate the complementary area between vector and inserted genes used for mega-primer amplification. The plasmid backbone was amplified by PCR with primers pT7NZbas\_fw (5'-GGTTCTAGCGGCGGTAGCGGCTAAAAGCTTGAAGCTGAGTTGGCT-3') and pT7NZbas\_rv (5'-CTACCGCTCTGAAAGTACAGATCCTCGCTACCGCCGCTCTGGAA CAGAGCTTCCAAATTCG-3') (in total 30 cycles; each cycle: 98 °C/15 s; 62 °C/30 s; 72 °C/10 min; 20 min at 72 °C final extension). BM3 WT and GDH genes were amplified by PCR from plasmid DNA using ZBFw\_BM3/ZBRv\_BM3 (ZBFw\_BM3: AGCGAGGATCTGTACTTTCAGAGCGGTAGCATGACAATTAAGAAATGCCTCAGC-3'; ZBRv\_BM3: 5'-GCCGCTACCGCCGCTAGAACCCCGCCACACGTCTTTTGCG TATC-3') and Zbas\_GDH\_fw/Zbas\_GDH\_rv (Zbas\_GDH\_fw: 5'AGCGAGGATCTGTACT TTCAGAGCGGTAGCATGTATACAGATTTAAAAGATAAAGTAG-3'; Zbas\_GDH\_rv 5'-GCCGCTACCGCCGCTAGAACCCTATTAGCCTCTTCCTGCTTGGAAAGAAG-3') as primers. The following PCR programs were used to execute amplification of BM3 WT and GDH: BM3 WT: 98 °C/15 s; 55 °C/15 s; 68 °C/5 min, one fill-up cycle: 10 min at 68 °C final extension; GDH: 98 °C/15 s; 55 °C/15 s; 72 °C/1 min; 25 cycles; 5 min at 72 °C final extension. Successful PCR

## Tailor-made, Self-sufficient and Recyclable Monooxygenase Catalyst Based on Co-immobilized Cytochrome P450 BM3 and Glucose Dehydrogenase

amplification was verified by agarose gel-electrophoreses and template DNA was removed from PCR mixtures by DpnI (Thermo Scientific, U.S.) digest overnight at 37 °C following the supplier's manual. The digested PCR products were purified by PCR clean-up KIT (Blirt DNA GDANSIC, Poland) and mixed in a 2:1 gene to vector ratio (2 mol gene to 1 mol vector; 100 ng vector was used) followed by 25 cycles of DNA amplification using Q5 DNA polymerase (95 °C/15 s; 55 °C/30 min; 72 °C/10 min). PCR products were directly transformed without further treatment into chemical competent Top10 cells (New England Biolabs, U.S.). To verify successful DNA assembly, colony PCR was performed using gene specific primers for GDH and P450 BM3 WT. Clones harboring the constructs with correct size were sequenced and used for protein expression (see Supporting Information for full length DNA and amino acid sequences of fused constructs).

### *Enzyme expression*

Z\_P450 BM3 was produced from *E. coli* strain Lemo21 cell cultures that were grown in 1-L Erlenmeyer flasks at 37 °C using an agitation rate of 110 rpm. Flasks contained 200 mL terrific broth medium supplemented with 0.05 mg/mL kanamycin and 0.034 mg/mL chloramphenicol. At OD<sub>600</sub> of 1.0, the protein expression was induced upon addition of 0.5 mM isopropyl β-D-1-thiogalactopyranoside (IPTG) and 0.5 mM aminolevulinic acid (heme pre-cursor). The induced cells were cultivated for 40 h at 15 °C and harvested by centrifugation (4500 x g, 15 min, 4 °C). The cell pellet was resuspended (1:1 by volume) in potassium phosphate buffer (50 mM, pH 7.5). The suspension was centrifuged, and the cell pellet was stored until use at -20 °C. Z\_GDH was produced from *E. coli* strain Lemo21 cells grown in 1-L baffled shaken flasks contained 200 mL Lennox broth medium supplemented with 0.05 mg/mL kanamycin and 0.034 mg/mL chloramphenicol under the same condition used for Z\_P450 BM3 expression. At OD<sub>600</sub> of 1.0, expression of the Z\_GDH gene was induced by addition of 0.5 mM IPTG. The induced cells were cultivated overnight at 25 °C and harvested with the same procedure mentioned above.

Cell lysis preparation and enzyme purification procedure are described in Supporting Information.

## **Immobilization of enzymes**

### *Immobilization of single enzyme*

Enzyme immobilization via  $Z_{\text{basic2}}$  was performed as reported elsewhere in detail (Bolivar & Nidetzky, 2012a). Briefly, ReliSorb SP400 (~100 mg) was incubated under mild stirring in potassium phosphate buffer (50 mM, pH 7.5, 250 mM NaCl). *E. coli* cell extract containing Z\_P450 BM3 (4  $\mu\text{M}$ ) or Z\_GDH (60-90 U/mL), with total protein concentration varied between 18 to 24 mg/mL, was supplemented with NaCl (250 mM) followed by adjusting the pH to 7.5. The carriers (~100 mg) were then mixed with 1 mL of cell extract and incubated under gentle mixing at room temperature (~25 °C) for 1 h. If not mentioned otherwise, an end-over-end rotator (20 rpm) was used for mixing. At the end of incubation time, samples were taken from the supernatant after sedimentation of the carriers, and the residual enzyme concentration (Z\_P450 BM3;  $\mu\text{M}$ ) or enzyme activity (Z\_GDH; U/mL) in the supernatant was measured using the assays described later. The immobilization step was repeated four times under the conditions described with an intermediate washing step with loading buffer in each round. For each step, the immobilization yield (%) was calculated as  $100 \times (c_0 - c) / c_0$ , where  $c_0$  is the initial enzyme activity/concentration, and  $c$  is the enzyme activity/concentration in solution after the immobilization.

### *Co-immobilization of P450 BM3 WT and GDH*

The immobilization conditions were the same as mentioned before. The P450 BM3-GDH co-immobilization was performed sequentially. After the immobilization of Z\_P450 BM3 (four loading steps), the carriers were washed with the loading buffer, and then incubated with cell extract

containing Z\_GDH at room temperature for 1 h (one loading step). Afterwards the carriers were washed with loading buffer and kept until use at 4 °C.

### **Z\_P450 BM3 activity assay**

The procedure of Omura and Sato was used to measure the active Z\_P450 BM3 concentration (Omura & Sato, 1964). To evaluate the catalytic activity of Z\_P450 BM3, anisole was used as a substrate. Therefore, 0.6 nmol of free enzymes or 6 mg of carriers with the same amount of bound enzyme were incubated with anisole (20 mM) in 1 mL of potassium phosphate buffer (50 mM, pH 7.5) for 5 minutes. Unless mentioned otherwise, anisole was pre-dissolved in ethanol to give a final ethanol concentration of 2.2 % (v/v) in the reaction mixture. The reaction was commenced by adding NADPH (0.2 mM final concentration) and incubated under gentle mixing at room temperature. At defined time points, samples were withdrawn and the concentration of produced guaiacol was measured by 4-AAP assay (Dennig et al., 2013) Coupling efficiency of free and immobilized enzyme were determined by measuring the concentration of guaiacol obtained after full depletion of NADPH (monitored spectrophotometrically at 340 nm under the stirred condition at 25 °C).

To test the dependence of enzyme activity on the concentration of NADPH, the same reaction setup was performed using different concentration of NADPH (0.1-1.6 mM). The samples were taken at defined time and the concentration of guaiacol was measured accordingly.

### **Z\_GDH activity assay**

Z\_GDH activity was obtained from the initial rate measurements that recorded the formation of NADPH spectrophotometrically at 340 nm. The reaction was performed in potassium phosphate buffer (50 mM, pH 7.5), containing NADP<sup>+</sup> (5 mM), glucose (200 mM) and the enzyme solution in appropriate dilution at 25 °C. One unit (U) of GDH activity corresponds to the amount of enzyme that produces 1 μmol of NADPH per minute. Furthermore, the activity of soluble and immobilized preparations of Z\_GDH were studied at different concentrations of NADP<sup>+</sup>. Reactions consisted of

Tailor-made, Self-sufficient and Recyclable Monooxygenase Catalyst Based on Co-immobilized Cytochrome P450 BM3 and Glucose Dehydrogenase

0.03 U soluble or immobilized enzyme and  $\text{NADP}^+$  (0.5-10 mM) in a final volume of 1 mL of potassium phosphate buffer (50 mM, pH 7.5). Reaction was started by adding glucose (200 mM final concentration) under the stirred condition at 25 °C.

### **Evaluation of enzyme co-immobilizates in hydroxylation reactions**

#### *Time-course measurement of anisole hydroxylation reaction*

Each reaction contained anisole (20 mM),  $\text{NADP}^+$  (0.8 mM) and 100 mg of carriers (9 nmol Z\_P450 BM3 and 70 U of Z\_GDH) in a final volume of 5 mL potassium phosphate buffer (50 mM, pH 7.5). Catalase (1000 U/mL) was added to one of the reaction mixture to remove  $\text{H}_2\text{O}_2$  potentially formed during uncoupling of Z\_P450 BM3. Reactions were performed in 15 mL tubes under gentle mixing at room temperature. Samples were taken at defined time-points and analyzed with the 4-AAP assay.

#### *Time-course measurement of lauric acid hydroxylation reaction*

The reaction setup contained lauric acid (2 mM),  $\text{NADP}^+$  (0.1 mM), free enzymes or 20 mg carriers (1.8 nmol Z\_P450 BM3 and 14 U Z\_GDH, respectively) and catalase (1000 U/mL) in a final volume of 5 mL potassium phosphate buffer (50 mM, pH 7.5). Lauric acid was pre-dissolved in ethanol to give a final ethanol concentration of 2.2 % (v/v) in the reaction mixture. The formation of hydroxylated products was determined by GC-MS analysis. The same reaction setup was operated with native carriers (no catalyst bound) and the taken sample was calculated as 100 % substrate in GC-MS analysis (single point calibration). For GC-MS analysis, samples were acidified with HCl (3 M) and extracted with an equal volume of EtOAc that contained 0.1 % (V/V) 1-octanol as the internal standard. Following that, the organic phase dried over  $\text{Na}_2\text{SO}_4$  to remove traces of water. Samples were centrifuged, and the taken sample (120  $\mu\text{L}$ ) was mixed with MeOH (60  $\mu\text{L}$ ) and  $\text{CH}_2\text{N}_2$  (10  $\mu\text{L}$ ).

### *Scale-up and reusability study of co-immobilized enzymes*

To test the reusability of co-immobilized enzymes, lauric acid was used as the substrate. Each cycle of reaction contained lauric acid (2 mM), NADP<sup>+</sup> (0.8 mM), catalase (1000 U/mL) and 100 mg carriers (9 nmol Z\_P450 BM3 and 70 U of Z\_GDH) in a final volume of 5 mL potassium phosphate buffer (50 mM, pH 7.5). Each cycle was stopped after 15 minutes, and the sample was withdrawn and analyzed by GC-MS. To perform another reaction cycle, the carriers were separated, washed with 4 mL loading buffer and added to a fresh reaction mixture.

## **Results and Discussion**

### *Preparation and characterization of enzymes*

A chimeric Z\_P450 BM3 was constructed by fusing the binding module, Z<sub>basic2</sub> to the N-terminal part of P450 BM3 WT. Z\_P450 BM3 was functionally expressed in *E.coli*. Using anisole as the substrate, cell extracts containing Z\_P450 BM3 showed specific activity of 0.02 U/mg, while the total protein content was 20 mg/mL. The Z\_P450 BM3 was obtained highly purified in the expected mass of 127.29 kDa (Figure S1). The chimeric construct was expressed in *E. coli* to a level of 6.6 % of total intracellular protein indicating a sufficient expression of the enzyme. The purified Z\_P450 BM3 displayed a specific activity of 0.3 U/mg, which represents a moderate conservation of the specific activity of the native enzyme (0.65 U/mg) reported in literature (Dennig et al., 2013). Unexpectedly, the coupling efficiency of Z\_P450 BM3 (40 %) was around 4-fold higher than the reported values for the untagged protein (Dennig et al., 2013). Note: the coupling efficiency was defined as  $100 \times [\text{product}]/[\text{consumed NADPH}]$ . Results indicate that fusion to Z<sub>basic2</sub>, to some extent, interfered with the P450 BM3 activity. The chimeric construct of GDH was designed by the fusing Z<sub>basic2</sub> to the N-terminus of enzyme. The *E.coli* cell extract containing Z\_GDH displayed a specific activity of 3.4 U/mg and the total protein content was 21 mg/mL. The purified enzyme showed the calculated mass of 37.67 kDa (Figure S1) reaching expression level of 6 %, thus

indicating as useful expression of the GDH chimera. The specific activity of the purified Z\_GDH was determined as 57 U/mg while the specific activity of the native form was ~ 800 U/mg reported in literature (Nagao et al., 1992).

### **Immobilization of single enzymes**

ReliSorb SP400 was used as a support for the immobilization of enzymes. The carriers are spherical particles made from polymethacrylate-based material harboring sulfonate groups on the surface. The internal structure of ReliSorb SP400 displays available pores (80-100 nm) that should enable relatively unrestricted access of Z\_P450 BM3 (~ 9 nm) and Z\_GDH (7.8 nm) to the entire available surface area. Note: the characteristic diameters for the enzymes were calculated using the CalcTool protein mass calculator based on the numbers of amino acids.

To design the efficient co-immobilized enzymes system, at first, it is essential to study the binding capacity of carriers for each enzyme. Previously, we showed that the immobilization can be effectively performed directly from *E.coli* cell extract without previous purification due to exquisite selectivity of the immobilization (Wiesbauer et al., 2011). Therefore, to simplify preparation of heterogeneous catalysts, bacterial cell extract of each enzyme was used for the immobilization. The amount of bound enzyme (Z\_P450 BM3; nmol/g<sub>carriers</sub> or Z\_GDH; U/g<sub>carriers</sub>) and subsequently the immobilization yield (%) were calculated for each step. Figure 1 shows that in the first step > 90 % of offered enzyme bound to the carriers after 1 h incubation at room temperature. The immobilization yield decreased stepwise for both enzymes indicating the practical saturation of carriers with the respective enzyme. It is shown that unlike Z\_GDH, the maximum enzyme loading was not reached for Z\_P450 BM3, but a trend of approaching a “saturated” value was also noticeable in the experiment. In total, 100 nmol<sub>P450 BM3</sub>/g<sub>carriers</sub> and 1280 U<sub>GDH</sub>/g<sub>carriers</sub> (equivalent to 22 mg<sub>GDH</sub>/g<sub>carriers</sub>) were efficiently bound to the carriers. These results suggest that the binding capacity of ReliSorb SP400 for Z-enzyme constructs can be generally useful for the envisioned application.

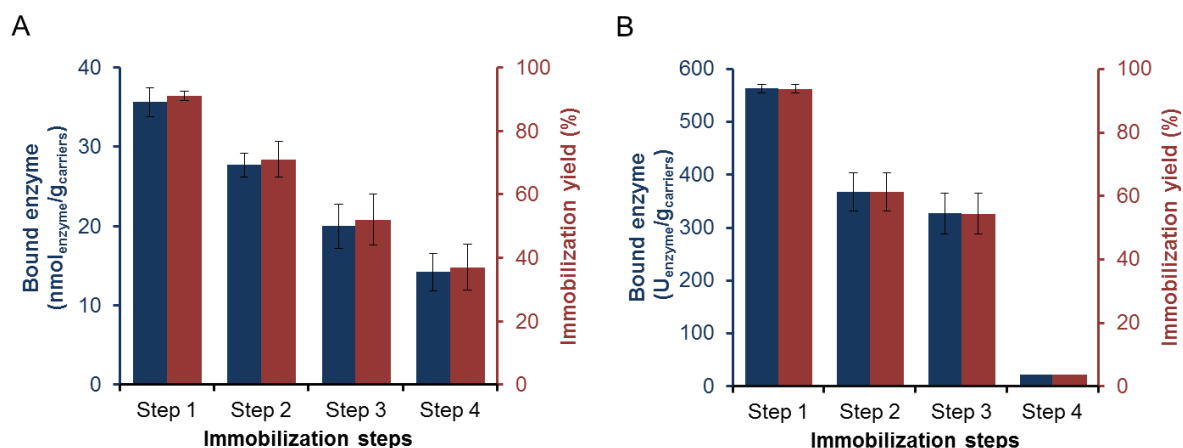


**Figure 1.** An analysis of enzyme immobilization on ReliSorb SP carriers. Panel A shows the immobilization of Z\_P450 BM3 in terms of bound enzyme on carriers and immobilization yield (%) in each step. Panel B shows the immobilization of Z\_GDH in the terms of bound enzyme on carriers and immobilization yield (%) in each step. The immobilization mix contained defined amount of enzymes, NaCl (0.25 M) and potassium phosphate buffer (50 mM, pH 7.5). The incubation time was 1h under gentle mixing at 25 °C. Error bars show standard deviations from 4 independent experiments.

### Characterization of immobilized Z\_GDH

It is quite common for immobilized enzymes that the actual activity of solid immobilizate ( $E_{obs}$ ) is not the same as, typically lower than, expected from bound enzyme obtained from immobilization yield ( $E_{bound}$ ), where the ratio between them is generally referred to as the effectiveness factor ( $\eta = E_{obs}/E_{bound}$ ).  $E_{obs}$  for Z\_GDH was studied and the measured activity was 4-fold lower than  $E_{bound}$ . To explore this effect more precisely, we studied the dependence of initial rates on  $NADP^+$  concentrations (0.5 to 10 mM) for both free and immobilized Z\_GDH. Figure 2A illustrates the initial-rate measurements of free enzyme where the obtained  $K_m$  (~3 mM) has a reasonable agreement with the  $K_m$  value (1.9 mM) reported in literature (Nagao et al., 1992). By contrast, Figure 2B shows that GDH immobilizates was able to retain a linear dependence of reaction velocity on the  $NADP^+$  concentrations up to 10 mM. The shape of the curve suggests a transport hindrance of the  $NADP^+$  through the ReliSorb harboring sulfonate groups, which it can be plausible given the

negatively charged state of the molecule. The calculated  $\eta \sim 0.25 \pm 0.05$  showed suitability of the immobilization for the good preservation of enzyme functionality on solid phase.

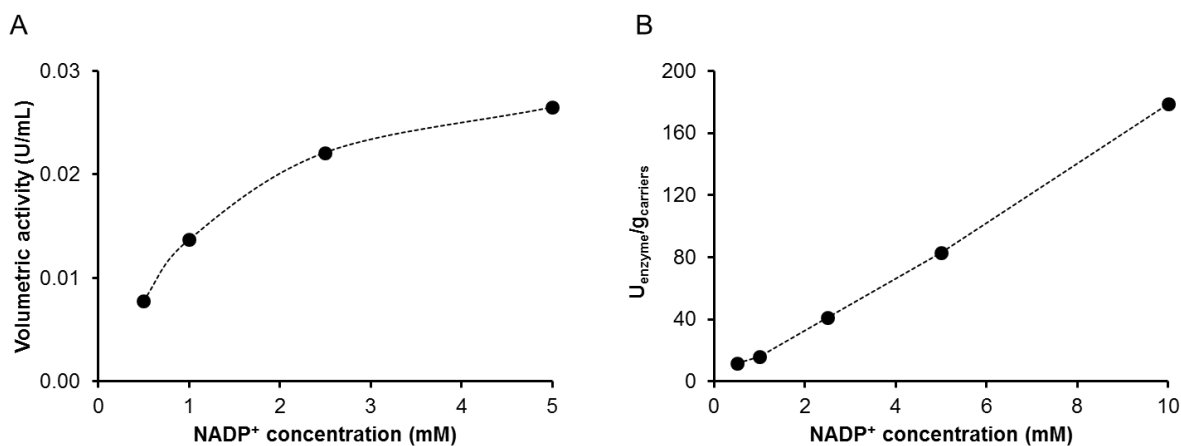


**Figure 2.** Kinetic profile of free and immobilized Z\_GDH at different concentration of NADP<sup>+</sup>. Panel A illustrates the effect of initial rates of free enzyme (0.03 U/mL) and Panel B shows the effect of initial rates of immobilized enzyme. The reactions were commenced by adding glucose (200 mM) in 50 mM potassium phosphate; 25°C, pH 7.5.

### Characterization of immobilized Z\_P450 BM3

The hydroxylation of anisole was used to assay the performance of immobilized Z\_P450 BM3. Conditions of the experiment were designed to capture the initial linear product formation as shown in Figure 3A. From the graph,  $E_{obs}$  for the immobilized Z\_P450 BM3 can be reliably calculated and compared with the maximum expected based on the amount of the enzyme immobilized:  $E_{bound}$ . As a result, the immobilized enzyme exhibited the  $\eta \sim 0.4$  that supports the notion that oriented immobilization on ReliSorb carriers through Z<sub>basic2</sub> module succeeded in maintaining, to some extent, the original enzyme activity in the immobilization procedure. The coupling efficiency of the Z\_P450 BM3 immobilizates was also measured which showed roughly the same amount obtained from free enzyme ( $\sim 40-50\%$ ). Considering  $\eta$ , it seems that the reaction rate of immobilizate is slower than the free one, however, coupling efficiency showed that irrespective of reaction time, the amount of

## Tailor-made, Self-sufficient and Recyclable Monooxygenase Catalyst Based on Co-immobilized Cytochrome P450 BM3 and Glucose Dehydrogenase

product is the same after complete depletion of NADPH for both free and immobilized enzymes. Therefore, using enzyme immobilizates, it is plausible that production yield of anisole hydroxylation could raise within the long-term operation in the presence of sufficient NADPH.

To investigate the sufficiency of NADPH concentration on the catalytic performance of Z\_P450 BM3, the productivity of immobilized P450 BM3 at different NADPH concentrations (0.1-1.6 mM) was examined. Figure 3B illustrates the increase in the range from 0.1 to 0.4 mM NADPH where it had a gradual decrease at 0.8 mM NADPH followed by the sharp decline at 1.6 mM NADP. It is possible that the enzyme might be inactivated due to uncoupling pathways which could produce superoxide and peroxide during the reaction. Although 0.4 mM showed the highest catalytic activity, we considered 0.8 mM NADPH as a value to be adequate for the long-term operation of Z\_P450 BM3, in case some amount of NADPH degrades during reactions.

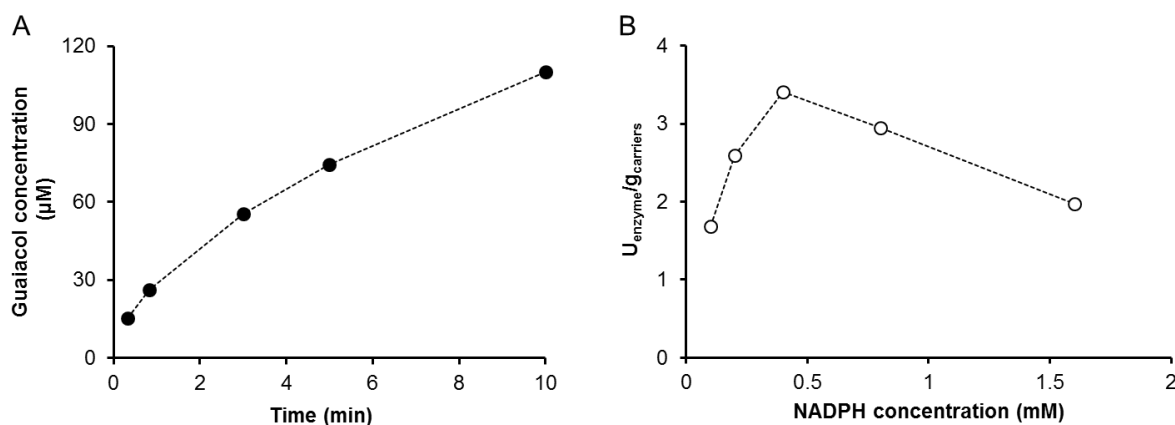


**Figure 3.** An analysis of immobilized Z\_P450 BM3 in the terms of conversion rate and NADPH dependency. Panel A shows the product formation per time using 0.2 mM NADPH. Panel B shows the effect of NADPH concentration on the activity of enzyme. The reaction mixture contained 20 mM anisole in 50 mM potassium phosphate; 25°C, pH 7.5.

### **Co-immobilization of Z\_P450 BM<sub>3</sub> and Z\_GDH**

Having in mind the application of immobilized P450 BM3 for long-term operation and considering the continuous requirement of expensive cofactor (NADPH), we co-immobilized Z\_P450 BM3 and Z\_GDH. Previously we proved that our immobilization technique can be efficiently applied to load sufficient amount of each enzyme. As the main benefit, immobilization of enzymes occurred under the same conditions (50 mM potassium phosphate buffer, pH 7.5, 250 mM NaCl), consequently, the co-immobilization of enzymes can be done with no changes in situation. However, due to low activity of Z\_P450 BM3 WT for anisole (0.3 U/mg) and the high activity of Z\_GDH (57 U/mg), the aim was to maximize quantity of bound Z\_P450 BM3 as this might be the limiting catalyst in the overall reaction. Therefore Z\_P450 BM3 immobilized on the carrier in four repetitive steps ( $100 \text{ nmol}_{\text{enzyme}}/\text{g}_{\text{carriers}}$ ) followed by adding Z\_GDH (90 U/mL). Results are shown in Figure 4 where the high immobilization yield of Z\_GDH (~80 %) indicated the vacant spaces remained after P450 BM3 immobilization. Due to ionic and therefore competitive adsorption of both enzymes to the carrier, 10 % of initially immobilized Z\_P450 BM3 leaked from the carriers during co-immobilization. Therefore, at the end,  $90 \text{ nmol}_{\text{P450BM3}}/\text{g}_{\text{carriers}}$  and  $700 \text{ U}_{\text{GDH}}/\text{g}_{\text{carriers}}$  was obtained. This system showed the facile and practical procedure for immobilized multienzymatic systems.

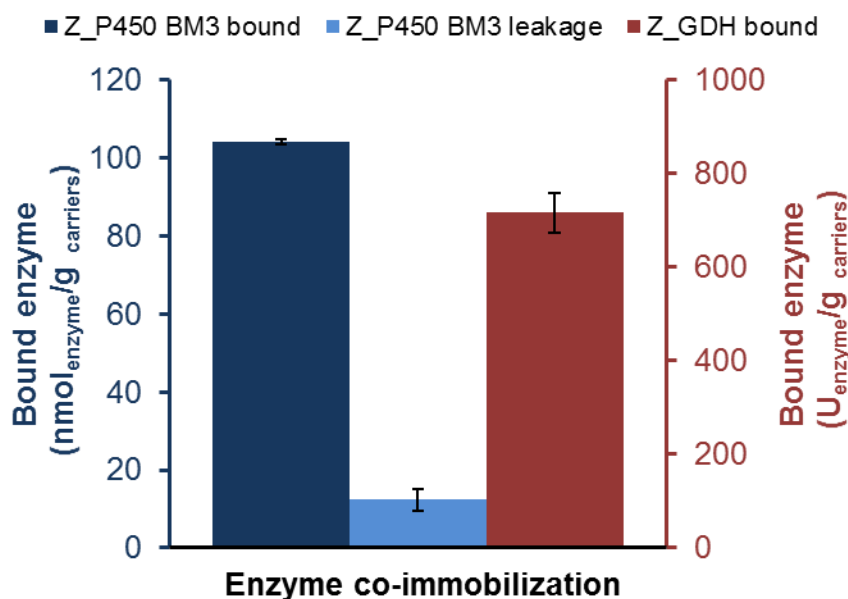


**Figure 4.** An analysis of co-immobilization of Z\_P450 BM<sub>3</sub> and Z\_GDH. The immobilization mix contained defined amount of enzymes, NaCl (0.25 M) and potassium phosphate buffer (50 mM, pH 7.5). The incubation time was 1 h under gentle mixing at 25 °C.

### Evaluation of co-immobilized enzymes as the self-sufficient system

To demonstrate that NADPH was indeed being produced and recycled by the co-immobilized enzyme preparations, the hydroxylation of anisole was kept as assay reaction. Goals: feasibility of cofactor recycling and studying the performance of the co-immobilizates on conversion profile of anisole. Therefore, using the co-immobilized P450 BM<sub>3</sub>-GDH (1.8 μM Z\_P450 BM<sub>3</sub> and 14 U/mL Z\_GDH), the hydroxylation of anisole was operated under the long-term operation in the presence of air from headspace. Note: the concentration of oxygen available for the reaction was not measured at this point, since we were just interested in time-point measurements of anisole hydroxylation. The pH of the reaction monitored, and no significant change observed over time. Figure 5 shows the time-dependent conversion of anisole hydroxylation where the amount of product increased linearly up to 2 mM which was lower compared with the data reported (Dennig et al., 2013). As mentioned before, the low conversion of the reaction might be related to the uncoupling pathways where

## Tailor-made, Self-sufficient and Recyclable Monooxygenase Catalyst Based on Co-immobilized Cytochrome P450 BM3 and Glucose Dehydrogenase

increasing levels of  $\text{H}_2\text{O}_2$  affects the stability of enzyme. To tackle this problem, catalase (1000 U/mL) was added to the reaction (not bound to carriers). Figure 5 shows that the amount of product rose by 2-fold using catalase indicating significant amount of  $\text{H}_2\text{O}_2$ . The total product concentration reached 4 mM, corresponding to a total turnover (TTN;  $\mu\text{mol total product} \cdot \mu\text{mol catalyst}^{-1}$ ) of  $\sim 2000$  and the cofactor was recycled  $>10$  times (40% coupling efficiency). The co-immobilizates proved the efficient cofactor regeneration system where the initial reaction rates can be transferred to continuous product formation. However, the low obtained conversion, expected for P450 BM3 WT, might be associated to the high uncoupling efficiency (Dennig et al., 2013).

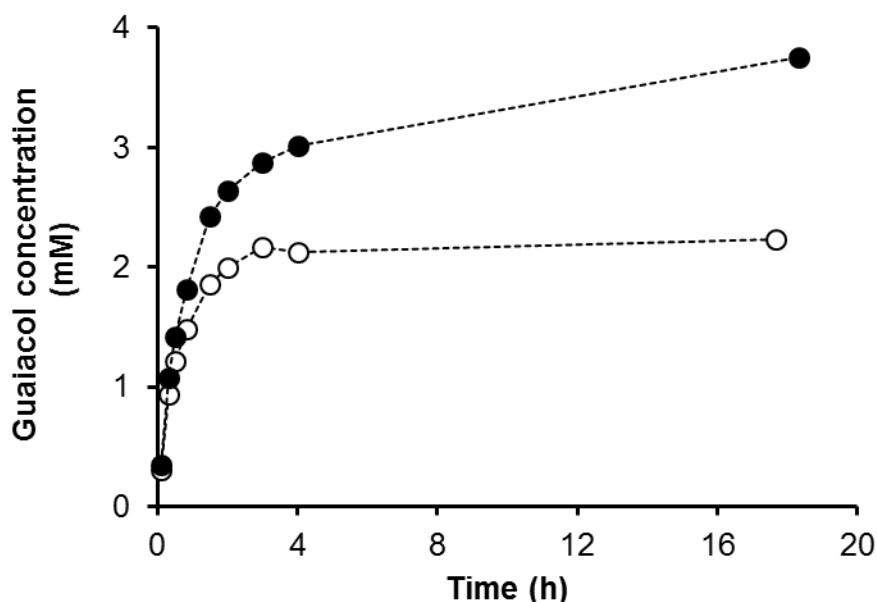


**Figure 5.** Time course analysis of product formation with co-immobilized enzymes system. The reaction was performed in the presence (●) and in the absence (○) of catalase. The reaction mixture contained 1.8  $\mu\text{M}$  Z\_P450 BM3, 14 U/mL Z\_GDH, 1000 U/mL catalase, 20 mM anisole, 0.8 mM  $\text{NADP}^+$  and 200 mM glucose in 50 mM potassium phosphate; 25°C, pH 7.5.

### **Analyzing the efficiency performance of co-immobilized system**

To exploit the suitability of the co-immobilizates, we chose the hydroxylation of lauric acid as the target reaction for P450 BM3 WT where the uncoupling inactivation might not have effect on the overall performance of the system. First, the hydroxylation of lauric acid was performed at high concentration of NADP<sup>+</sup> (0.8 mM) and co-immobilized enzymes (1.8 μM Z\_P450 BM3 and 14 U/mL Z\_GDH) under air headspace conditions. The full conversion was obtained after 15 minutes reaction and the calculated TTN was 1100. Encouraged by the results, we decreased the amount of applied enzymes (0.36 μM Z\_P450 BM3 and 2.8 U/mL Z\_GDH) to capture the kinetic of the conversion and study specific catalyst productivity. The concentration of NADP<sup>+</sup> was also decreased (0.1 mM) to study the potential of cofactor recycling at high level. Using the same amount of free and immobilized, the hydroxylation of lauric acid was studied. Figure 6 shows that activity of free enzyme was 3-fold higher than the immobilized one ( $\eta \sim 0.3$ ), which can be assigned to diffusion limitation of substrates in the porous carrier catalyst. A TTN of 5500 was calculated as well as 20 cycles of NADPH regeneration. Results decisively confirmed that the co-immobilized Z\_P450 BM3 and Z\_GDH can fulfill the application of heterogenous P450 BM3 in biocatalytic reactions.

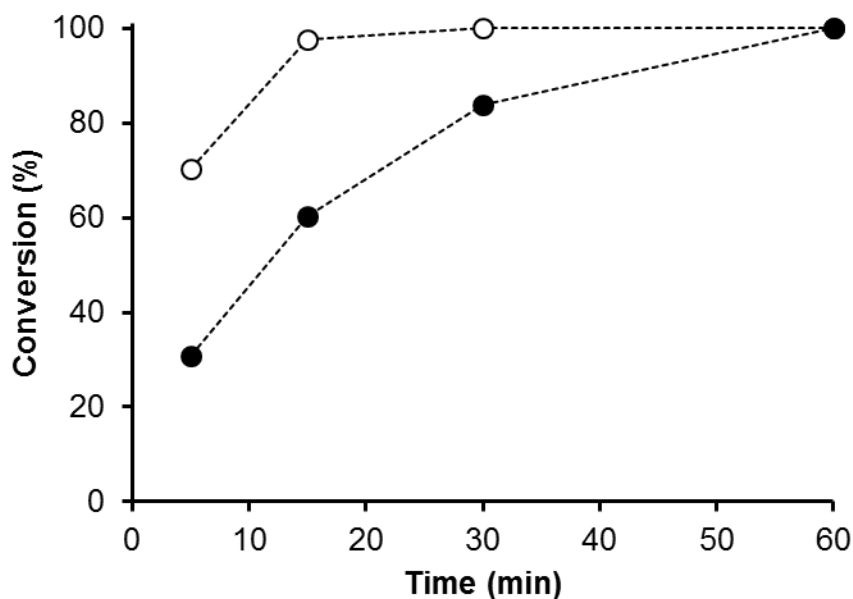


**Figure 6.** Time course of lauric acid hydroxylation reaction. The reaction was performed with free (○) and immobilized (●) enzymes. The reaction was a mixture of 0.36  $\mu\text{M}$  Z\_P450 BM3, 2.8 U/mL Z\_GDH, 1000 U/mL catalase, 2 mM lauric acid, 0.1 mM  $\text{NADP}^+$  and 200 mM glucose in 50 mM potassium phosphate; 25°C, pH 7.5.

### Co-immobilized enzymes reuse

A beneficial parameter for heterogenous catalyst is its reusability which can compensate the time and cost used for immobilization compared to whole cells. Therefore, the BM3-GDH co-immobilizates (1.8  $\mu\text{M}$  Z\_P450 BM3 and 14 U/mL Z\_GDH) were tested and reused for up to 20 catalytic cycles under air headspace conditions. Figure 7 shows the reusability of the system in which more than 90 % conversion was obtained for up to 10 cycles followed by a gradual decline reaching the half lifetime after 19 cycles of reuse. After the first 10 cycles where 2 mM lauric acid was efficiently converted into hydroxylauric acid, the corresponding TTN reached to  $\sim 11000$ .

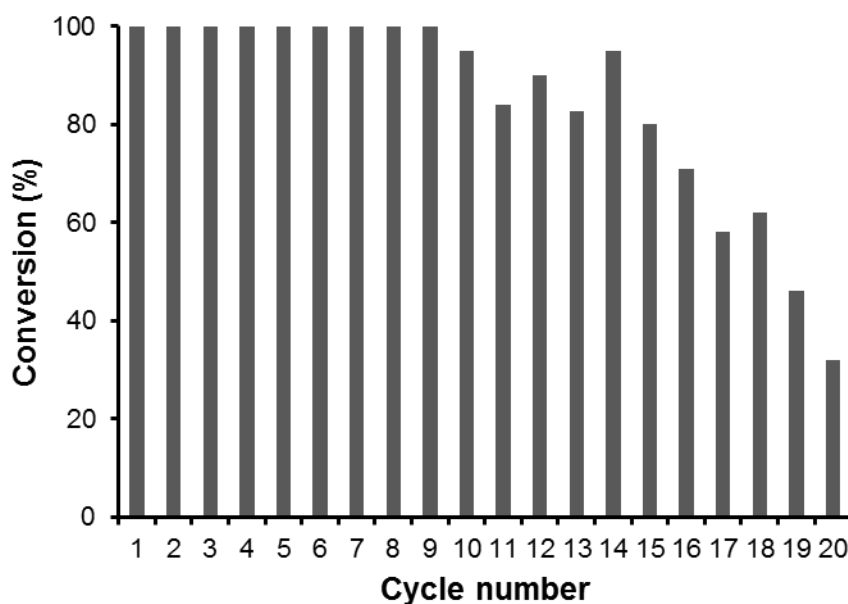


**Figure 7.** Evaluation of the reusability of co-immobilized enzyme system. The conversion (%) of the lauric acid hydroxylation versus number of cycles was studied for 20 cycles. Each column is defined as one cycle. The reaction mixture contained 1.8  $\mu\text{M}$  Z\_P450 BM3, 14 U/mL Z\_GDH, 1000 U/mL catalase, 2 mM lauric acid, 0.8 mM  $\text{NADP}^+$  and 200 mM glucose in 50 mM potassium phosphate; 25°C, pH 7.5.

## Conclusion

This study reveals, and shows a practical application of P450 BM3 as a heterogeneous biocatalyst on porous solid supports applied for the hydroxylation of lauric acid. Using enzymes as fusion proteins with the cationic binding module  $Z_{\text{basic}2}$ , P450 BM3 was co-immobilized with GDH on ReliSorb SP carriers. Tailored electrostatic complementarity between  $Z_{\text{basic}2}$  and the carrier surface, each enzyme could be immobilized on the carriers in controllable amount, thus maximizing the relative portion of the limiting P450 BM3 in total enzymes co-immobilizates. Using lauric acid as the ideal substrate of P450 BM3 WT, we demonstrated the full conversion of substrate hydroxylation under sufficient coupling to the regeneration of NADPH from glucose. The system showed high reusability which provided the opportunity to boost the amount of hydroxylated fatty acid in total. This approach offers

Tailor-made, Self-sufficient and Recyclable Monooxygenase Catalyst Based on Co-immobilized Cytochrome P450 BM3 and Glucose Dehydrogenase

the stable immobilized P450 BM3 combined with the efficient cofactor regeneration system which can be easily used by other P450s.

### **Acknowledgments**

We thank Prof. Dr. Georg Sprenger (University of Stuttgart) for kindly providing the plasmid containing the gene of *gdhIV* from *Bacillus megaterium*.

## References

- Bahrami, A., Vincent, T., Garnier, A., Larachi, F., Boukouvalas, J., & Iliuta, M. C. (2017). Noncovalent Immobilization of Optimized Bacterial Cytochrome P450 BM3 on Functionalized Magnetic Nanoparticles. *Industrial & Engineering Chemistry Research*, 56(39), 10981-10989. doi:10.1021/acs.iecr.7b02872
- Bolivar, J. M., Gascon, V., Marquez-Alvarez, C., Blanco, R. M., & Nidetzky, B. (2017). Oriented Coimmobilization of Oxidase and Catalase on Tailor-Made Ordered Mesoporous Silica. *Langmuir*, 33(20), 5065-5076. doi:10.1021/acs.langmuir.7b00441
- Bolivar, J. M., & Nidetzky, B. (2012a). Oriented and selective enzyme immobilization on functionalized silica carrier using the cationic binding module Z basic2: design of a heterogeneous D-amino acid oxidase catalyst on porous glass. *Biotechnol Bioeng*, 109(6), 1490-1498. doi:10.1002/bit.24423
- Bolivar, J. M., & Nidetzky, B. (2012b). Positively charged mini-protein Zbasic2 as a highly efficient silica binding module: opportunities for enzyme immobilization on unmodified silica supports. *Langmuir*, 28(26), 10040-10049. doi:10.1021/la3012348
- Dennig, A., Busto, E., Kroutil, W., & Faber, K. (2015). Biocatalytic One-Pot Synthesis of l-Tyrosine Derivatives from Monosubstituted Benzenes, Pyruvate, and Ammonia. *ACS Catalysis*, 5(12), 7503-7506. doi:10.1021/acscatal.5b02129
- Dennig, A., Lülldorf, N., Liu, H., & Schwaneberg, U. (2013). Regioselective o-Hydroxylation of Monosubstituted Benzenes by P450 BM3. *Angewandte Chemie International Edition*, 52(32), 8459-8462. doi:10.1002/anie.201303986
- Di Nardo, G., & Gilardi, G. (2012). Optimization of the bacterial cytochrome P450 BM3 system for the production of human drug metabolites. *Int J Mol Sci*, 13(12), 15901-15924. doi:10.3390/ijms131215901

Tailor-made, Self-sufficient and Recyclable Monooxygenase Catalyst Based on Co-immobilized Cytochrome P450 BM3 and Glucose Dehydrogenase

- Ducharme, J., & Auclair, K. (2018). Use of bioconjugation with cytochrome P450 enzymes. *Biochimica et Biophysica Acta (BBA) - Proteins and Proteomics*, 1866(1), 32-51. doi:10.1016/j.bbapap.2017.06.007
- Hernandez-Martin, A., von Buhler, C. J., Tieves, F., Fernandez, S., Ferrero, M., & Urlacher, V. B. (2014). Whole-cell biotransformation with recombinant cytochrome P450 for the selective oxidation of Grundmann's ketone. *Bioorg Med Chem*, 22(20), 5586-5592. doi:10.1016/j.bmc.2014.06.005
- Hollmann, F., Hofstetter, K., & Schmid, A. (2006). Non-enzymatic regeneration of nicotinamide and flavin cofactors for monooxygenase catalysis. *Trends Biotechnol*, 24(4), 163-171. doi:10.1016/j.tibtech.2006.02.003
- Kang, J. Y., Ryu, S. H., Park, S. H., Cha, G. S., Kim, D. H., Kim, K. H., Yun, C. H. (2014). Chimeric cytochromes P450 engineered by domain swapping and random mutagenesis for producing human metabolites of drugs. *Biotechnol Bioeng*, 111(7), 1313-1322. doi:10.1002/bit.25202
- Lee, J. H., Nam, D. H., Lee, S. H., Park, J. H., Park, S. J., Lee, S. H., Jeong, K. J. (2014). New platform for cytochrome p450 reaction combining in situ immobilization on biopolymer. *Bioconjug Chem*, 25(12), 2101-2104. doi:10.1021/bc500404j
- Lee, S. H., Kwon, Y. C., Kim, D. M., & Park, C. B. (2013). Cytochrome P450-catalyzed O-dealkylation coupled with photochemical NADPH regeneration. *Biotechnol Bioeng*, 110(2), 383-390. doi:10.1002/bit.24729
- López-Gallego, F., Jackson, E., & Betancor, L. (2017). Heterogeneous Systems Biocatalysis: The Path to the Fabrication of Self-Sufficient Artificial Metabolic Cells. *Chemistry – A European Journal*, 23(71), 17841-17849. doi:10.1002/chem.201703593

Tailor-made, Self-sufficient and Recyclable Monooxygenase Catalyst Based on Co-immobilized Cytochrome P450 BM3 and Glucose Dehydrogenase

- Lu, Y., & Mei, L. (2007). Co-expression of P450 BM3 and glucose dehydrogenase by recombinant *Escherichia coli* and its application in an NADPH-dependent indigo production system. *J Ind Microbiol Biotechnol*, 34(3), 247-253. doi:10.1007/s10295-006-0193-1
- Mateo, C., Palomo, J. M., Fernandez-Lorente, G., Guisan, J. M., & Fernandez-Lafuente, R. (2007). Improvement of enzyme activity, stability and selectivity via immobilization techniques. *Enzyme and Microbial Technology*, 40(6), 1451-1463. doi:10.1016/j.enzmictec.2007.01.018
- Maurer, S. C., Schulze, H., Schmid, R. D., & Urlacher, V. (2003). Immobilisation of P450 BM-3 and an NADP<sup>+</sup> Cofactor Recycling System: Towards a Technical Application of Heme-Containing Monooxygenases in Fine Chemical Synthesis. *Advanced Synthesis & Catalysis*, 345(67), 802-810. doi:10.1002/adsc.200303021
- Miyazaki, K. (2011). Chapter seventeen - MEGAWHOP Cloning: A Method of Creating Random Mutagenesis Libraries via Megaprimer PCR of Whole Plasmids. In C. Voigt (Ed.), *Methods in Enzymology* (Vol. 498, pp. 399-406): Academic Press.
- Müller, C. A., Akkapurathu, B., Winkler, T., Staudt, S., Hummel, W., Gröger, H., & Schwaneberg, U. (2013). In Vitro Double Oxidation of n-Heptane with Direct Cofactor Regeneration. *Advanced Synthesis & Catalysis*, 355(9), 1787-1798. doi:10.1002/adsc.201300143
- Munro, A. W., Leys, D. G., McLean, K. J., Marshall, K. R., Ost, T. W., Daff, S., Dutton, P. L. (2002). P450 BM3: the very model of a modern flavocytochrome. *Trends Biochem Sci*, 27(5), 250-257. doi:10.1016/S0968-0004(02)02086-8
- Nagao, T., Mitamura, T., Wang, X. H., Negoro, S., Yomo, T., Urabe, I., & Okada, H. (1992). Cloning, nucleotide sequences, and enzymatic properties of glucose dehydrogenase isozymes from *Bacillus megaterium* IAM1030. *J Bacteriol*, 174(15), 5013-5020. doi: 10.1128/jb.174.15.5013-5020.1992

Tailor-made, Self-sufficient and Recyclable Monooxygenase Catalyst Based on Co-immobilized Cytochrome P450 BM3 and Glucose Dehydrogenase

- Nowak, C., Pick, A., Lommès, P., & Sieber, V. (2017). Enzymatic Reduction of Nicotinamide Biomimetic Cofactors Using an Engineered Glucose Dehydrogenase: Providing a Regeneration System for Artificial Cofactors. *ACS Catalysis*, 7(8), 5202-5208. doi:10.1021/acscatal.7b00721
- O'Reilly, E., Kohler, V., Flitsch, S. L., & Turner, N. J. (2011). Cytochromes P450 as useful biocatalysts: addressing the limitations. *Chem Commun (Camb)*, 47(9), 2490-2501. doi:10.1039/c0cc03165h
- Omura, T., & Sato, R. (1964). THE CARBON MONOXIDE-BINDING PIGMENT OF LIVER MICROSOMES. I. EVIDENCE FOR ITS HEMOPROTEIN NATURE. *J Biol Chem*, 239, 2370-2378.
- Ortiz de Montellano, P. R. (2010). Hydrocarbon Hydroxylation by Cytochrome P450 Enzymes. *Chemical Reviews*, 110(2), 932-948. doi:10.1021/cr9002193
- Park, J. H., Lee, S. H., Cha, G. S., Choi, D. S., Nam, D. H., Lee, J. H., Park, C. B. (2015). Cofactor-free light-driven whole-cell cytochrome P450 catalysis. *Angew Chem Int Ed Engl*, 54(3), 969-973. doi:10.1002/anie.201410059
- Pham, S. Q., Gao, P., & Li, Z. (2013). Engineering of recombinant E. coli cells co-expressing P450<sub>pyr</sub><sup>TM</sup> monooxygenase and glucose dehydrogenase for highly regio- and stereoselective hydroxylation of alicycles with cofactor recycling. *Biotechnol Bioeng*, 110(2), 363-373. doi:10.1002/bit.24632
- Santos, J. C. S. d., Barbosa, O., Ortiz, C., Berenguer-Murcia, A., Rodrigues, R. C., & Fernandez-Lafuente, R. (2015). Importance of the Support Properties for Immobilization or Purification of Enzymes. *ChemCatChem*, 7(16), 2413-2432. doi:10.1002/cctc.201500310
- Schewe, H., Holtmann, D., & Schrader, J. (2009). P450(BM-3)-catalyzed whole-cell biotransformation of alpha-pinene with recombinant Escherichia coli in an aqueous-organic

- Tailor-made, Self-sufficient and Recyclable Monooxygenase Catalyst Based on Co-immobilized Cytochrome P450 BM3 and Glucose Dehydrogenase
- two-phase system. *Appl Microbiol Biotechnol*, 83(5), 849-857. doi:10.1007/s00253-009-1917-8
- Schoemaker, H. E., Mink, D., & Wubbolts, M. G. (2003). Dispelling the Myths--Biocatalysis in Industrial Synthesis. *Science*, 299(5613), 1694-1697. doi:10.1126/science.1079237
- Tran, D. N., & Balkus, K. J. (2011). Perspective of Recent Progress in Immobilization of Enzymes. *ACS Catalysis*, 1(8), 956-968. doi:10.1021/cs200124a
- Tran, N. H., Nguyen, D., Dwaraknath, S., Mahadevan, S., Chavez, G., Nguyen, A., Cheruzel, L. E. (2013). An efficient light-driven P450 BM3 biocatalyst. *J Am Chem Soc*, 135(39), 14484-14487. doi:10.1021/ja409337v
- Urlacher, V. B., & Eiben, S. (2006). Cytochrome P450 monooxygenases: perspectives for synthetic application. *Trends Biotechnol*, 24(7), 324-330. doi:10.1016/j.tibtech.2006.05.002
- Urlacher, V. B., & Girhard, M. (2012). Cytochrome P450 monooxygenases: an update on perspectives for synthetic application. *Trends Biotechnol*, 30(1), 26-36. doi:10.1016/j.tibtech.2011.06.012
- Wang, X., Saba, T., Yiu, H. H. P., Howe, R. F., Anderson, J. A., & Shi, J. (2017). Cofactor NAD(P)H Regeneration Inspired by Heterogeneous Pathways. *Chem*, 2(5), 621-654. doi:10.1016/j.chempr.2017.04.009
- Weber, E., Sirim, D., Schreiber, T., Thomas, B., Pleiss, J., Hunger, M., Urlacher, V. B. (2010). Immobilization of P450 BM-3 monooxygenase on mesoporous molecular sieves with different pore diameters. *Journal of Molecular Catalysis B: Enzymatic*, 64(1-2), 29-37. doi:10.1016/j.molcatb.2010.01.020
- Whitehouse, C. J. C., Bell, S. G., & Wong, L.-L. (2012). P450BM3 (CYP102A1): connecting the dots. *Chemical Society Reviews*, 41(3), 1218-1260. doi:10.1039/C1CS15192D
- Wiesbauer, J., Bolivar, J. M., Mueller, M., Schiller, M., & Nidetzky, B. (2011). Oriented Immobilization of Enzymes Made Fit for Applied Biocatalysis: Non-Covalent Attachment to

Tailor-made, Self-sufficient and Recyclable Monooxygenase Catalyst Based on Co-immobilized Cytochrome P450 BM3 and Glucose Dehydrogenase

Anionic Supports using Zbasic2 Module. *ChemCatChem*, 3(8), 1299-1303.  
doi:10.1002/cctc.201100103

Wu, H., Tian, C., Song, X., Liu, C., Yang, D., & Jiang, Z. (2013). Methods for the regeneration of nicotinamide coenzymes. *Green Chemistry*, 15(7), 1773. doi:10.1039/c3gc37129h

Zernia, S., Ott, F., Bellmann-Sickert, K., Frank, R., Klenner, M., Jahnke, H. G., Beck-Sickinger, A. G. (2016). Peptide-Mediated Specific Immobilization of Catalytically Active Cytochrome P450 BM3 Variant. *Bioconjug Chem*, 27(4), 1090-1097.  
doi:10.1021/acs.bioconjchem.6b00074

# Supporting Information

## **Tailor-made, Self-sufficient and Recyclable Monooxygenase Catalyst Based on Co-immobilized Cytochrome P450-BM3 and Glucose Dehydrogenase**

Donya Valikhani<sup>1</sup>, Juan M. Bolivar<sup>1</sup>, Alexander Dennig<sup>1</sup>, and Bernd Nidetzky<sup>1,2</sup>

<sup>1</sup>Institute of Biotechnology and Biochemical Engineering, Graz University of Technology, NAWI Graz, Petersgasse 12, 8010 Graz, Austria

<sup>2</sup>Austrian Centre of Industrial Biotechnology (acib), Petersgasse 14, 8010 Graz, Austria

Corresponding author (B.N.)

e-mail: bernd.nidetzky@tugraz.at; phone: +43 316 873 8400

## S1. Enzymes

### S1.1. DNA sequences and amino acid sequences of Z-enzyme constructs

#### T7-Tag (gene 10 leader)

#### Z<sub>basic2</sub>-Tag

#### Linker between Z<sub>basic2</sub> Tag and BM3/GDH

#### GDH/P450 BM3 WT

GDH IV from *Bacillus megaterium*: synthetic gene (WP\_013055759.1)

#### Assembled open reading frame: “Z\_GDH” construct (after DNA sequencing):

ATGGCTAGCATGACTGGTGGACAGCAAATGGGTTCGCGGATCCGTAGACAACAATTCA  
ACAAAGAACGTCGCCGTGCTCGCCGTGAAATCCGTCACTTACCTAACTTAAACCGTGAA  
CAACGCCGTGCTTTCATTCGTTCCCTGCGTGATGACCCAAGCCAAAGCGCTAACTTGCTA  
GCAGAAGCTAAAAAGCTAAATGATGCTCAGGCGCCGAAACCGAATAGCGGCGGTAGCG  
AGGATCTGTACTTTCAGAGCGGTAGCATGTATACAGATTTAAAAGATAAAGTAGTTGTA  
ATTACAGGTGGATCAACAGGTTTAGGACGTGCAATGGCTGTTTCGTTTCGGTCAAGAAGA  
AGCAAAAGTTGTTATTA ACTATTACAACAATGAAGAAGAAGCTTTAGATGCGAAAAAA  
GAAGTAGAAGAAGCAGGCGGACAAGCAATCATCGTTCAAGGCGACGTAACAAAAGAA  
GAAGACGTTGTAAACCTTGTTCAAACAGCTATTAAGAATTTCGGAACATTAGACGTTAT  
GATTAATAACGCTGGTGTGAAAACCCAGTTCCTTCTCATGAGCTATCTTTAGACA ACTG  
GAACAAAGTTATTGATACAACTTAACAGGTGCATTCTTAGGAAGCCGTGAAGCAATTA  
AATATTTTCGTTGAAAATGACATTAAGGAAACGTTATTAACATGTCCAGCGTTCACGAA  
ATGATTCCTTGCCATTATTTGTTCACTACGCAGCAAGTAAAGGCGGTATGAAACTAAT  
GACGGAAACATTGGCTCTTGAATATGCGCCAAAAGGTATCCGAGTAAATAACATTGGAC  
CAGGTGCGATGAACACACCAATTAACGCTGAAAAATTCGCTGATCCTGTACAACGTGCA  
GACGTAGAAAGCATGATTCCAATGGGTTACATCGGTAAGCCAGAAGAAGTAGCAGCAG  
TTGCAGCATTCTTAGCATCATCACAAGCAAGCTATGTAACAGGTATTACATTATTTGCTG  
ATGGTGGTATGACGAAATACCCTTCTTTCCAAGCAGGAAGAGGCTAA

#### Amino acid sequence [Z\_GDH]

MTGGQQMGRGSVDNKFNKERRRARREIRHLPNLNREQRRAFIRSLRDDPSQSANLLAEAK  
KLND AQAPKPNSSGSEDLYFQSGSMYDLDKDKVVVITGGSTGLGRAMAVRFGQEEAKVVI  
NYYNNEEEALDAKKEVEEAGGQAIIVQGDVTKEEDVVNLVQTAIKEFGTLDVMINNAGVE  
NPVPSHELSDLNWNKVIDTNLTGAFLGSREAIKYFVENDIKGNVINMSSVHEMI PWPLFV  
HYAASKGGMKLMTETLALEYAPKGI RVNNIGPGAMNTPINA EKFPADPVQ RADVESMI PMG  
YIGKPEEVA AVAAFLASSQASYVTGITL FADGGMTKYPSFQAGRG

**Assembled open reading frame: “Z\_P450 BM3WT” (after DNA sequencing):**

ATGGCTAGCATGACTGGTGGACAGCAAATGGGTTCGCGGATCCGTAGACAACAATTCACAAAGAACGTCGCCGTGCTCGCCGTGAAATCCGTCACCTAACCTAAACCGTGAA  
CAACGCCGTGCTTTCATTTCCTGCGTGATGACCCAAGCCAAAGCGCTAACTTGCTAGCAGAAAGCTAAAAGCTAAATGATGCTCAGGCGCCGAAACCGAATAGCGGCGGTAGCG  
AGGATCTGTACTTTCAGAGCGGTAGCATGACAATTAAGAAATGCCTCAGCCAAAAAC  
GTTTGGAGAGCTTAAAAATTTACCGTTATTAACACAGATAAACCGGTTCAAGCTTTGATGAAAATTGCGGATGAATTAGGAGAAATCTTTAAATTCGAGGGCGCTGGTTCGTGTAACG  
CGCTACTTATCAAGTCAGCGTCTAATTAAGAAGCATGCGATGAATCACGCTTTGATAAACTTAAGTCAAGCGCTTAAATTTGTACGTGATTTTGCAGGAGACGGGTTATTTACAA  
GCTGGACGCATGAAAAAATTGGAAAAAAGCGCATAATATCTTACTTCCAAGCTTCAGTCAGCAGGCAATGAAAGGCTATCATGCGATGATGGTCGATATCGCCGTGCAGCTTGTTC  
AAAGTGGGAGCGTCTAAATGCAGATGAGCATATTGAAGTACCGGAAGACATGACACGT  
TTAACGCTTGATACAATTGGTCTTTGCGGCTTTAACTATCGCTTTAACAGCTTTTACCGA  
GATCAGCCTCATCCATTTATTACAAGTATGGTCCGTGCACTGGATGAAGCAATGAACAA  
GCTGCAGCGAGCAAATCCAGACGACCCAGCTTATGATGAAAACAAGCGCCAGTTTCAA  
GAAGATATCAAGGTGATGAACGACCTAGTAGATAAAATTATTGCAGATCGCAAAGCAA  
GCCGTGAACAAAGCGATGATTTATTAACGCATATGCTAAACGGAAAAGATCCAGAAAC  
GGGTGAGCCGCTTGATGACGAGAACATTCGCTATCAAATTATTACATTCTTAATTGCGG  
GACACGAAACAACAAGTGGTCTTTTATCATTGCGCTGTATTTCTTAGTGAAAAATCCAC  
ATGTATTACAAAAGCAGCAGAAGAAGCAGCAGAGTTCTAGTAGATCCTGTTCCAAG  
CTACAAACAAGTCAAACAGCTTAAATATGTCGGCATGGTCTTAAACGAAGCGCTGCGCT  
TATGGCCAACTGCTCCTGCGTTTTCCCTATATGCAAAGAAGATACGGTGCTTGGAGGA  
GAATATCCTTTAGAAAAAGGCGACGAACTAATGGTTCTGATTCTCAGCTTCACCGTGA  
TAAAACAATTTGGGGAGACGATGTGGAAGAGTTCCGTCCAGAGCGTTTTGAAAATCCAA  
GTGCGATTCCGCAGCATGCGTTTAAACCGTTTGGAAACGGTCAGCGTGCGTGTATCGGT  
CAGCAGTTCGCTCTTCATGAAGCAACGCTGGTACTTGGTATGATGCTAAAACACTTTGA  
CTTTGAAGATCATACAAACACTACGAGCTGGATATTAAGAAACTTTAACGTTAAAACCTG  
AAGGCTTTGTGGTAAAAGCAAATCGAAAAAATTCGCTTGGCGGTATTCCTTCACCT  
AGCACTGAACAGTCTGCTAAAAAAGTACGCAAAAAGGCAGAAAACGCTCATAATACGC  
CGCTGCTTGTGCTATACGGTTCAAATATGGGAACAGCTGAAGGAACGGCGCGTGATTTA  
GCAGATATTGCAATGAGCAAAGGATTTGCACCGCAGGTCGCAACGCTTGATTACACGC  
CGGAAATCTTCCGCGCGAAGGAGCTGTATTAATTGTAACGGCGTCTTATAACGGTCATC  
CGCTGATAACGCAAAGCAATTTGTCGACTGGTTAGACCAAGCGTCTGCTGATGAAGTA  
AAAGGCGTTCGCTACTCCGATTTGGATGCGGCGATAAAAACCTGGGCTACTACGTATCA  
AAAAGTGCCTGCTTTTATCGATGAAACGCTTGCCGCTAAAGGGGCAGAAAACATCGCTG  
ACCGCGGTGAAGCAGATGCAAGCGACGACTTTGAAGGCACATATGAAGAATGGCGTGA  
ACATATGTGGAGTGACGTAGCAGCCTACTTTAACCTCGACATTGAAAACAGTGAAGATA  
ATAAATCTACTCTTCACTTCAATTTGTCGACAGCGCCGCGGATATGCCGCTTGCGAAAA  
TGCACGGTGCCTTTTCAACGAACGTCGTAGCAAGCAAAGAACTTCAACAGCCAGGCAGT  
GCACGAAGCACGCGACATCTTGAAATTGAACTTCCAAAAGAAGCTTCTTATCAAGAAGG  
AGATCATTTAGGTGTTATTCCTCGCAACTATGAAGGAATAGTAAACCGTGTAAACAGCAA  
GGTTCGGCCTAGATGCATCACAGCAAATCCGTCTGGAAGCAGAAGAAGAAAAATTAGC  
TCATTTGCCACTCGCTAAAACAGTATCCGTAGAAGAGCTTCTGCAATACGTGGAGCTTC  
AAGATCCTGTTACGCGCACGCGAGCTTCGCGCAATGGCTGCTAAAACGGTCTGCCCGCCG  
CATAAAGTAGAGCTTGAAGCCTTGCTTGAAGCAAGCCTACAAAGAACAAGTGCTGG  
CAAAACGTTTAAACAATGCTTGAAGTCTTGAAGAAATACCCGGCGTGTGAAATGAAATTC

```
AGCGAATTTATCGCCCTTCTGCCAAGCATAACGCCC GCGCTATTACTCGATTTCTTCATCA  
CCTCGTGTGCGATGAAAAACAAGCAAGCATCACGGTCAGCGTTGTCTCAGGAGAAGCGT  
GGAGCGGATATGGAGAATATAAAGGAATTGCGTCGAACTATCTTGCCGAGCTGCAAGA  
AGGAGATACGATTACGTGCTTTATTTCCACACCGCAGTCAGAATTTACGCTGCCAAAAG  
ACCCTGAAACGCCGCTTATCATGGTTCGGACCGGGAACAGGCGTTCGCGCCGTTTAGAGGC  
TTTGTGCAGGCGCGCAAACAGCTAAAAGAACAAGGACAGTCACTTGGAGAAGCACATT  
TATACTTCGGCTGCCGTTACCTCATGAAGACTATCTGTATCAAGAAGAGCTTGAAAAC  
GCCCAAAGCGAAGGCATCATTACGCTTCATAACCGCTTTTTCTCGCATGCCAAATCAGCC  
GAAAACATACGTTTCAGCACGTAATGGAACAAGACGGCAAGAAATTGATTGAACTTCTT  
GATCAAGGAGCGCACTTCTATATTTGCGGAGACGGAAGCCAAATGGCACCTGCCGTTGA  
AGCAACGCTTATGAAAAGCTATGCTGACGTTACCAAGTGAGTGAAGCAGACGCTCGCT  
TATGGCTGCAGCAGCTAGAAGAAAAGGCCGATACGCAAAGACGTGTGGGCTGGGTA  
A
```

### Amino acid sequence: [Z\_P450 BM3]

```
MTGGQQMGRGSVDNKFNKERRRARREIRHLPLNLNREQRRAFIRSLRDDPSQSANLLAEAK  
KLNDAQAPKPNSSGSEDLVFQSGSMTIKEMPQPKTFGELKNLPLLNTDKPVQALMKIADE  
LGEIFKFEAPGRVTRYLSSQRLIKEACDESFRDKNLSQALKFVRDFAGDGLFTSWTHEKN  
WKAHNI LLPSFSQQAMKGYHAMMVDIAVQLVQKWERLNADEHIEVPEDMTRLTLDTIGL  
CGFNRYRNSFYRDQPHFITSMVRALDEAMNKLQRANPDDPAYDENKRQFQEDIKVMNDL  
VDKIIADRKASGEQSDDLTHMLNGKDPETGEPLDDENIRYQIITFLIAGHETTSGLLSF  
ALYFLVKNPHVLQKAAEEAARVLVDPVPSYKQVKQLKYVGMVLNEALRLWPTAPAFSLYA  
KEDTVLGGEYPLEKGD ELMVLI PQLHRDKTIWGDVVEEFRPERFENPSAIPQHAFKPFNG  
GQRACIGQQFALHEATLVLGMMLKHFDFEDHTNYELDIKETLTLKPEGFVVKAKSKKIPL  
GGIPSPSTEQSAKKVRKAENAHTPLLVLVYGSNMGTAEGTARDLADIAMSKGFAPQVAT  
LD SHAGNLPREGAVLIVTASYNHPPDNAKQFVDWLDQASADEVKGVRYSVFGCGDKNWA  
TTYQKVPAFIDETLAAKGAENIADRGEADASDDFEGTYEEWREHMWSDVAAYFNLDIENS  
EDNKSTLSLQFVDSAADMPLAKMHGAFSTNVVASKELQQPGSARSTRHLEIELPKEASYQ  
EGDHLGVI PRNYEGIVNRVTARFGLDASQQIRLEAEEKLAHLPLAKTVSVEELLQYVEL  
QDPVTRTQLRAMAAKTVCPPHKVELEALLEKQAYKEQVLAKRLTMLELLEKYPACEMKFS  
EFIALLP SIRPRYYSISSPRVDEKQASITVSVVSGEAWSGYGEYKGIASNYLAELQEGD  
TITCFISTPQSEFTLPKDPETPLIMVGP GTGVAPFRGFVQARKQLKEQGQSLGEAHL YFG  
CRSPHEDYLYQEELNAQSEGIITLHTAFSRMPNQPKTYVQHVMEQDGKKLIELLDQGAH  
FYICGDGSQMAPAVEATLMKSYADVHQVSEADARLWLQQLLEEKGRYAKDVWAG
```

### S1.2. Enzyme purification

The cell pellet was thawed on ice and resuspended in potassium phosphate buffer (50 mM, pH 7.5).

Resuspended cells were placed on ice and disrupted by sonication. Lysed cells were centrifuged (20000 x g, 10 min, 4°C) for entire removal of cell debris and the clear supernatant was used for further experiments. Protein was purified at 25 °C using pre-packed (1.6 cm × 2.5 cm; 5 mL) HiTrap SPFF columns (GE Healthcare Life Sciences) fitted on a ÄKTA prime plus system. The column was

## Tailor-made, Self-sufficient and Recyclable Monooxygenase Catalyst Based on Co-immobilized Cytochrome P450 BM3 and Glucose Dehydrogenase

equilibrated with buffer A (50 mM potassium phosphate buffer, pH 7.5) and 10 mL of the cell extract were loaded onto the column. Protein elution was performed using a continuous salt gradient from 0 to 100% of buffer B (50 mM potassium phosphate buffer containing 2 M NaCl, pH 7.5) in 75 mL at a flow rate of 3 mL min<sup>-1</sup>. The target protein (all constructs) eluted at around 40-50% buffer B. Pooled fractions were collected and buffer was exchanged to buffer A. Protein purification was monitored by SDS-PAGE. Protein elution profile during fractionation and SDS-PAGE are shown in Figure S1.

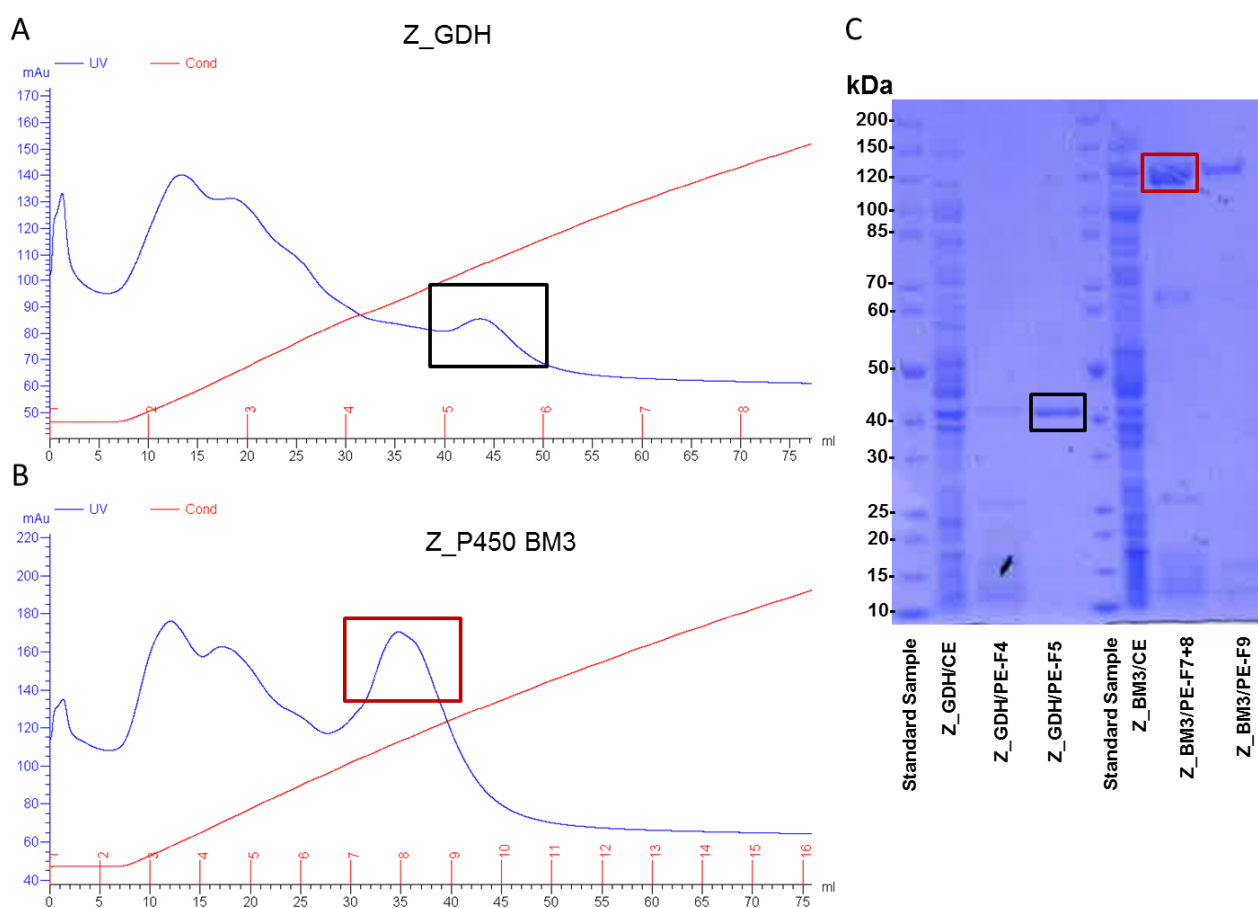


**Figure S1.** Purification of Z\_P450 BM3 and Z\_GDH. Panel A and Panel B show protein elution profile during fractionation of *E. coli* cell extract on HiTrap SPFF columns. Panel C shows the purification of Z-enzyme constructs analyzed by SDS PAGE, comparing the purified enzyme (PE) and the corresponding cell extract (CE). Thermo Scientific PageRuler™ Unstained Protein Ladder was used as the size standard.

## Scientific record

### Publications

#### **Multivalency Effects on the Immobilization of Sucrose Phosphorylase in Flow Microchannels and Their Use in the Development of a High-Performance Biocatalytic Microreactor**

Donya Valikhani, Juan M. Bolivar, Martin Pfeiffer, Bernd Nidetzky

*ChemCatChem*, 2017, 9, 161 – 166

#### **A Spring in Performance: Silica Nanosprings Boost Enzyme Immobilization in Microfluidic Channels**

Donya Valikhani, Juan M. Bolivar, Martina Viefhues, David N. McIlroy, Elwin X. Vrouwe, Bernd Nidetzky

*ACS Appl. Mater. Interfaces*, 2017, 9, 34641–34649

#### **Tailor-made resealable micro(bio)reactors providing easy integration of *in situ* sensors**

Martina Viefhues, Shiwen Sun, Donya Valikhani, Bernd Nidetzky, Elwin X Vrouwe, Torsten Mayr, Juan M. Bolivar

*J. Micromech. Microeng.*, 2017, 27, 065012

### Oral presentation

**Wall-coated enzyme microreactors for biocatalytic process development.** Donya Valikhani, Juan M. Bolivar, Martin Pfeiffer, Bernd Nidetzky, 18<sup>th</sup> DocDay, 2017, Graz, Austria

### Flash presentation

**Multivalency Effects on the Immobilization of Sucrose Phosphorylase in Flow Microchannels for the Development of a High-Performance Biocatalytic Microreactor.**

Donya Valikhani, Juan M. Bolivar, Martin Pfeiffer, Bernd Nidetzky, Implementation of Microreactor Technology in Biotechnology, 2017, Bled, Slovenia

## Poster presentation

**Use of silica nanosprings and electrospun nanofibers for the development of wall-coated enzyme microreactors.** Donya Valikhani, Juan M. Bolivar, Filip Strniša, David N. McIlroy, Polona Žnidaršič Plazl, Bernd Nidetzky, Implementation of Microreactor Technology in Biotechnology, 2017, Bled, Slovenia

**The application of oxygen sensor layers integrated in resealable flowcells for immobilized enzyme reactions.** Donya Valikhani, Martina Viefhues, Shiwen Sun, Juan M. Bolivar, Torsten Mayr, Bernd Nidetzky, EUROPTRODE-Conference on Optical Chemical Sensors and Biosensors, 2016, Graz, Austria

**Reversible oriented immobilization of sucrose phosphorylases in a glass microreactor.** Donya Valikhani, Juan M. Bolivar, Martin Pfeiffer, Bernd Nidetzky, 15<sup>th</sup> DocDay, 2016, Graz, Austria

**Reversible oriented immobilization of sucrose phosphorylases in a glass microreactor: the role of multivalency due to protein oligomerization.** Donya Valikhani, Juan M. Bolivar, Marco A. Tribulato, Martin Pfeiffer, Bernd Nidetzky, Implementation of Microreactor Technology in Biotechnology, 2015, Opatija, Croatia